Fatigue Assessment for Failed Bridge Deck Closure Pour

Elias Alexander Rivera

Thesis submitted to the faculty of the Virginia Polytechnic Institute and State University
in partial fulfillment of the requirements for the degree of

Master of Science
In
Civil Engineering

Committee Members
William J. Wright, Chair
Richard E. Weyers
Carin L. Roberts-Wollmann

May, 1 2012
Blacksburg, VA

Keywords: Fatigue, Bridge Deck, Closure Pour, Reinforcing Steel, Construction Joint

Fatigue Assessment for Failed Bridge Deck Closure Pour

Elias Alexander Rivera

ABSTRACT

After 17 years in service, a 3 ft by 3 ft closure pour section of an Interstate 81 (I-81) bridge deck failed by punching through near Marion, Virginia. Visual inspection noted that there was considerable corrosion on some of the reinforcing bars in the vicinity of the construction joint, while other failure bars had little or no corrosion. Sections of the bridge deck were cut and delivered to Virginia Tech for further investigation.

It was clear from an initial investigation that shrinkage of the deck concrete had caused the construction joints to open and thereby allow water and chlorides to enter the joint. In addition, it was observed that several bars across the closure pour construction joints had suffered significant section loss due to corrosion, but it was not clear if fatigue and strength failure of the reinforcing bars were also contributing factor in the closure pour failure.

To study the problem four fatigue tests and five strength tests performed. The specimens included six slab strips cut from the I-81 bridge deck, with the 3-ft closure pour included, and three additional specimens that were cast in the laboratory to represent a base line for performance. A three-point loading setup was used for both fatigue and strength tests. However, for the final strength and fatigue tests, a jacking system was designed and implemented in an effort to open the closure pour construction joints to simulate the open joints of the I-81 bridge.

The objectives of this research program are to provide a better understanding of the closure pour failure mechanism, develop inspection procedures for Virginia Department of Transportation (VDOT) to assess its bridge inventory containing similar construction joints, and to develop recommendations for future construction of similar construction joints.

ACKNOWLEDGEMENTS

First and foremost, I would like to take this opportunity to express my sincere thanks to Dr. William J. Wright for his guidance and patience throughout the course of this research study. His role as committee chair and mentor has had a tremendous impact during my time at Virginia Tech. I would also like to thank the members of my advisory committee, Dr. Richard E. Weyers and Dr. Carin L. Roberts-Wollmann, for serving as part of the committee and for their kindness and thoughtfulness in reviewing this report. I am appreciative of their guidance and support during this process.

I am fortunate to have been given the opportunity to study and work at Virginia Tech and I would like to express my gratitude to the Charles E. Via, Jr. Department of Civil and Environmental Engineering and the Via Endowment Program for blessing me with the honor of the Via Fellowship. My time in Blacksburg would not have been the same if it were not for the Department's trust and generosity.

I want to thank my colleague and dear friend Ebrahim Abbas who was part of this project and played a major role throughout its entirety. His help and support has been a great blessing. The instruction and aid of Dr. David Mokarem, Mr. Brett Framer, and Mr. Dennis Huffman at the Thomas M. Murray Structural Engineering Laboratory were vital, and I am thankful to them as well. I would also like to thank David Padilla, Shainur Ahsan, Kedar Halbe, and William Collins for their helping hands.

I would like to extend a special thanks to my parents, Byron and Ximena, and brother, Byron Jr. Their support, love, and prayers have been a pillar of strength throughout my academic career, especially in graduate school. Finally, I would like to express my gratitude to the supreme Structural Engineer who wrote the laws that govern nature and continues to reveal them through research.

TABLE OF CONTENTS

LIST OF FIGURES

LIST OF TABLES

CHAPTER 1: INTRODUCTION

1.1 Background

In 1992 a number of bridge decks on Interstate 81 were replaced in Smyth County Virginia near the city of Marion. In this effort, epoxy coated reinforcing (ECR) bars were used for the concrete deck instead of the uncoated reinforcing (black bars) used in the original deck (Sprinkel, et al., 2010). A staged-construction approach was carried out to avoid closing the bridge to traffic. For two-lane bridges, it involved the use one lane and shoulder for through traffic while one side of the deck was replaced with a new slab. A 3-ft gap was left between the new and old deck portions. The reinforcing bars from the new deck sections extended into the 3 ft. gap. Once the first new slab section was cured, traffic was diverted onto the new deck section and the second half of the deck was replaced. Finally a closure pour was placed between the two new deck sections to fill the gap and bond the two sections together. This created two cold joints in the deck that extended the entire length of the bridge in the longitudinal direction. The bridge girder spacing was 8 ft. on center and the 3 ft closure pour strip was centered between the girders. The lane striping on the deck placed the left wheel load path of the right lane directly over the closure pour.

Seventeen years after the deck replacement, on April 2, 2009, a 3 ft x 3 ft section of the closure pour failed by punching through on the southbound bridge at mile marker 43. Since the failed section was located at the end of the deck, it fell onto the bridge's end diaphragm directly below it. When the failed section was being repaired, it became apparent the entire closure pour strip was in poor condition requiring immediate replacement (Sprinkel, et al., 2010). The failed closure pour section is shown in Figure1-1. This photograph was taken after the concrete had been removed to reveal the reinforcing bars.

Figure 1-1. Failed Closure Pour Section (Sprinkel, et al., 2010)

Three weeks prior to the failure, a 1/8 in. transverse crack across the closure pour was noticed during a routine inspection. This crack formed one of the boundaries of the failed section as shown across the top of Figure 1-1. The post-failure examination showed that a total of eighteen No. 5 reinforcing bars had been sheared along the boundaries of the failed section. Ten were in the transverse direction across the closure pour construction joints, while eight were in the longitudinal direction. The examination also revealed that the ECR had sustained section loss due to corrosion at the location of the construction joints. Figure 1-2 shows two transverse bars that have cracked along the closure pour joint after concrete was removed. The brown coloration of the epoxy coating indicates that corrosion is occurring on the surface of the bars at the failure location. The bars have transverse fractures and are completely severed in planes that are offset from the plane of the construction joint.

Figure 1-2. Sheared Bars at Closure Pour with Corrosion Damage (Sprinkel, et al., 2010)

The failed section was repaired by cutting out an 8-ft section of the deck along the entire bridge that spanned between the two adjacent steel girders which enclosed the closure pour. Expansive concrete with Type K cement and MMFX2 (corrosion resistant) reinforcement was used in replacing the 8-ft section (Sprinkel, et al., 2010). This repair widened the closure pour section and moved the construction joints to the center of the bridge girders to provide direct support for the joints. This contrasts with the original 3 ft closure pour where the joints had no vertical support.

1.2 Results of Initial Investigation

Four slab sections that were cut out from the southbound bridge were taken to the Structures and Materials Research Laboratory at Virginia Tech to be inspected and analyzed. The dimensions for three slabs were roughly 55 in. by 122 in. (the greater dimension being parallel to the closure pour joints). The fourth slab's dimensions were 55-1/2 in. by 97-5/8 in., the larger dimension also being in the same direction as the joints. The investigation, lead by Richard E. Weyers and Michael M. Sprinkel, was

conducted to determine the condition of the slab and the cause of the closure pour failure. The results were outlined and reported by the Virginia Department of Transportation in Sprinkel et al. (2010). The scope of the investigation included an assessment of the conditions of the construction joints, the Epoxy Coated Reinforcement and the deck concrete, and an assessment of the design details used for the closure pour joint.

The investigation included visual inspection and nondestructive evaluation (NDE) of the closure pour deck sections both at the bridge site and in the laboratory at Virginia Tech. NDE methods to assess corrosion damage included current flow, resistivity, and electrical potential measurements of the reinforcing bars. In addition, the chloride ion content and permeability of concrete samples were measured. It was determined that shrinkage of the closure pour concrete had caused the joints to open enough to leak (more than 0.007 in.). Water and chlorides from de-icing salts had infiltrated through the open joints and come in direct contact with the transverse ECR bars across the joints. A joint width of 0.012 in. and 0.014 in. was measured, respectively, for sides 1 and 2 of slab 1. For slab 2, the joint widths were 0.015 in. and 0.008 in. for sides 1 and 2 respectively.

The final report concluded that the chloride ion content at the joint walls was high enough to propagate corrosion throughout the slab depth near the joints, the ECR had corroded at a high rate at the joint locations, the epoxy coating of the rebars did not protect against corrosion at the joints and transverse cracks, the corrosion in the ECR extended several inches into the concrete adjacent to the joints, there was adhesion loss of the epoxy coating supplying little protection against corrosion, and the leaking environment at the joints and cracks was as severe as a splash zone in a marine location. The report recommended that corrosion resistant reinforcement should be used in concrete decks with construction joints and cracks greater than 0.007 in. and that expansive deck concrete should be used in closure pour locations to minimize shrinkage. The report also recommended that closure pour joints should be placed directly over girders to provide support to the joint and eliminate shear force in the transverse reinforcing steel.

1.3 Objective and Scope of Research

It was clear from the initial investigation that some of the bars across the closure pour construction joints had suffered significant section loss to corrosion. The combination of the smooth vertical concrete joint and joint opening due to shrinkage created a condition where most of the shear across the joints was carried by the reinforcing steel. Section loss in some of the bars transfer additional shear to the undamaged bars and elevate the shear stress in the corroded bars. Some of the bars at the failure surface appeared to have experienced a shear-type failure with little or no section loss due to corrosion. It could not be determined if the failure mode of the bars was a strength failure or a fatigue failure from visual inspection. The section loss in the surrounding bars can be expected to elevate both the maximum shear stress and the cyclic stress range in the undamaged bars. The fact that there is little necking or distortion of the bar cross section at the failure location tends to favor the fatigue failure assumption. The location of the closure pour under the wheel path of trucks on the bridge caused a high number of load cycles during the17 years of service.

The main objectives of this research investigation are to develop a deeper understanding of the failure mechanism of the I-81 closure pour; develop inspection procedures for Virginia Department of Transportation (VDOT) to assess its bridge inventory containing similar closure pour construction joints; and to develop recommendations for future construction of bridge decks with construction joints resistant to this type of failure. The development of inspection procedures is important since there are other bridges in Virginia that have closure pours constructed with similar details. Once the failure is fully understood, the inspection procedures can address the safety concerns that arose from the I-81 deck failure and help prevent and future occurrences.

A total of six slab specimens from the I-81 bridge deck were tested at Virginia Tech, three to determine the static strength and three to determine the fatigue resistance. Both test types were performed in a one-way, three-point loading configuration. In addition, three similar slab sections were cast in the laboratory to serve as control specimens that

have no pre-existing damage. Two of these new specimens were subjected to static strength tests and one to cyclic fatigue testing.

The remaining chapters of this report discuss how the experimental program was developed and implemented and what conclusions were drawn from the results. They are organized in the following way: Chapter 2 is a literature review on fatigue of reinforcing steel in concrete; Chapter 3 discusses the development of the test plan and describes the test specimens, the setup for strength and fatigue tests, the equipment used in testing, and presents a test matrix; Chapter 4 provides the material properties of the slabs and other components, describes the instrumentation and data acquisition, testing procedures, and describes the jacking system implemented for the final two tests; the test results are presented and discussed in Chapter 5 for both strength and fatigue tests; and Chapter 6 summarizes the conclusions and offers recommendations. The appendix chapters are organized as follows: Appendix A presents the plots of the individual tested specimens; Appendix B provides figures of the bridge cross-section and the deck slab sketches with the test specimens' cut location; Appendix C includes the I-81 specimens' dimensions and bar cover depths; Appendix D presents photographs of the failed test specimens with the cracks emphasized; and Appendix E provides detailed calculations that were completed throughout the course of this study.

1.4 Development of Test Plan

In a continuous reinforced concrete beam or slab (without construction joints), the reinforcing bars bond with the surrounding concrete and behave compositely when the system is subjected to bending. The I-81 deck failure occurred at closure pour joints with no shear engagement of the concrete across the joints. This condition causes the steel reinforcement across the joint to behave differently. In addition to axial stress due to slab bending, the bars are subjected to shear and local bending stresses due to shear deformation across the joint. This results in a complicated stress state in the bars consisting of axial stress, local bending stress, and shear stress. The closure pour joints were formed and cast with vertical edges without providing any shear engagement

between the concrete on the two sides of the joint. In addition, shrinkage caused the joints to open thereby minimizing frictional contact in the concrete. This joint detail, that forces the reinforcing steel to carry both the moment and shear across the joint, is not typical and no references were found in the literature pertaining to this condition. The I-81 closure pour was located directly in the wheel path of truck traffic and the wheel loads cause cyclic stress in the reinforcing steel. This raises the possibility that fatigue was a contributing factor to the failure. The closure pour failed after 17 years of service and some of the bars were severely corroded at the failure location. However, other bars appeared to have recently failed without significant corrosion. This suggests that both corrosion and fatigue may have been contributing factors.

The direct shear at the construction joints can be estimated from standard wheel loads. However, it is hypothesized that localized concrete crushing at the edge of the joint in contact with the reinforcing bars may have been caused by this direct shear. If so, local bending of the bars in an "S" shape manner would have caused high distortional bending stresses in addition to shear and bending stresses. Figure 1-3 illustrates this scenario. The gray areas are the locations where the local concrete crushing would take place.

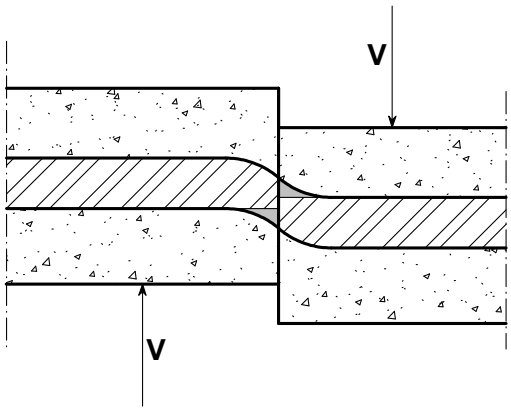

Figure 1-3. Localized Concrete Crushing Will Allow "S" Shaped Local Bending

Visual inspection of the ECR during the preliminary investigation showed that there was damage to the epoxy coat of some of the bars at the joint. It is hypothesized that the aforementioned cyclic local distortional bending along with the debonding of the epoxy coating may have caused a mechanical breakdown of the epoxy coat and further

accelerated corrosion. An interaction between corrosion and fatigue that would cause the bars to deteriorate at a faster rate is also a possibility.

The test plan was developed to test specimens under a loading configuration that approximates the level of shear and moment present across the closure pour joint in the I-81 bridge. Testing of the closure pour joint is complicated since the joint represents a structural discontinuity in the slab. Axial force transfer across the joint occurs through a combination of concrete bearing contact and forces in the reinforcing steel. Shear force transfer occurs through a combination of frictional and interface contact between the two concrete faces and shear force in the rebars. Therefore, analysis of the force transfer mechanism at the joints is a non-linear problem that is dependent on the joint opening gap and the level of axial force across the joint.

No guidance could be found in the literature on testing of joints similar to those in the I-81 bridge. Lacking any guidance on testing protocols, the initial tests were conducted to simulate the moment and shear loads across the joint that are present in the I-81 bridge. When the slab sections were cut and removed from the bridge it released any axial forces that might have been present due to shrinkage and constraint. It became apparent after the initial testing that the gap openness and axial force have a significant effect of behavior. Therefore, the experimental procedures were altered on the final two tests to jack open the joints prior to testing with an external jacking system. In retrospect, it would have been preferable to conduct more replicate tests with the external jacking system. However, this realization only came after analyzing the results from the early tests.

CHAPTER 2: LITERATURE REVIEW

2.1 Review of Fatigue

Structural engineering elements can be subjected to different types of cyclic loadings that if magnitude and frequency are sufficient, can greatly decrease the element's service life and ultimately lead to failure. The stresses caused by these loadings are usually much lower than the ultimate and yield strength of the structural element. Microscopic physical damage can result from the repeated application of these stresses, and continue to accumulate until a crack or other types of macroscopic damage develops. This process and the resulting failure due to repeated loading is called fatigue (Dowling, 2007). A common case of fatigue loading is in bridge decks where the trucks passing over the bridge are the main source of loading. Fatigue failure of the bridge deck reinforcing steel in service has not been documented in continuous bridge decks. However, these observations do not necessarily apply to the unique conditions existing in the closure pour construction joint in the I-81 bridge.

The stress-based approach for fatigue analysis presented by Dowling is considered in this study. In this approach, the nominal (or average) stresses in the critical region of the element under fatigue loading are the basis for analysis. Considering mean stress and adjusting for stress raisers leads to the determination of the nominal stress range that is resisted under repeated loading.

Cyclic stresses are often characterized by the stress range, $\Delta\sigma$, or the difference between the maximum and minimum stresses that result from cyclic loading. Moreover, the stress amplitude, σ_a, is defined as half the stress range and the mean stress, σ_m, is defined as the average of the maximum and minimum stresses. The results from fatigue tests at different stress ranges can be combined in a stress-life curve, or S-N curve. A form of stress (stress range, amplitude of stress, or nominal stress) is plotted on the y-axis and the number of cycles to failure is plotted on the x-axis. Each test represents a point on the S-N curve. If enough test points are included, the full S-N curve for a material under a specific fatigue loading condition—usually uniaxial—can be constructed. Generally, for materials such

as reinforcing steel, the S-N plot shows that number of cycles to failure decreases as the stress range increases. However, there is a stress range level where failure rarely occurs and the fatigue life is said to be virtually infinite. This lower bound stress range level is called the endurance limit or fatigue threshold. The number of cycles to failure is usually plotted on logarithmic scale since it changes rapidly with stress range level and could span over several orders of magnitude. Figure 2-1 shows the S-N plot of concrete reinforcing steel from a single manufacturer. Wight and MacGregor present this plot based on an investigation on the fatigue of reinforcing bars (Helgason and Hanson, 1974). The statistically-determined tolerance limits for the data are shown on plot, with the lower limit being critical for design.

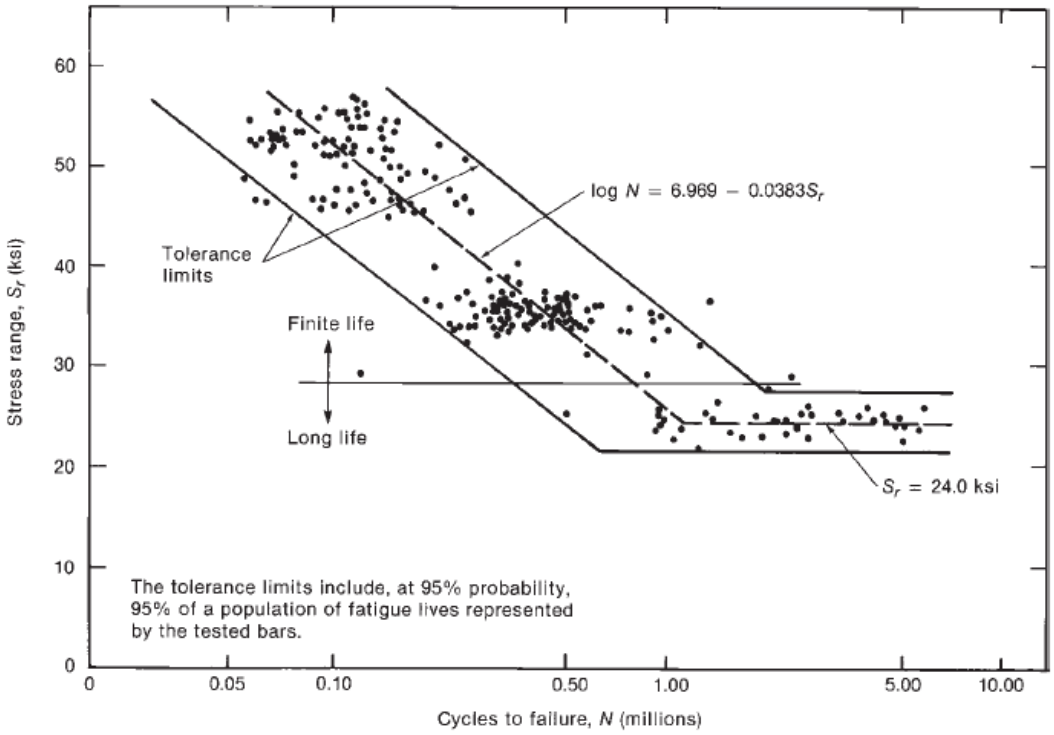

Figure 2-1. S-N Plot of Tests Conducted on Steel Reinforcing Bars (Wight and MacGregor, 2009)

Most of the literature on the fatigue of reinforcing steel presents the results of uniaxial testing (tensile and compressive stresses applied in the longitudinal direction). The reinforcing steel across the open construction joints on the I-81 closure pour were subjected to more complicated loading conditions consisting of direct shear, localized bending distortion, and tension from the global bending of the slab. Dowling presents an

approach for the analysis of elements subjected to multiaxial fatigue. For the case of ductile materials where the cyclic loads are completely reversed, have the same frequency, and are in-phase or 180 degrees out-of-phase, he argues it is reasonable that the fatigue life of the element is governed by the amplitude of the octahedral shear stress. A similar relationship to that used for the octahedral shear yield criterion was used to formulate the following equation for the effective stress amplitude:

$$\bar{\sigma}_a = \frac{1}{\sqrt{2}}\sqrt{(\sigma_{1a} - \sigma_{2a})^2 + (\sigma_{2a} - \sigma_{3a})^2 + (\sigma_{3a} - \sigma_{1a})^2} \tag{2-1}$$

Here, σ_{1a}, σ_{2a}, and σ_{3a} are the amplitudes of the principal stresses. When using Equation 2-1, in-phase amplitudes are considered positive and 180 degrees out-of-phase are considered negative.

If non-cyclic loads are present in addition to the cyclic loads, the aforementioned relationship is not fully effective. Dowling approaches this case by assuming that the mean stress variable and the hydrostatic stress value are proportional. From the mean stresses in the principle directions, the effective mean stress is taken as:

$$\bar{\sigma}_m = \sigma_{1m} + \sigma_{2m} + \sigma_{3m} \tag{2-2}$$

The effective stress amplitude and mean values can be calculated from the amplitude and mean values of the stress components for any coordinate axes, using stress invariants. The resulting expressions for amplitude and mean stresses are as follows:

$$\bar{\sigma}_a = \frac{1}{\sqrt{2}}\sqrt{(\sigma_{xa} - \sigma_{ya})^2 + (\sigma_{ya} - \sigma_{za})^2 + (\sigma_{za} - \sigma_{xa})^2 + 6(\tau_{xya}^2 + \tau_{yza}^2 + \tau_{zxa}^2)} \tag{2-3}$$

$$\bar{\sigma}_m = \sigma_{xm} + \sigma_{ym} + \sigma_{zm} \tag{2-4}$$

These two stresses, along with the material-specific empirical constant, σ'_f (often approximately equal to the pure tensile true fracture strength), can be amalgamated into an equivalent completely reversed uniaxial stress:

$$\sigma_{ar} = \frac{\overline{\sigma}_a}{1 - \frac{\overline{\sigma}_m}{\sigma'_f}} \tag{2-5}$$

The stress value given by Equation 2-5 can be used to compare with the completely reversed S-N curve of a material in a uniaxial stress cyclic loading.

2.2 Fatigue of Reinforcing Steel

Under ordinary conditions, there have not been any reported fatigue failures of reinforcing bars in service (Helgason, et al., 1976). The reason for this is because the stress range in bars in bridge decks is less than the fatigue threshold of steel rebars (presented later in this section). A closure pour scenario, such as the I-81 bridge, presents an unusual condition due to the presents of the construction joints without a shear key engagement. This research study attempts to relate the bar stress range of the test specimens to the results from previous research investigations.

Several research investigations have been conducted on the fatigue behavior of reinforcing steel. However, none were identified where the bars were in a similar multiaxial cyclic loading condition as the bars in this study. The majority of the investigations tested reinforcing steel bars under a uniaxial (tensile) cyclic loading. The remainder of this section summarizes the findings of investigations with such loading conditions.

A major investigation completed by the Portland Cement Association (PCA) and sponsored by the National Cooperative Highway Research Program (NCHRP) was carried out in an effort to establish the fatigue strength of deformed bars and produce design guidelines based on a statistical analysis. The test program, a review of literature, test results, and final conclusions and recommendations were thoroughly presented by Helgason et al. (1976). In all tests, a single reinforcing steel bar from American manufacturers was longitudinally encased in a rectangular or T-shaped concrete beam as the main reinforcement. Proper shear reinforcement was provided and a crack former was

included at midspan. The test setup consisted of a four-point loading configuration in which the ends were simply supported and loading ram(s) applied load at third points of the beam span to maintain a constant moment in the central region. The cyclic load was applied in sinusoidal manner at the nominal rates of 250 or 500 cycles/min.

A total of 353 tested were performed in which the major test variables considered included stress range, minimum stress, bar deformation geometry, bar grade (Gr. 40, 60, and 75), bar size (No. 5, 6, 8, 10, and 11), and effective beam depth (6, 10, and 18 in.). The authors observed that the predominant variable influencing rebar fatigue strength was the stress range of the applied load. They also found that: increasing the minimum stress while keeping the stress range constant, reduces the fatigue strength; bars with larger diameters have lower fatigue strength than those with smaller diameters; higher grades of reinforcing steel have a higher fatigue strength; and that embedded manufacturer's labels and transverse lugs cause concentration of stresses at juncture with the bar's barrel. Furthermore, the fatigue strength was affected by the ratio of the radius of the lug's base to its height (r/h).

The lowest stress range that resulted from testing was 21.3 ksi (fatigue threshold for reinforcing bars), which corresponded to a Grade 60 No. 11 bar with a minimum stress of 17.5 ksi (tension) and 1,250,000 cycles at failure. A lower bound two-part curve was formulated for design from a statistical analysis of entire set of tests.

$$\log N = 6.1044 - 0.0407 f_r - 0.0138 f_{\min} + 0.0071 f_u - 0.0566 A_s + 0.3233 D(r/h) \quad (2\text{-}6)$$

$$f_r = 21 - 0.33 f_{\min} + 8(r/h) \quad (2\text{-}7)$$

Where:

f_r = stress range, ksi
$f_{\min}$ = corresponding minimum tensile (positive) or maximum compressive (negative) stress, ksi
(r/h) = ratio of lug base radius to height
$\log N$ = base 10 logarithm of the number of cycles to failure
f_u = tensile strength of bar, ksi
A_s = nominal area of bar, in^2

D = nominal bar diameter, in.

Equation 2-6 corresponds to fatigue lives between 10,000 and 1 million cycles and Equation 2-7 corresponds to those above 1 million cycles (Rabbat and Corley, 1984). When the r/h ratio is not known, it is recommended that a value of 0.3 be used. Several codes and design guides have adopted Equation 2-7, or a similar form, as the limiting specification for design (Corley, et al., 1978). Figure 2-2 shows an S-N plot of the NCHRP test results (unlabeled points) and the long-time test results (numerically labeled) added by Rabbat and Corley (1984). Here, the curve label "Equation 2" corresponds to Equation 2-6 and the curve labeled "Equation 1" corresponds to Equation 2-7. The purpose of Rabbat and Corley's investigation was to verify that the validity of Equation 2-7 at higher number of cycles since the NCHRP tests were stopped after the specimens reached 5 million loading cycles. For the six tests performed, Grade 60 No. 8 bars were used from 5 different manufacturers, and with a stress range varying from 24.8 to 26.5 ksi. These bars were left over from the NCHRP investigation, so their characteristics were already well-documented.

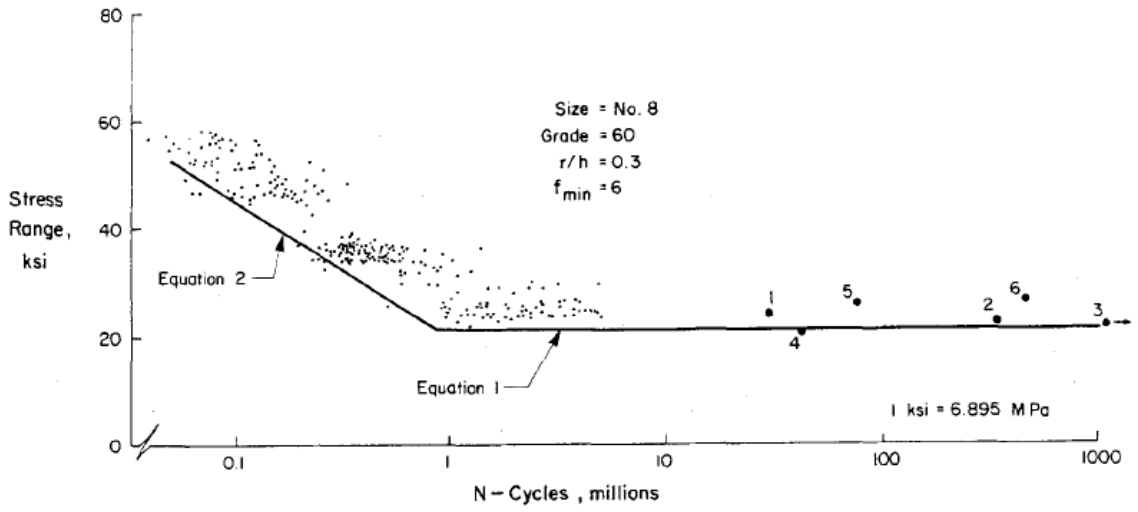

Figure 2-2. Fatigue Test Results with Lower Bound Equations (Rabbat and Corley, 1984)

The most common bar size that was used in the NCHRP study, as well as other reinforcing steel fatigue studies, is No. 8. The former reported that for No. 8 Grade 60 bars from five American manufacturers and a minimum tensile stress of 6 ksi, the fatigue

limit ranged from 23.0 to 28.5 ksi. For the current I-81 closure pour investigation, No. 5 Grade 60 bars were used on the actual bridge deck and on the laboratory cast specimens. Therefore, the endurance limit of No. 5 Grade 60 becomes an obvious target. A study was conducted that relates the stress range of different size bars (MacGregor, et al., 1971).Since the NCHRP did not outline a specific endurance limit for No. 5 Grade 60 (not critical for the formulation of the design equation), the work of MacGregor et al can be extrapolated to attain an estimate. In their study, they tested bars varying in size (No. 5, 8, and 11) and Grade (40, 60, 75). Other variables were present, such as stress concentration factors due to transverse lugs, beam depth, minimum stress level (about 0.1 of yield strength), and concrete strength. Their results show that the fatigue strength (at 2 or 5 million cycles) of No. 5 Grade 60 bars is about 1.08 relative to that of No. 8 Grade 60 bars. Considering this relationship, the fatigue limit (at 2 or 5 million cycles) of No. 5 Grade 60 bars ranges from 24.8 to 30.8 ksi.

In ductile materials a process called damage intensification occurs during cyclic loading which eventually leads to failure. This process starts at a microscopic level where slip bands, or regions with high deformation due to shearing between crystal planes, are developed by crystal grains with a relatively unfavorable orientation to the applied stress. Some slip bands develop into cracks within the grains which spread and join other similar cracks forming a larger crack that induces failure (Dowling, 2007). Fatigue failure results when the fatigue crack grows under cyclic loading to the extent where the net section fails due to the overload. Looking at the cross section of the failed crack surface, the area adjacent to the initiation point (focal point) of the crack is relatively smooth in texture, while the overload region is rough and forms a shear lip oriented approximately 45 degrees to the applied stress.

In the NCHRP investigation, it was observed that all fatigue cracks initiated at the base of a transverse lug or at a manufacturer's identification mark. The role of these geometric deformations in creating stress concentrations is evident. Most specimens had a single crack focal point, but a few had developed a second. As expected, the region of the crack adjacent to the focal point had a smooth texture, while the tensile overload region had a rougher texture. Figure 2-3 shows a fracture face of one of the test specimens oriented the

same way when embedded in the beam for testing. The described fracture face texture is clear and the focal point is at the location of a transverse lug.

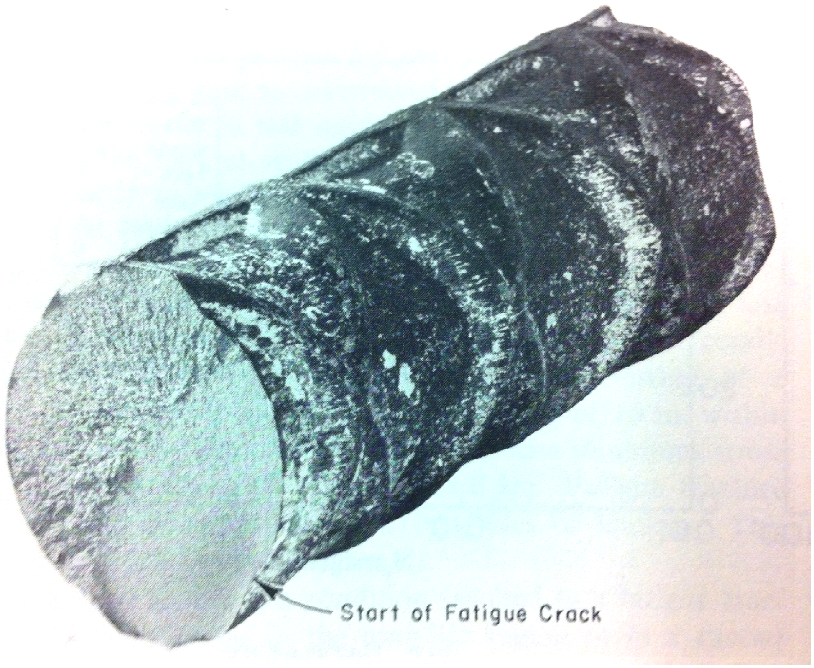

Figure 2-3. Fracture Face of Fatigue-Failed Test Bar (Helgason, et al., 1976)

CHAPTER 3: DEVELOPMENT OF EXPERIMENTAL PROGRAM

3.1 Test Specimens

The goal of this experimental program is to identify the actual failure mechanism that occurred on the I-81 closure pour. A total of nine test specimens were tested; six were cut from salvaged sections of the actual bridge slab and three were cast new in the laboratory. Four of the specimens were tested under cyclic fatigue loading and five were tested under static loading to determine the ultimate strength and failure mode. Three slab specimens from the actual bridge deck were fatigue tested using a three point loading setup, which is described in more detail in the upcoming sections. One of the new cast specimens was also tested under cyclic loading, but the test setup was altered to open up the joint as discussed in Section 3.4. In addition, three slab specimens from I-81 and two new cast specimens were subjected to strength tests using the same three-point loading setup. The following two sections will discuss the I-81 and new cast specimens in more detail.

3.1.1 I-81 Specimens

When the closure pour was being repaired, four large sections of the deck (including the 3-ft closure pour) were saw cut out of the bridge and sent to the Thomas M. Murray Structures and Materials Research Laboratory at Virginia Tech for assessment and testing. The condition of the slabs was assessed both visually and using a variety of non-destructive evaluation techniques to detect internal corrosion of the reinforcing steel. After the initial investigation, the slabs were cut into smaller strips for the structural fatigue and strength tests. A total of eight test specimens were cut from the four large slab sections that were removed from the I-81 southbound deck. The resulting specimens were about 22 in. wide and 54 in. long with the depth equal to the full 9 in. bridge deck thickness. Each specimen has two closure pour joints transversely located along the length about 9 in. from each end. There were slight dimensional differences due to construction tolerances and cutting precision. Figure 3-1 shows the 3-ft closure pour section located in the center with about 9 in. of adjacent slab on each side. The figures in Appendix B indicate the exact location of the eight specimens in the four original slabs.

Figure 3-1. Typical Specimens Cut From the I-81 Bridge Deck

The 9-in. end portions of the deck slab are too short to fully develop the reinforcing bars to reach the flexural capacity of the specimen. Although the moment at the joint location is not expected to reach the flexural capacity during testing, there was still concern that the reinforcing bars might slip jeopardizing the results of the tests. Ordinary measures to splice additional length to the bars were rejected since this would have required excavating around the ends of the reinforcing bars. This might have damaged the end blocks and altered the conditions at the closure pour joints. Instead, the ends of the reinforcing steel bars were capped with ¼-20 bolts and fender washers. Before tightening the bolts, epoxy was applied to ensure uniform bearing on the concrete. While this did not necessarily eliminate the problem, it enhanced the development length and reduced the chance of the bars slipping during testing.

3.1.2 New Cast Specimens

Three new slab specimens were constructed in the laboratory to closely match the actual conditions in the I-81 closure pour. The new slab specimens are intended to serve as undamaged controls for both the strength and fatigue tests. Before testing the specimens, however, shrinkage and rate of corrosion were closely monitored as the concrete aged for

a parallel study focusing on shrinkage and corrosion within the overall investigation (Abbas, 2011). The main difference between the new slabs and the I-81 specimens is the end sections were longer to avoid the aforementioned development length concerns. Therefore, the total length of the specimens is 104 in., opposed to the 54-in. length of the I-81 specimens. The other two dimensions are essentially the same with an 8 ½-in. thickness and 22-in. width. Both the new specimens and the I-81 specimens were tested with roller supports at the same locations; hence the longer end sections did not alter the testing conditions.

The casting sequence for the new specimens simulated the construction sequence used for the I-81 deck. The 3 ft. closure pour strip in the I-81 deck was located at midspan between two of the longitudinal steel beams 8 ft. on center. There was no structural support directly underneath the closure pour joints. The main sections of the bridge deck were cast first and allowed to cure before placement of the closure pour. When the closure pour was placed, the two deck sections served as rigid boundary conditions to constrain shrinkage across the closure pour. As the closure pour concrete shrank during curing, it thus tended to open the closure pour gap and introduce stress in the reinforcing steel.

To simulate this construction sequence, the two end sections of the new specimens were formed and compositely connected to two beams, 8 ft apart, which were bolt-connected to the structural floor. The two end sections were allowed to cure before casting the center closure pour section. Therefore, the casting setup was designed so that the ends were restrained to the supporting steel beams. The end sections were compositely connected to the support beams in two ways: the ends of the specimens were bolted to the supporting beams, and shear studs were incorporated at the end region. The bolted end can be seen in Figure 3-2.

To simulate the staged construction conducted in the placement of the I-81 closure pour, the concrete for the specimens was poured 30 days apart. The two end sections of the specimens were placed first, followed by the middle portion (closure pour). Figure 3-2 shows the formwork used to cast the end sections. The epoxy coated reinforcing bars

were placed in the same configuration present in the I-81 deck. Figure 3-3 shows the reinforcing steel and formwork before the first placement of concrete. Figures 3-4 and 3-5 show the formwork setup just prior to the second concrete placement 30 days after the first placement. Removal of the end forms from the first placement left a vertical smooth face on the two end sections that served as the form for the second placement. The resulting joint does not provide any shear connection between the concrete on either side.

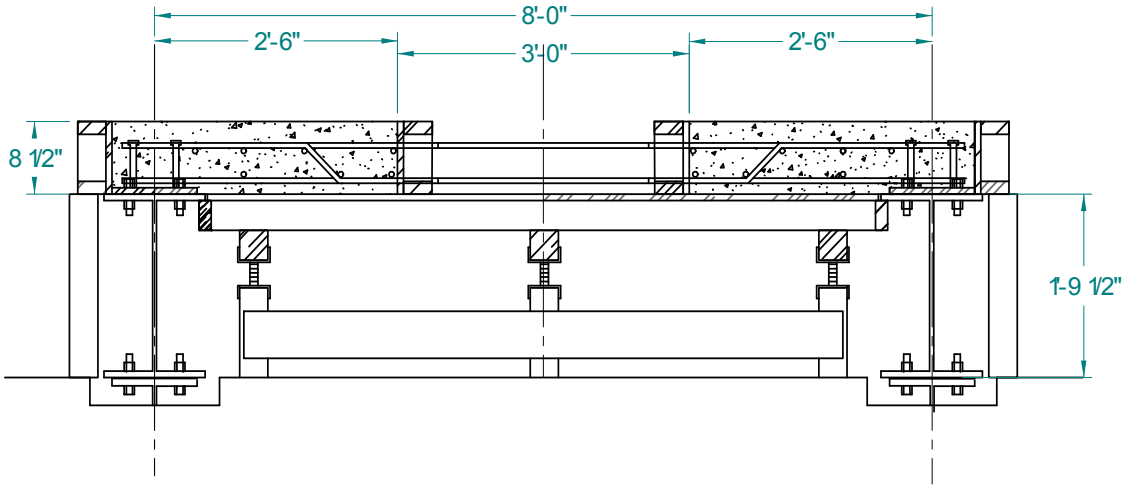

Figure 3-2. Setup of First Concrete Placement

Figure 3-3. Formwork of Cast Slabs with Reinforcing Steel in Place

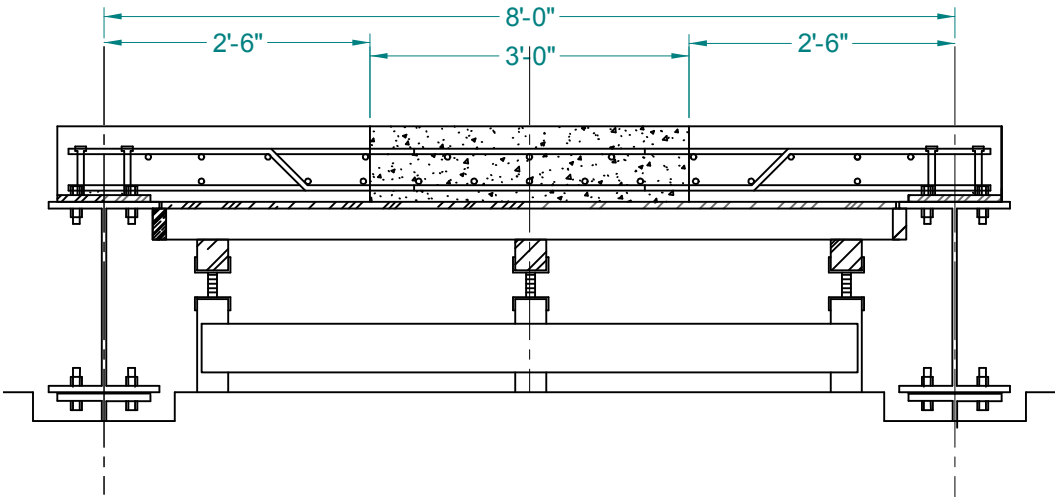

Figure 3-4. Setup of Second Concrete Placement

Figure 3-5. Closure Pour Section Prior to Second Concrete Placement

3.2 Overview of Test Setup

A three-point loading configuration was used for all tests to simulate the effect of a wheel load on the center of the closure pour. With the specimens simply supported at the ends, as shown in Figure 3-6, the loading configuration induces one-way bending in a strip of the deck slab. Positioning the supports for the simple-span specimens at 4 ft, closely replicated the moment and shear across the closure pour joint in the continuous-span slab present in the I-81 deck. This can be observed in Figure 3-7; the shear and moment that would be expected in a transverse continuous slab with a wheel load at the center are simulated by supporting the specimens at 4 ft on center.

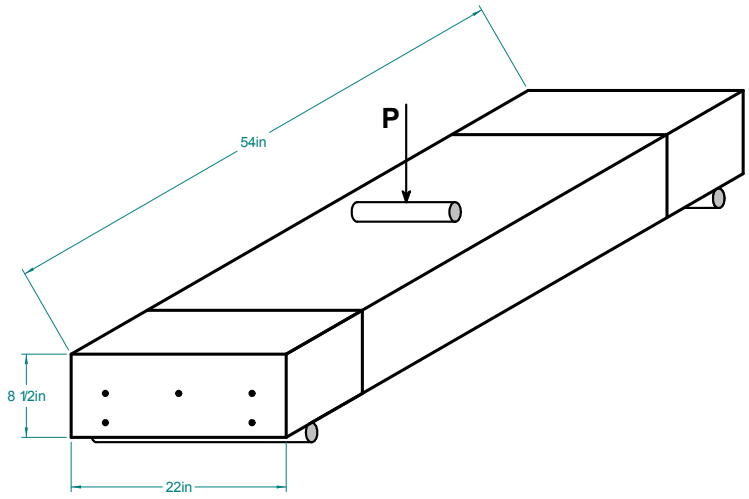

Figure 3-6. Transverse Section of the Closure Pour Slab Tested in One-Way Bending

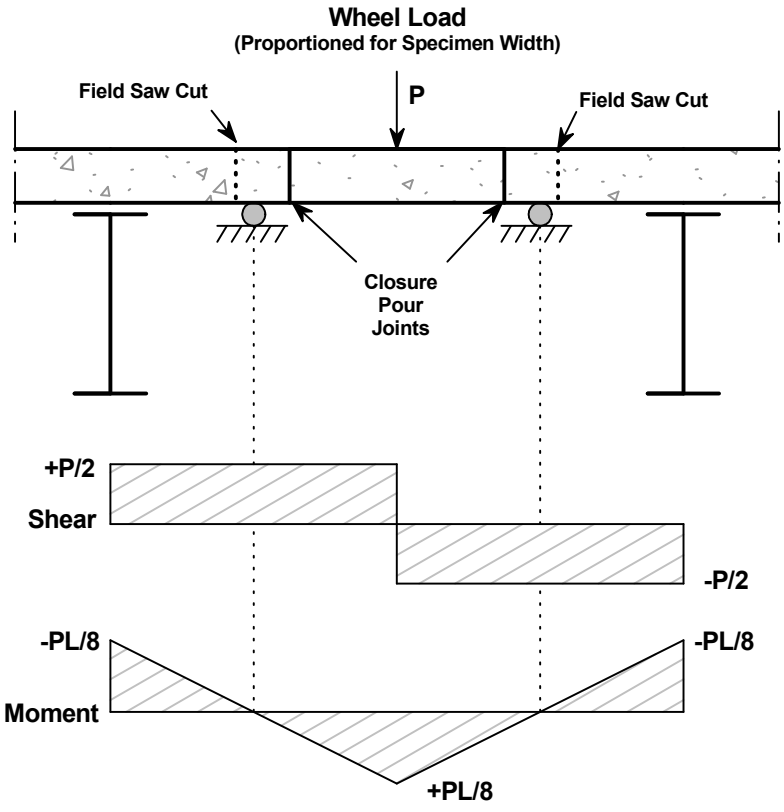

Figure 3-7. Test Conditions Designed to Simulate the Moment and Shear on the I-81 Bridge

The actual load applied to a bridge deck by a truck's wheel is a pressure area instead of a point load. Application of a point load directly to concrete could cause local crushing if the load's magnitude is high enough. A 20-in. by 10-in. elastomeric pad was used in series with a load spreading device to simulate the contact pattern of a tandem truck wheel on the bridge deck. This is the wheel load patch used for evaluation of local deck loading specified in the AASHTO LRFD Bridge Design Specifications (AASHTO, 2010). Figure 3-8 shows a the idealize test setup which includes simple supports and the load actuator with the tire contact area pad.

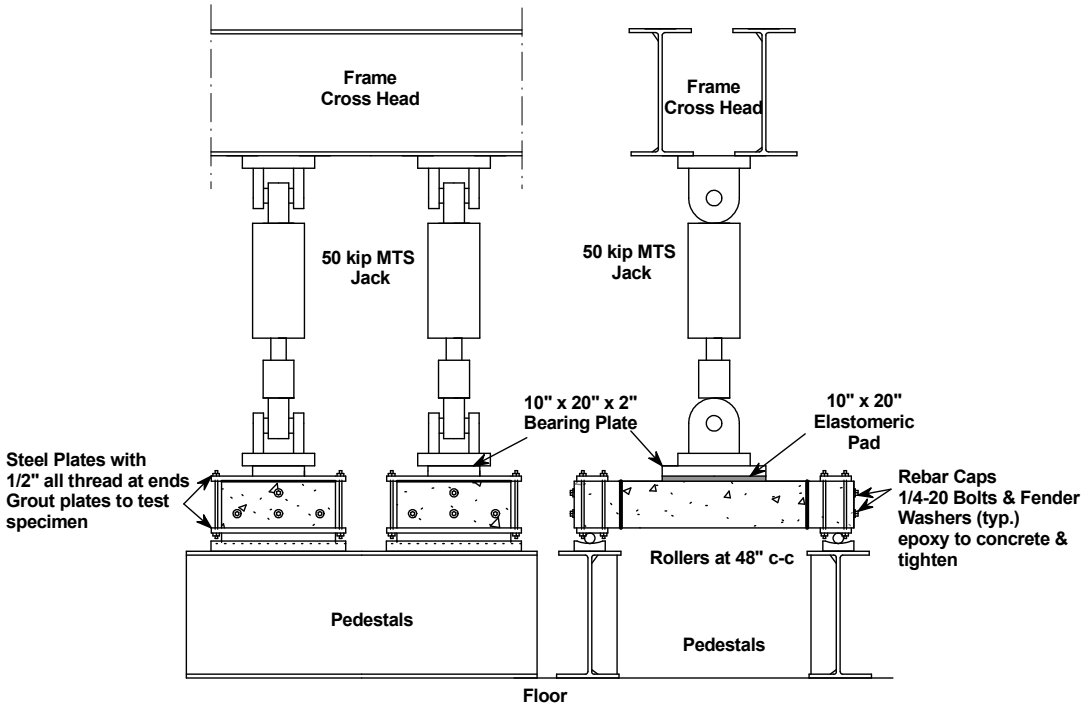

Figure 3-8. Idealized Setup for Fatigue and Strength Tests

3.2.1 Fatigue Test Setup

The three-point loading fatigue tests were setup as shown in Figure 3-8. Steel bearing plates were attached to the specimens at the support roller locations to prevent local crushing of the specimens under direct contact with the supports. A thin layer of grout

was applied between the specimens and the bearing plate to even out slab imperfections and ensure uniform contact pressure along the length of the rollers. Once the steel plates were attached to the specimens, the specimens were placed on roller supports resting on alignment pedestals consisting of stiffened steel I-beams. The pedestals were bolted to the strong floor of the laboratory. A MTS hydraulic actuator was attached to a cross head frame that spanned transversely over the specimens. The cross head was part of a frame system assembled with A325 bolts and fixed to the laboratory floor. The entire setup was assembled prior to loading is shown in Figure 3-9. Two parallel setups were utilized to enable two simultaneous fatigue tests. The wooden struts shown were to prevent the actuators from kicking out laterally or pushing the specimens to the sides during loading.

The major difference between the actual setup shown in Figure 3-9 and the original idealized setup from Figure 3-8 is that a stiffened steel I-section was used to spread the jack load over the wheel patch area. This I-section was bolted in series to the MTS actuator and used as an extension since the actuator could not extend down to the top surface of the specimens. During loading, it was in direct contact with the elastomeric pad.

Figure 3-9. Complete Setup for Fatigue Loading

3.2.2 Strength Test Setup

The strength tests could not be performed at the same location as the fatigue tests since the required loads exceed the MTS actuator capacity. Therefore, a slightly different setup was used for the strength tests. The setup was essentially the same as the fatigue tests with a different loading actuator. Figure 3-10 shows the strength test setup. Since strength tests are relatively short in duration compared to fatigue tests, there was no need to assemble two simultaneous testing setups. The same roller supports were used as well as the same type of frame assembly and I-section pedestals.

Figure 3-10. Complete Setup for Strength Tests

The static actuator was a manually controlled Enerpac hydraulic ram with a load cell placed in series with the actuator. The same I-section was used to apply the wheel load to the specimens through the elastomeric pad.

3.3 Test Equipment

This section describes the equipment used for both test setups in detail. It includes the supports, end constraining plates, the I-section used in loading the specimens, and the hydraulic actuators used for both tests.

3.3.1 Roller Supports and End Constraining Plate

The supports used in all the tests were of the roller type, shown in Figure 3-11. These had been previously assembled in the laboratory for general lab use. A 4-in. diameter steel bar (32-in. length) sits on a semicircular steel cradle welded to a 5-in. channel-section base. The steel bar and semicircular plates were greased to reduce friction.

Figure 3-11. Roller-Type Support Used for all Tests

As previously mentioned, the slab specimens were not in direct contact with the roller supports. The concrete end blocks were sandwiched between two steel plates and clamped with four steel rods at the corners. The was done for two reasons: 1) to provide a bearing plate to prevent concrete crushing under direct contact with the roller; and 2) to add some additional constraint to the end block to help prevent cracking that might affect development length. The plates used were 7 in. by 30 in. by ½ in. and four ½-in. rods were used to align the plates and hold them together. Figure 3-12 shows the entire assembly in place with the grout layer between the specimen and the bottom plate. The rods were welded to the bottom plate and fastened to the top plate with nuts and washers. To stiffen the top plate and prevent bending from tightening the nuts, a channel section was welded to the top plate. There were a total of four plate assemblies constructed. Two used channel sections for plate stiffness and two used angle sections.

Figure 3-12. Steel Plate Assembly at Support Locations with Grout Layer

3.3.2 Loading I-Section

Since the stroke extension of both actuators (MTS and Enerpac) was not sufficient to make direct contact with the specimens, a 20-in. long W12x87 steel section was used as an extension for all tests. Once centered on top of the elastomeric pad, the actuator applied the load directly to the top of the section. Its weight was accounted for in the data analysis. Figure 3-13 shows the section with four ½-in. plates (two shown) that were welded to the web and flanges for stiffness purposes.

Figure 3-13. Stiffened W12x87 Section Used as Loading Extension

3.3.3 Hydraulic Actuators

Two 55-kip MTS hydraulic actuators were used for the fatigue tests. Both are a 244.31 model and have dynamic and static stroke limits of 6.0-in.and 6.4-in., respectively. They are each computer-controlled through an MTS 407 Controller. The load control setting was used instead of stroke control to keep the load constant if the specimen stiffness decreases during testing. The 3,000 psi MTS hydraulic pump (hydraulic power supply) was also controlled with the 407 controller. The actuators have built-in force and displacement transducers that are calibrated to provide direct readout on the 407 Controller.

A 200-ton RR 200-13 Enerpac actuator was used for the strength tests. It is also a hydraulic-powered actuator, but the loading is controlled manually via a 30,000-series Enerpac 115-volt pump. The ram applies and releases load by extending forward and retracting backwards. An external load cell was used to monitor the applied load. Figure 3-14 shows the MTS and the Enerpac actuators.

Figure 3-14. Actuators Used for Testing (MTS on Left, Enerpac on Right)

3.4 Jacking System Setup

In the initial investigation it was evident the construction joints of the I-81 bridge closure pour were open enough to increase the load on the transverse reinforcing bars and also permit water and chlorides to enter the joint and come in contact with the bars. The joint widths were not measured directly on the bridge before four closure pour sections were cutout and transported to Virginia Tech. It is possible that the slab cutting procedure released constraint across the closure pour thereby allowing the gap to close to some degree. The early test results indicated the amount of openness and constraint across the closure pour joint has a significant effect on the fatigue performance of the test specimen. Fully open joints have all of the shear force resisted by the reinforcing steel while partially closed joints have some of the shear force carried by frictional contact of the concrete. Therefore, it was determined that joint openness has a more significant effect on fatigue performance than originally envisioned. For this reason, the set-up for the final fatigue test on Specimen A was modified to increase the crack opening using an external jacking arrangement. The following sections include a general overview of the jacking system designed to open the joints and detailed description of its components.

The joint width of the I-81 closure joints solely from stresses due to concrete shrinkage was determine to be 0.017 in. using a method similar to a fully restrained concrete member model (Gilbert, 1992). The calculations of the joint widths and stresses due to

shrinkage are detailed in Appendix E. The models presented by Gilbert and in Appendix E are an approximation to the conditions in the I-81 closure pour since they assume a concentric steel area at the slab midspan, thereby not accounting for the eccentricity introduced by the bar layout across the joints.

3.4.1 Overview of Jacking System

The opening of the joints was implemented with the use of two screw jacks, one on each side of the specimens along the long dimension. This is essentially a reverse post-tensioning system that adds tension instead of the usual compression to the specimen. Jacking along the sides prevented the jacking system from interfering with the loading actuators, instrumentation, and roller supports. In addition to the jacks, there were other attachments assembled in the laboratory that formed part of the jacking system. Figure 3-15 shows the entire jacking system setup where a jacking strut is fabricated by attaching the base of a screw jack (with tack welds) to a square HSS section. The jacking strut bears against a steel anchor plate system to transfer force from the strut to the specimen.

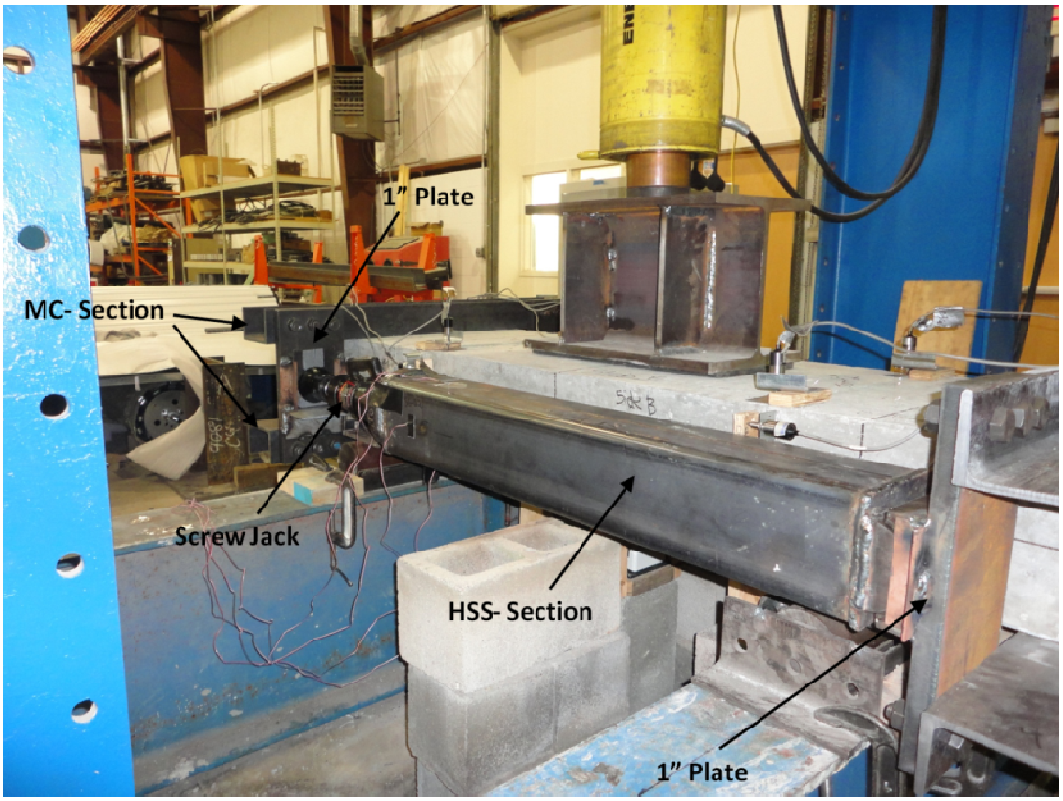

Figure 3-15. Jacking System Set Up with Jacking Struts Bearing Against Steel Plates at Both Ends

Four 42-in. steel MC6x18 (channel-type) sections were attached to the end blocks of the slab specimens, two at each end, one on the top surface and the other at the bottom. They were placed such that the webs were flush to the concrete surface and the flanges stood normal to the surface. They were each attached with five post-installed expansion anchor bolts. The bolts were evenly spaced at 3½ in. on-center and placed along the centerline of the MC sections' webs. The top and bottom MC sections were installed 11 in. from the roller support on center. Therefore, the two MC sections on each end were spaced 70 in. from each other since the supports were spaced at 48 in.

A set of four 1-in. steel plates was bolted to the overhanging portion of the MC sections' flanges; one is shown below in Figure 3-16. Three bolts were used to connect the plates to the top MC section and three were also used to connect to the bottom MC section. These plates served as the contact points for each end of the jacking struts. The screw jacks applied force to the middle of the steel plates, which then transferred the load to the MC sections. Since the MC sections were bolted to the end slab sections, an axial load was applied to the entire specimen through the anchor bolts at the four MC section connections and thus the construction joints were opened.

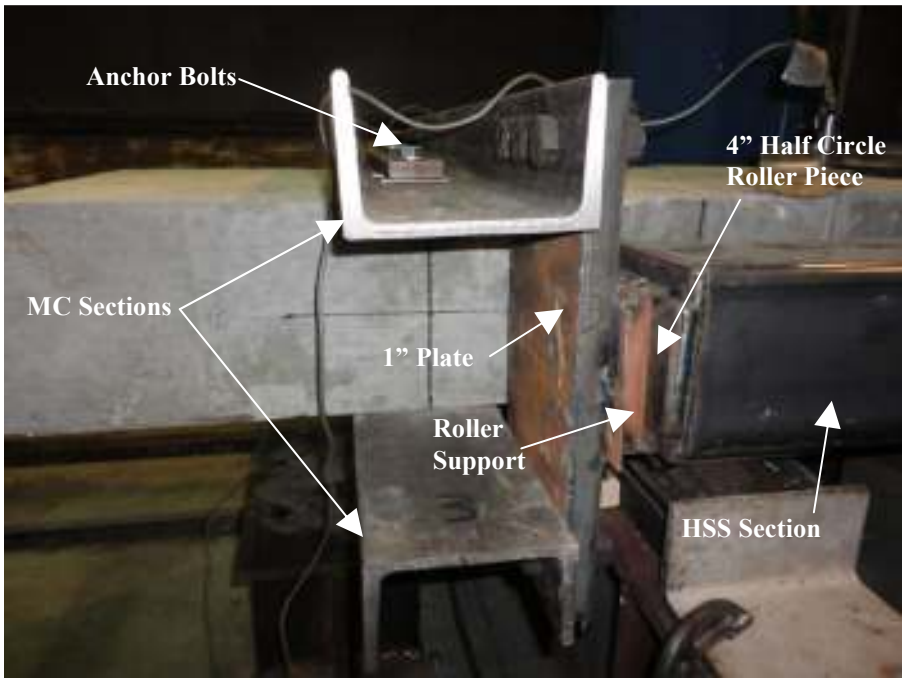

Figure 3-16. Bearing Plates Bolt-Connected to MC Channel Sections

The jacking strut was placed with its centerline axis at the mid-depth of the slab specimens (4.375 in. from the bottom), and it was laterally offset 5.25 in. from the side face of the slab specimens.

Pivot points were added to each end of the jacking strut to allow the strut to remain straight while the concrete specimens bend during testing. A 4-in. diameter steel half circle roller section was welded to the HSS end of the strut. A roller support for the 4-in. roller was attached to the 1-in. plate such that the jacking segment was placed at the intended location (4.375 in. from the bottom and 5.25 in. from the side face of the specimen). The jack screw device has a pivot point at the load pad that allows rotation of the jack end. The attached roller and roller support can be seen in Figure 3-16 above.

3.4.2 Components and Materials of Jacking Setup

As previously described, the jacking struts were fabricated from a commercially available screw jack welded to an HSS steel section. The screw jacks used were 25-ton Torin Big Red jacks, model SJ25. The screw bar allowed overall minimum and maximum heights of 16.625 in. and 26.375 in., respectively. Two 40-in. HSS 6 x 6 x 1/4 sections (grade A-500) were capped with 6 x 6 x ½ in. plates welded to each end to distribute the jacking load. At one end of the HSS segment the screw jack was tack welded to the 6 x 6 in. end plate, and the half circle steel roller (4 in. diameter and 6 in. length) was welded to the other end.

The bearing plates for the jacking struts 7 x 16 x 1 in. grade A514 high strength steel. These were attached to the flanges of the channel sections with ¾-in. A325 bolts. MC 6 x 18 channel sections were bolted across the top and bottom of the slab specimens. As previously mentioned, anchor bolts were used to attach these segments to the slab specimens. The anchor bolts were ¾-in. diameter Power-Bolt mechanical expansion anchors. The total length of each bolt was 4¼ in. and they were installed to the minimum embedment length of 3 in. into the concrete slabs. The installation procedure and capacity check were done according to the manufacturer's specifications. There were a total of five anchor bolts used to attach each of the four MC sections to the concrete specimens. The bolts connecting the top and bottom channels were offset to avoid interference.

3.5 Test Matrix

A total of nine tests were conducted for this research investigation. Table 3-1 displays the specific I-81and cast specimens and their corresponding tests (strength or fatigue) and setup. Here, the basic setup refers the setup described in Section 3.2, while the jacking system setup is described in Section 3.4. Only six of the eight I-81 specimens were used, three were strength tested and three fatigue tested. The specimens that were not used (Specimens 5 and 6) were kept as alternates. One of the cast specimens, Specimen C, was tested with the basic setup, as the I-81 specimens. However, the remaining cast specimens, A and B, were tested with the jacking system setup.

Table 3-1. Test Matrix

	Basic Setup		**Jacking System Setup**	
	I-81 Specimens	New Specimens	I-81 Specimens	New Specimens
Strength Test	Specimen 1 Specimen 3 Specimen 8	Specimen C	-	Specimen B
Fatigue Test	Specimen 2 Specimen 4 Specimen 7	-	-	Specimen A

CHAPTER 4: IMPLEMENTATION OF EXPERIMENTAL PROGRAM

4.1 Material Properties

This section provides the material properties of the I-81 slab concrete as well as the material properties for the cast specimens.

4.1.1 I-81 Specimens

Samples were cored from the four slabs that were cut from the I-81 bridge and delivered to Virginia Tech for the initial investigation. These 17-year-old cores were taken from both the main deck and closure pour portions of the slabs. Following ASTM testing procedures, the compressive strength, modulus of elasticity, and unit weight of the concrete was determined (Abbas, 2011). Table 4-1 displays the properties for the closure pour concrete, and Table 4-2 displays the properties for the main deck concrete. The tensile strength in both tables was determined as the modulus of rupture defined by Section 9.5.2.3 in the ACI 318-08 Code (ACI, 2008).

Table 4-1. I-81 Closure Pour Concrete Material Properties

Concrete Type	Core Number	Compressive Strength (psi)	Modulus of Elasticity (10^6 psi)	Unit Weight (lb/ft^3)	Tensile Strength (psi)
Closure	S1C1	6760	4.26	147.5	617
Closure	S1C2	8510	4.50	147.0	692
Closure	S2C1	7590	4.49	146.4	653
Closure	S2C4	7730	-	146.5	659
Average		**7650**	**4.42**	**146.8**	**655**

Table 4-2. I-81 Bridge Deck Core Properties of Adjacent Slab Portions

Concrete Type	Core Number	Compressive Strength (psi)	Modulus of Elasticity (10^6 psi)	Unit Weight (lb/ft^3)	Tensile Strength (psi)
Deck	S2C2	4620	3.19	142.9	510
Deck	S2C3	6760	4.5	142.9	617
Deck	S2C5	5600	3.58	143.1	561
Average		**5660**	**3.76**	**143.0**	**563**

4.1.2 Cast Specimens

The new specimens were cast with two different concrete placements that were 30 days apart. The first placement was for the outer sections of the specimens (deck), and the second placement was for the center (closure pour) section. The mix design proportions are presented in Table 4-3, while Table 4-4 provides the unit weight, slump, air entrainment and temperature measured from both placements. Cylinder tests were conducted to measure compressive strength, splitting tensile strength, and modulus of elasticity at different concrete age for both placements. The tests were performed at 7, 28, 56, and 90 days in accordance with ASTM C39/C39M-10. The results were averaged and are presented in Table 4-5 and Table 4-6 for the first and second placements, respectively.

Table 4-3. Cast Specimens Mix Design Properties

Material	First Placement		Second Placement	
	Total Batched	Per cy	Total Batched	Per cy
Cement Type I, lbs.	2545	(636)	2535	(634)
Fly Ash, lbs.	635	(159)	665	(166)
Coarse Aggregate, lbs.	7060	(1765)	6980	(1745)
Fine Aggregate, lbs.	3840	(960)	3800	(950)
Water, lbs.	982	(246)	1130	(283)
Total, lbs.	15062	(3766)	15110	(3778)
AEA, fl. oz	6	(1.5)	5	(1.25)
MD W/R, fl. oz	76	(19)	76	(19)
Retarder, fl. oz	63	(16)	63	(16)

Table 4-4. Properties of First and Second Concrete Placements

Properties	First Placement	Second Placement
Unit Weight (lbs./ft^3)	139.5	139.9
Slump (in.)	4.75	5.5
Air Entrainment (%)	4	5.5
Temperature (^{o}F)	70	60

Table 4-5. Concrete Strength Properties of First Placement (Deck)

Age (Days)	Average Compressive Strength (psi)	Average Splitting Tensile Strength (psi)	Average Modulus of Elasticity (x 10^6 psi)
7	5930	610	4.05
14	5920	685	4.46
29	6510	720	4.53
56	6630	740	4.60
90	6650	760	4.58

Table 4-6. Concrete Strength Properties of Second Placement (Closure Pour)

Age (Days)	Average Compressive Strength (psi)	Average Splitting Tensile Strength (psi)	Average Modulus of Elasticity (x 10^6 psi)
7	4930	585	4.90
28	6140	605	5.46
56	6280	645	5.80
90	6400	650	6.11

4.1.3 Reinforcing Steel

The new cast specimens were constructed with the same size and grade of reinforcing steel that was used in the I-81 deck. These were epoxy-coated Grade 60 No. 5 bars whose yield stress was determined to be 67.5 ksi from tensile tests. The purpose of using epoxy coated reinforcing (ECR) in the I-81 deck was to resist corrosion and increase the service life of the reinforcing steel.

4.2 Instrumentation

The instrumentation used in the experimental investigation consisted of load cells, displacement transducers, and unidirectional strain gages. All these instruments were wired to a PC-controlled data acquisition system to provide signal conditioning and processing of the raw data. The acquisition system was a Vishay System 5000 controlled by the StrainSmart 5000 v3.10 software running on a PC with a Windows XP operating system. Each instrument was allotted a separate channel and received an individual assignment for data output. User-defined assignments were also programmed to convert the raw data into engineering units. For example, there were user-defined assignments programmed to calculate the axial load of the jacking segment from the strain gage

readings and HSS section material properties. The data collected from all the assignments in the software was reduced and stored in Excel spreadsheet files.

Three different load cells were used for all tests in the experimental investigation. Two of these load cells were part of the MTS actuator system used for the fatigue tests. These MTS Force Transducer model 661.22C-01 load cells have a 55-kips load capacity and a 2 mV/V nominal output sensitivity at full scale load. The third load cell was used along with the Enerpac actuator for all the strength tests. This load cell is a Transducer Techniques model CLC-100k, which has a 100-kip load capacity and a 2 mV/V nominal output sensitivity.

The two primary types of displacement transducers used were linear variable differential transformers (LVDT's) and wire-type cable-extension position transducers (wire potentiometers). The LVDT's were TransTek model 350-000 transducers with a 6 to 28 VDC excitation, a working range of ±0.05-in., a mechanical travel of 0.16 in., and a non-linearity rating of less than 0.5 percent of full scale. The wire pots were Celesco model PT 101-0010-111-5110 transducers with a full stroke range of 10 in., a 2 mV/V full scale output, an accuracy rating of 0.15 percent of full scale, and a life cycle of 500,000.

A unidirectional strain gage was mounted on each face of the HSS members used for the jacking struts (four per member). The strain readings from the four strain gages were averaged to cancel out any bending and the axial strut force was calculated based on a cross-sectional area of 5.24 in^2 and an elastic modulus of 29,700 ksi. Micro-Measurements C2A-13-250LW-350 universal general purpose strain gages were used. These have a grid resistance of 350 ohms and a gage factor of 2.13. In addition, for the three I-81 specimens' fatigue tests, demountable mechanical strain gages (DEMEC gage) were used to measure the closure pour joint opening at the side edges of the test specimens. These gages do not involve wiring since the readings are taken manually from DEMEC reference points placed on opposite sides of the joint.

There were a total of six LVDT's used for the I-81 specimens' strength tests (Specimens 1, 3, and 8). Two LVDT's measured the differential vertical displacement (shear displacement) occurring across each of the two joints, the other two were placed in

contact with the central bottom bar at each end of the specimen to monitor bar slippage. Also, one wire potentiometer measured the midspan vertical deflection at the bottom of the specimen. A 100-kip load cell directly measured the applied load. The same instrumentation setup was utilized for the first cast specimen test (Specimen C), with the exception that the two LVDT's used to monitor bar slippage were omitted. The addition length of the end blocks provided sufficient development length to fully develop the strength of the reinforcing bars. The strength test with the jacking system setup (Specimen B) used an additional eight LVDT's (twelve total); four per joint, to measure the horizontal joint displacement across the closure pour joints. Four were placed on each side face of the test specimens, two across the top of the joints and two across the bottom of the joints. In addition to the midspan wire pot, four additional wire pots were added along the specimen centerline of Specimen B to measure the deflected shape based on five points.

The same instrumentation setup used for the I-81 specimen strength tests was used in the I-81 slab fatigue tests, expect the MTS 55 kip load cell was used. However, there was a slightly different instrumentation configuration for the fatigue test of the cast specimen with the jacking system setup (Specimen A). For this test, four LVDT's measured the vertical joint displacement (two at each joint) and four LVDT's measured the horizontal joint displacement at one of the two joints. One wire pot was used at midspan to measure the vertical deflection.

4.3 Testing Procedures

This section describes the procedures conducted during the fatigue and strength tests and during the opening of the joints with the jacking system prior to testing.

4.3.1 Fatigue Tests

The same general procedure was followed for all of the fatigue tests. The only difference was for testing of Specimen A and Specimen 4. Prior to fatigue loading, Specimen A was

subjected to an axial force using an external jacking system to open the construction joint. This insured that there was no contact between concrete on either side of the joint. Therefore, the reinforcing bars are the sole carriers of shear and moment across the joint. With the exception of the pre-test jacking of Specimen A, the other test procedures were the same.

The cyclic load used for fatigue loading was originally selected to produce a realistic effect compared to wheel loads on the I-81 deck in service. The test specimens are cut out and tested under one-way bending opposed to the two-way plate bending in the I-81 deck. Therefore the loads were proportioned to approximately account for this effect. The baseline load for the I-81 deck was assumed to be a single AASHTO design truck wheel load of 16 kips (AASHTO, 2010). Using the provisions in Table 4.6.2.1.3-1 of the AASHTO LRFD Bridge Design Specifications, the wheel load is distributed over an equivalent 72 in. interior strip (see calculations in Appendix E). Using the ratio of the slab specimen width to the equivalent strip width (22 in. versus 72 in.), the wheel load can be scaled down to about 5 kips for the test specimens. However, for testing purposes, the load range was increased to half the AASHTO wheel load, or 8 kips. The intent of the increase was to accelerate testing and obtain fatigue failure at a practical number of load cycles. There is little basis in the literature upon which to base this decision, therefore it reflects the judgment of the research team. Specimen 4 was the first specimen tested at the 8 kip load range, but no fatigue failure was observed after 10 million loading cycles. This suggested that the wheel load needed to be further increased to trigger failure. Therefore, it was decided to increase the load range to a full wheel load (16 kips) for the remaining fatigue tests (Specimens 2, 7, and A). It is recognized that this load range is probably higher than the actual loads occurring in the I-81 bridge.

The procedure carried out for testing is as follows: First, the specimen was marked, grouted, aligned and placed in position on top of the roller supports with the MTS actuator directly over the center of the specimen. The top end constraint plates were then secured to the top of the specimen at each end. The instrumentation (LVDT's and midspan wire potentiometer) was then installed and tested to ensure proper operation. Before subjecting the specimen to cyclic loading, an elastic static test was run where the

specimen was slowly loaded and unloaded between 0 and 16.5 kips (8.5 kips for Specimen 4). The load rate was approximately 100 pounds per second. The actuator was then started to apply a sinusoidal cyclic load varying between 0.5 and 16.5 kips at a frequency of 3 hertz (3 cycles per second). Specimen 4 was cycled between 0.5 and 8.5 kips at the same frequency of 3 hertz. After 1,000 cycles were applied, the loading was stopped and another static test was performed. This static test procedure was repeated at 10^4, 10^5, 10^6, and 10^7cycles. Data was only recorded during the static tests, and for some of the longer cycling intervals the instrumentation was removed to reduce chances of damage.

4.3.2 Strength Tests

The same procedure was followed for the strength tests of all the specimens, except for Specimen B where the joints were opened with the jacking system prior to testing. The following steps were performed for the strength tests. The specimen was first marked, grouted, aligned and placed in position on top of the roller supports. The loading I-section was centered in position on top of the 20 in. by 10 in. elastomeric pad. The actuator ram was aligned to be plumb over the center of the load patch. The top end constraint plates and instrumentation were then attached and secured following the same procedures as defined for the fatigue tests. The data acquisition system was programmed to continuously record data during the test at 1 and 10 readings per second. Failure was defined as the peak load achieved on the load versus displacement curve. The actuator was then retracted and the acquisition system was stopped. Unlike the fatigue tests which used the computer-controlled MTS actuators, a uniform loading rate was not maintained for the static tests since the Enerpac actuator was manually controlled with an advance and retract controller. This results in a displacement controlled test. Initially, the load was slowly increased at about 1 to 2 kips every 2 to3 seconds. The same approximate displacement rate was maintained as the specimen became less stiff approaching the failure load.

4.3.3 Jacking Procedure

The jacking procedure was implemented to Specimen B (strength test) and Specimen A (fatigue test) prior to testing. The first step involved attaching the anchor blocks consisting of four channel-sections to the specimen using mechanical expansion bolt anchors. The anchor bolts were installed using the manufacturer's recommendations. The next step involved bolting the four 1-in. bearing plates to the overhanging ends of the channel-sections. Once the bearing plates were in place, the specimen was positioned on top of the support rollers. The jacking struts (jack, HSS, and half roller assembly) were positioned and aligned between the two plates on each side of the specimen. The jacking struts were parallel to the side face of the specimen and located at the mid-depth of the slab. Once the jacking struts were placed, the instrumentation was attached to the specimen. The data acquisition system was activated to record crack opening and jacking force while the struts were manually extend by turning the jack screw. Specimen B was jacked to a sustained axial load of 20 kips per jack. The construction joints were visually observed to be open at this load level. The same procedure was followed for Specimen A, but the maximum jacking load was about 18 kips per jack. Once the joints were opened by loading the jacking struts, the simulated wheel load was applied to the specimens following the same procedures for the un-jacked specimens.

CHAPTER 5: RESULTS & DISCUSSION

5.1 Strength Tests

There were a total of five strength tests conducted in this research investigation. Three tests were on slab specimens cut from the I-81 bridge deck (Specimens 1, 3 and 8). The remaining two were on the cast specimens, one with the basic setup (Specimen C) and the other with the jacking setup (Specimen B). Once the setup was complete, the specimens were loaded to failure.

The load-displacement curves for all strength tests are complied in Figure 5-1. Although the magnitude of the ultimate load varies between tests, the shape of the load versus displacement curves is similar between all tests. All specimens were loaded until a clear failure occurred where the applied load dropped off, with the exception of the first specimen tested, Specimen 3. It was to the indicated ultimate load (88.3 kips), but was unloaded before the applied load drop-off occurred. It was later retested, but the maximum load reached was 74 kips.

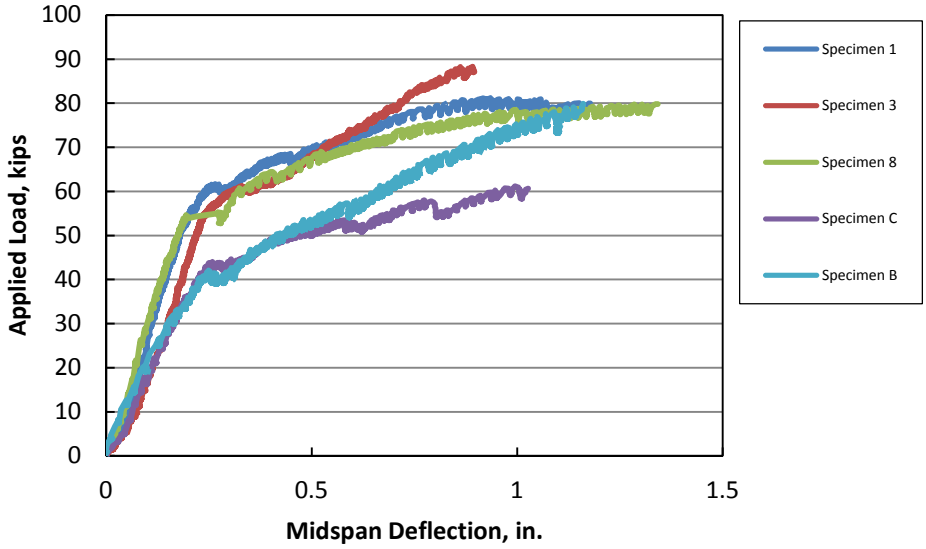

Figure 5-1. Load-Displacement Curves for Strength Tests

The three I-81 specimens (1, 3, and 8) all showed similar load versus displacement behavior. The shape of the curves can be described as bi-linear with a "kink" occurring between 55 and 61 kips. The initial portion of the curves has similar slopes indicating

similar elastic stiffness. The slopes are again similar in the portion of the curve immediately after the "kink". Greater divergence develops later in the test close to ultimate load when significant cracking is present in the concrete.

The two newly cast specimens (B and C) showed similar behavior that again can be described as bilinear. Compared to the I-81 specimens, the two newly cast specimens exhibited lower stiffness in the elastic portion of the curve. The "kink" occurs at approximately the same displacement but at a much lower load level. The immediate "post-kink" portion of all five curves appear to have similar slopes although the curves are lower for the newly cast specimens due to the lower load at the "kink". Again, the curves diverge at higher load levels approaching ultimate when significant cracking is present in the specimens.

Table 5-1 shows the maximum load and mid-span deflection measured during the test. Also shown, are the maximum calculated moments and shear based on the loading fixture geometry. The applied wheel load was not exactly a point load at midspan; it was rather a distributed load for a two-dimensional analysis. The load was applied to the specimens through a 10 by 20-in. elastomeric pad to represent a tandem truck wheel contact area, resulting in a 20 in. distributed load at the center of the specimen. Furthermore, as the load increases and the specimen deflects, the resulting curvature of the specimen will result in a non-uniform contact pressure under the load patch. The contact pressure will be higher at the edges approaching a two-point loading condition at higher loads. For simplicity, it was assumed that the resulting point load where located 8 in. from the slab center (2 in. from the edges of the elastomeric loading pad). Both loading cases are portrayed in Figure 5-2, where the actual loading bounded within the two cases, but closer to the two point load case.

The ultimate load is the highest load applied by the hydraulic ram that the slab withstood. Based on the setup and a roller support spacing of 48 inches, the ultimate shear is simply half the ultimate load. Similarly, the ultimate moment for the distributed load case is 9.5*P, while the ultimate moment for the two point load case is 8.0*P (See Appendix E for detailed calculations). The midspan deflection values listed are the deflections at the

time the slab reached the ultimate load. After this, the specimens continued to deflect at lower loads.

Table 5-1. Summary of Strength Test Results

Specimen Identification	Ultimate Load, kips	Midspan Deflection at Ultimate Load, in.	Ultimate Moment, (Distributed Load), in*kips	Ultimate Moment, (Two Point Load), in*kips	Ultimate Shear, kips
Specimen 1	81.2	0.926	771	650	40.6
Specimen 3	88.3	0.891	839	706	44.1
Specimen 8	79.8	1.340	758	638	39.9
Specimen C	61.2	0.996	581	490	30.6
Specimen B	79.9	1.161	759	639	39.9

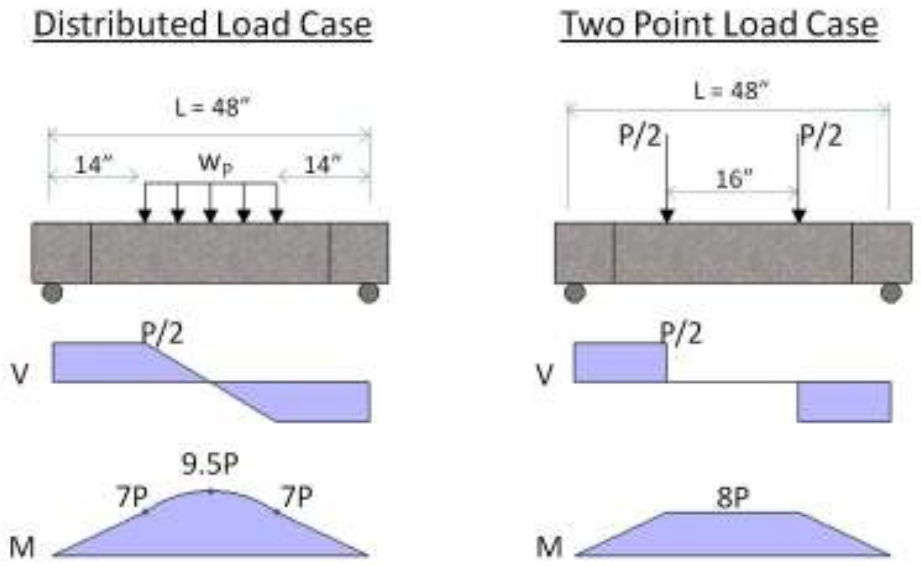

Figure 5-2. Two Extreme Loading Situations Resulting from Applied Wheel Load

Although the setup and testing procedures were the same for Specimens 1, 3, 8, and C, there was variability in the resulting ultimate load and corresponding midspan deflection for the four tests. While Specimens 1 and 8 failed at a similar load (81.2 and 79.8 kips), the corresponding deflections differed (0.926 and 1.340 in.) indicating a significant difference in stiffness between the two test specimens. While Specimen 3 failed at a higher load (88.3 kips), its midspan deflection (0.891) was less than those of Specimens 1

and 8. One possible reason for the stiffness variability is variations in the location of the reinforcing steel between the specimens. The slabs specimens were cut directly from the bridge deck, and while there was an effort to cut them with similar rebar configurations, none were exactly the same. The newly cast specimen (Specimen C) failed at a significantly lower load (61.2 kips) compared to the three specimens cut from the bridge deck, despite the specimen design and concrete mix being specified to replicate the I-81 specimens. Its midspan deflection, however, was in the same range as the other specimens. Specimen B was tested with the jacking setup and its ultimate values were close to those of the I-81 specimens.

5.1.1 I-81 Specimens

The load-displacement curves for the I-81 specimens along with the calculated shear and flexural limits are shown in Figure 5-3. The two flexural limits correspond to the two loading cases discussed in the previous section and were determined using a rectangular compression stress block assumption and a concrete strength of 7,650 psi (average value taken from core strength tests, see Chapter 4). The shear limit was determined base on shear strength of the concrete slab (See Appendix E for detailed calculations). The specimens were expected to fail somewhere within the flexural limits (53.6 and 60.0 kips), but they all failed above 79 kips. There are several factors that could have contributed to the higher capacity of the specimens. First, the flexural limits were determined using an average concrete strength from core tests taken from the closure pour region of the I-81 bridge deck. However, tests done on the cores taken from the I-81 specimens revealed that the average strength of the closure pour concrete and adjacent slab concrete was 7,650 and 5,660 psi, respectively (see Chapter 4). Since most of the specimens' volume consisted of the closure pour concrete, the overall strength of the specimens was most likely closer to 7,650 psi, rather than 5,660 psi. Another factor that could have affected the results is that the specimens were relatively short beams, where the assumptions used in the analysis of longer span beams do not apply. Shear is critical in short beams and shear deformations cannot be neglected. The rebar layout could also be a contributing factor since the bottom bars were truss bars, where the bar depth is not constant along the length of the slabs. Since the specimens were directly cut from the

bridge deck, the locations of the bars were not exactly the same in all specimens. The contribution of the construction joints is also uncertain. In addition, the actual yield and ultimate stress values are higher than the specified values. This, and with the calculations showing that the steel is in strain hardening at ultimate conditions, could also be reasons for the higher capacity of the specimens.

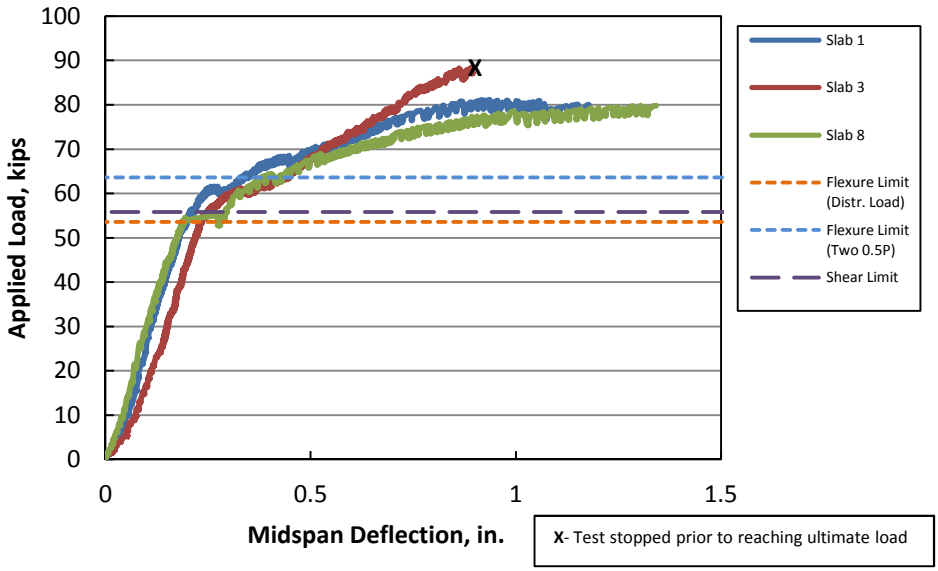

Figure 5-3. I-81 Specimens Load-Displacement Curves with Flexural and Shear Limits

The slab specimens behaved like a continuous beams despite the presence of the two construction joints. There was no measurable shear displacement across the joint until severe cracking occurred in the latter stages of testing. The specimens failed near the shear limit, but the shear plane shown in Figure 5-4 shows Specimen 1 after it was loaded to failure and it seems that the test-induced cracks (marked in red) are a mixture of shear and flexural cracks. If the cracks were purely shear cracks, they would have occurred closer to the roller supports. Furthermore, since the specimens are essentially short beams, it seems a though a punching failure occurred under the wheel load.

Specimens 3 and 8 had similar cracks form on their side faces. During the tests, the first cracks to form were the two shear cracks—oriented about 45 degrees from the horizontal—that started at the bottom face of the specimen about halfway between the supports and the specimens' midspan and continued upward toward the loading point. In the three tests, these cracks became visible close to the load where the "kink" occurred in

the load-displacement curves. After these cracks formed, smaller cracks began to branch out from them and other small ones formed in between them. There were sections of concrete that spalled off on the bottom face of the specimens, revealing the reinforcing bars.

Figure 5-4. Failed I-81 Specimen with Test-Induced Cracks (Marked in Red)

5.1.2 Cast Specimens

The load-displacement curves of the cast slabs and the calculated limits are shown in Figure 5-5. The limits shown are slightly different than the limits for the I-81 slabs since a concrete strength of 6,325 psi (from cylinder tests, see Chapter 4) was used in the calculation of the limits. The same factors mentioned in the previous section could have contributed to the specimens not failing at the predicted limits, with differences in the specimens' concrete strength and rebar placement. The average concrete strength values of the cast specimens were 6,140 and 6,510 psi for the closure pour placement and the adjacent slab placement, respectively. Also, there was more consistency with the rebar placement within the specimens since the specimens were cast in the laboratory, opposed to being cut directly from the bridge deck. It may be noteworthy that Specimen C, tested

under the basic setup (no jacking), failed closer to the two-point load case flexural limit than the other limits. The curve for Specimen B, tested with the jacking setup (opened joints), behaved almost the same as that of Specimen C until 50 kips. After this point, it continued to deflect and take more load until it failed close to 80 kips.

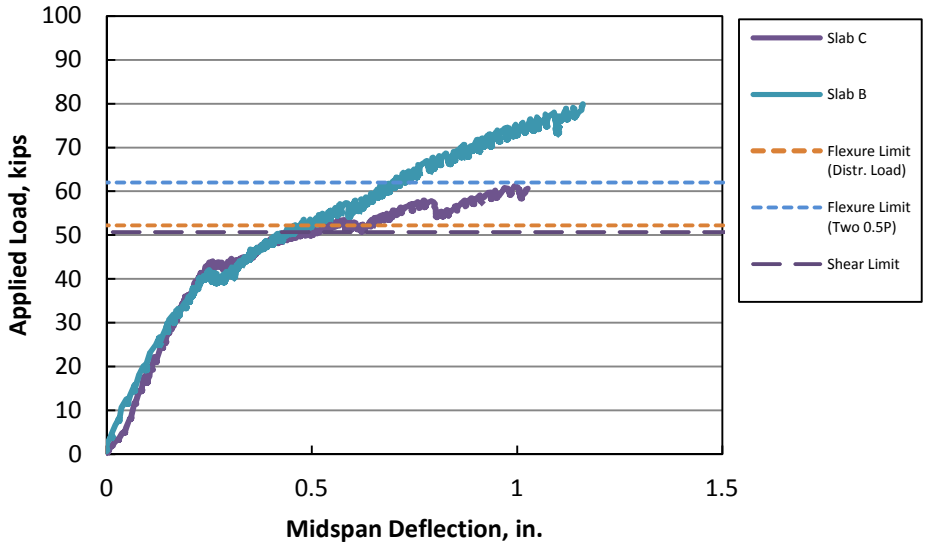

Figure 5-5. Cast Specimens Load-Displacement Curves with Flexural and Shear Limits

Specimen C did not have significant vertical joint deflections during the test, although around an applied load of 42 kips, some of the top surface concrete around the location of the LVDT's began to spall thereby affecting the readings. Up to that point the specimen still behaved as a beam without any shear deformation at the construction joints. Figure 5-6 shows the post-failure side face of Specimen C. There were fewer cracks compared to the I-81 specimens, but the two main cracks that started at the bottom surface and extended upward towards the loading point can be seen. The crack on the left did not start with a 45 degree inclination. It rather extended upward almost vertically until the specimen's mid-depth, and then it inclined toward the loading point. Similar cracks were formed on the other side of the specimen.

The main differences observed between Specimen C and the I-81 specimens are: 1) the ultimate load of Specimen C was significantly lower; 2) there was significant spalling of the concrete on the top face of Specimen C; and 3) there were fewer cracks compared to the I-81 specimens.

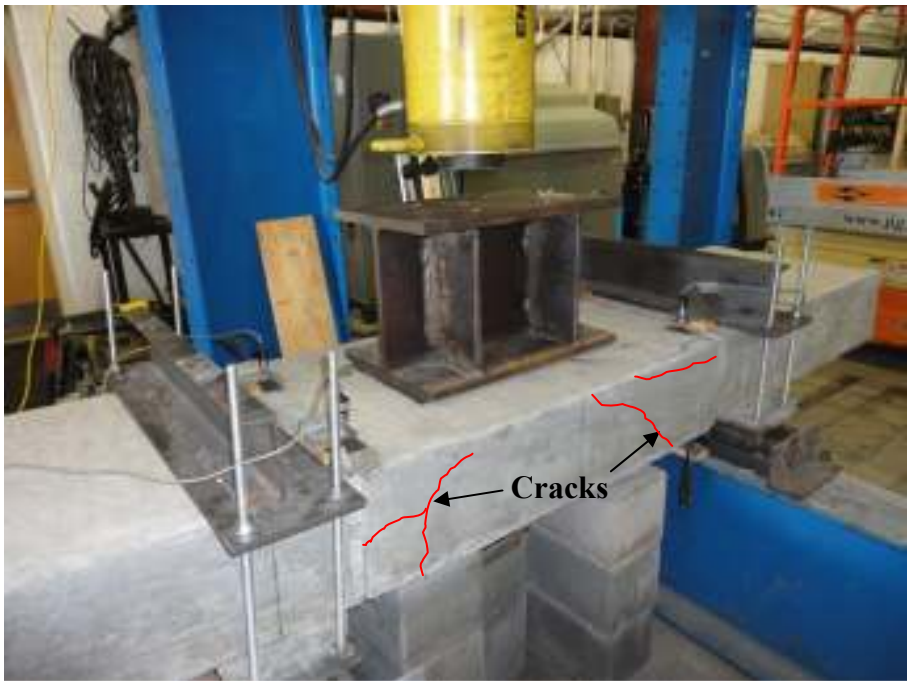

Figure 5-6. Failed Specimen C with Main Cracks Indicated

As mentioned before, Specimen B was tested using the jacking setup that required additional instrumentation. Since this was the first time the jacking setup was implemented, it was important to monitor joint behavior, both during the pre-test jacking and testing. Eight LVDT's were mounted (four per joint) to monitor the opening of the joints. Figure 5-7 shows a sketch of the Specimen B with the joints, sides, and LVDT's labeled. There were four additional wire pots used (five total) to monitor vertical deflection at five points along the specimen centerline throughout the test.

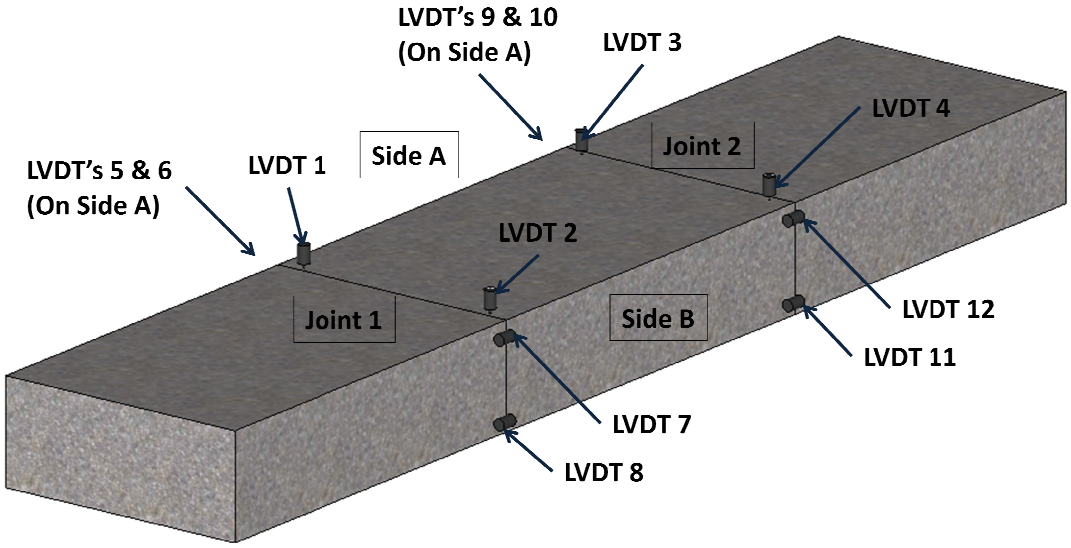

Figure 5-7. Specimen B with LVDT Locations for Strength Test

Prior to testing, the joints were opened with the stay-in-place jacking struts. It would have been ideal to open the joints to match the crack opening in the I-81 bridge prior to cutting of the slabs, but no crack opening measurements were taken prior to cutting the slabs. The jacking struts were placed along the specimen centerline resulting in a uniform axial force across the concrete section. However, there is an eccentricity at the joint since the rebar has an unsymmetrical arrangement with one top bar and three lower bars. This caused the crack to open more at the top compared to the bottom of specimen. This can be observed in Figures 5-8 and 5-9. The data collection did not begin until after the jacking struts were mounted with about1.5 kip force to hold the jacks in position. The LVDT values were zeroed relative to their readings at the beginning of the jacking process. It appears that LVDT 8 and 9 malfunctioned since no displacement was recorded during the test. The remaining LVDT readings show the top of the joints opening more than the bottom. The curves for all functioning LVDT's remained relatively linear indicating the reinforcing bars remained elastic during the jacking process. The jacking displacement was slowly increased until a load of 20 kips per strut (40 kips total axial load on the specimen). The curves shown in Figures 5-8 and 5-9 are were plotted with respect to the force in each individual jacking strut. The jacking force slowly decreased during the strength testing and the rate of decrease accelerated after the load exceeded

about 45 kips. This can be seen on Figure 5-10 where the jacking forces dropped to about 3.5 kips at failure. Jack A corresponds to the jacking strut that was on Side A of the specimen, and Jack B corresponds to the one on Side B.

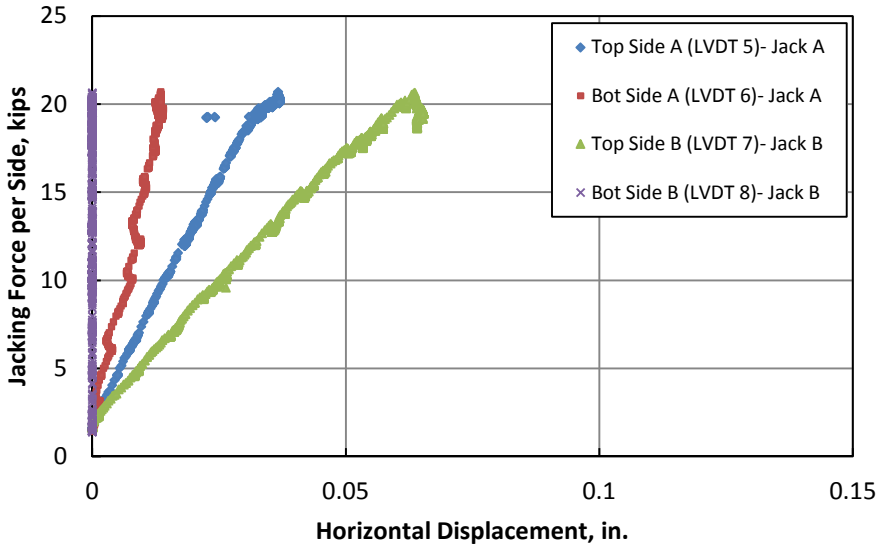

Figure 5-8. Joint Opening LVDT Readings at Joint 1 during Jacking

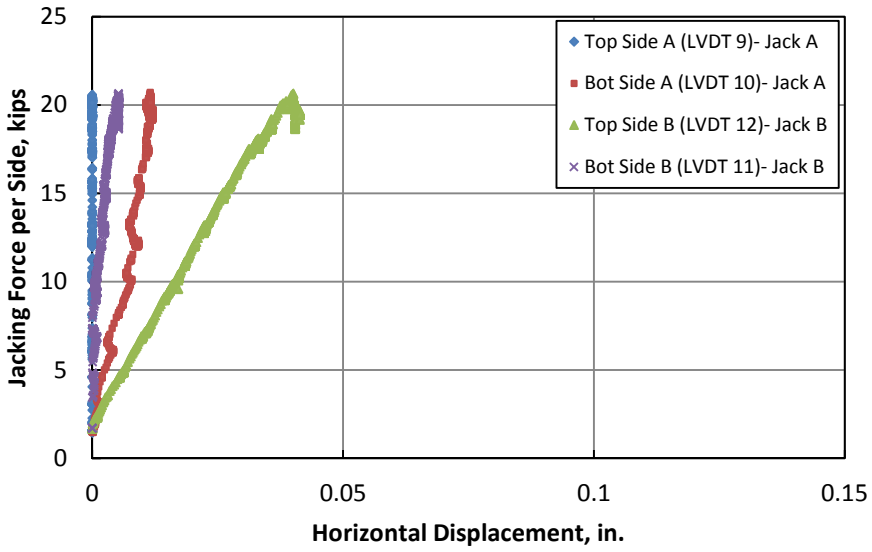

Figure 5-9. Joint Opening LVDT Readings at Joint 2 during Jacking

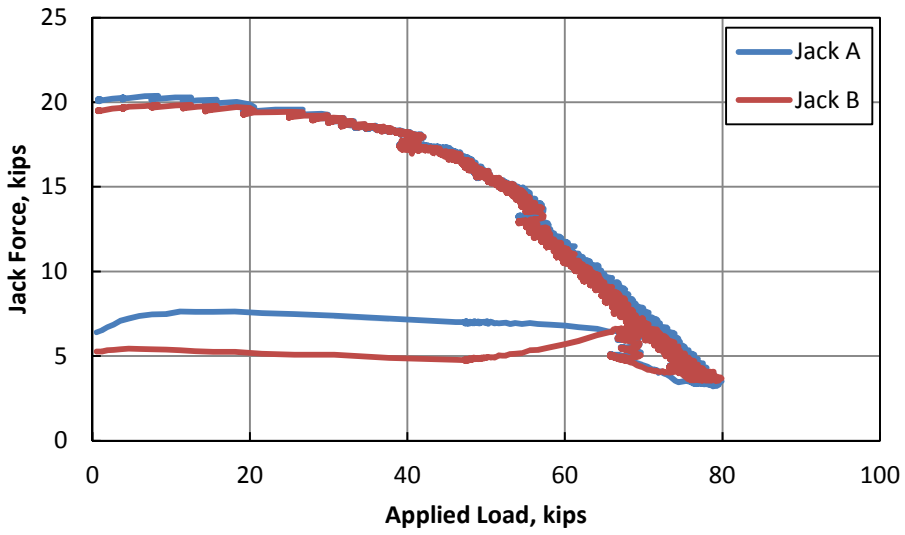

Figure 5-10. Jacking Forces during Strength Test (Specimen B)

The vertical deflected shape of Specimen B from the beginning of the test till failure is shown in Figure 5-11, while the zoomed-in deflected shape up until 20 kips of applied load is shown in Figure 5-12. The three middle deflection measurements were relatively constant at all load steps. Based on bending theory the midspan deflection would be expected to be higher compared to the other two locations. This indicates that the center region of the specimen is deflecting somewhat as a rigid body and shear deformation at the joints and crack locations are affecting the deflection response.

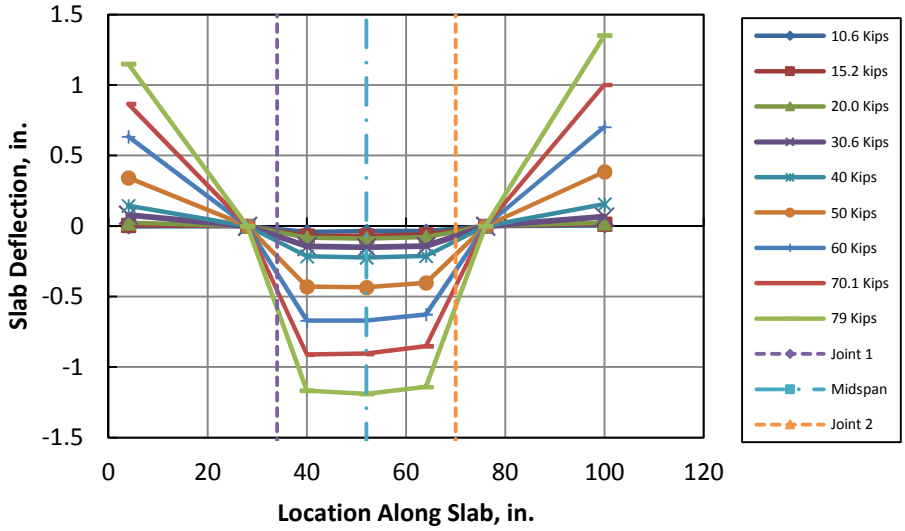

Figure 5-11. Deflected Shape of Specimen B Throughout Testing

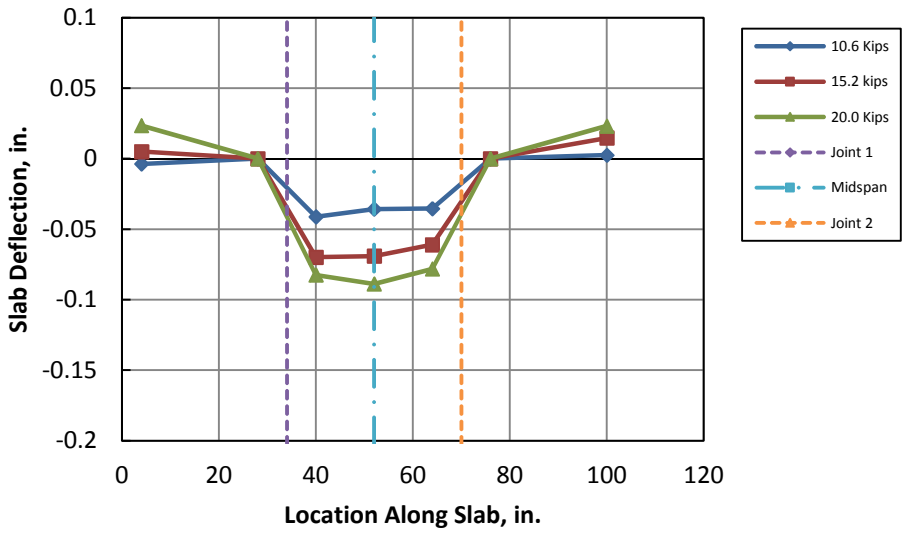

Figure 5-12. Deflected Shape of Specimen B up to 20 kips

Figure 5-13 is a photograph of the failed Specimen B once the instrumentation and jacks were removed. The test-induced cracks are marked in red. The two main cracks described in the other specimens, also appeared in Specimen B, but there were also additional cracks that formed on the sides of the specimen. These were located between the roller supports and the construction joints and are indicated in the picture. Refer to Appendix D for more photographs of failed Specimen B and the other strength test specimens.

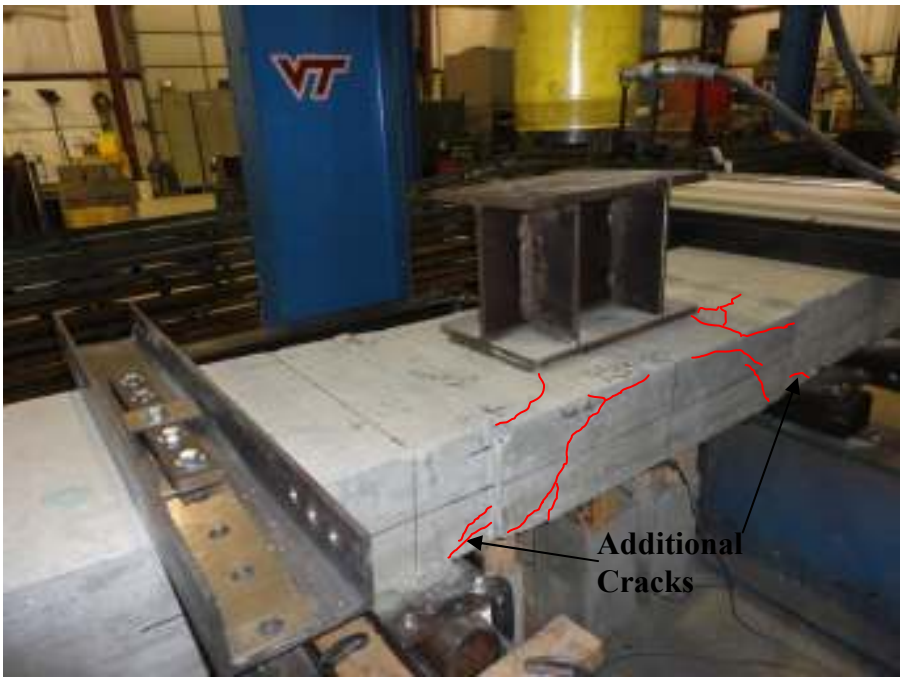

Figure 5-13. Failed Specimen B with Test-induced Cracks Marked

5.2 Fatigue Tests

There were a total of four specimens tested under fatigue loading in this research investigation. Three of these specimens were cut directly from the I-81 closure pour slabs and the remaining specimen was one of the laboratory cast specimens. The three I-81 specimens were tested with the basic test setup, while the cast specimen was tested with the applied axial force from the jacking setup. Both test setups are discussed in detail in Chapter 3. This section presents the results of fatigue tests and includes a discussion of the results.

The stiffness (load versus mid-span deflection) of the test specimens was periodically monitored over the duration of the fatigue test. A quasi-static load equal to the maximum cyclic fatigue load was applied while measuring mid-span deflection. The slope of the load versus displacement curve defines the specimen stiffness in kips/in. The stiffness measurements were performed before beginning the cyclic loading. In addition, static stiffness tests were performed after set numbers of fatigue cycles were applied to detect any change in stiffness due to the cyclic loading. The specimen stiffness was measured at

logarithmic cycle intervals corresponding to 10^0, 10^3, 10^4, 10^5, 10^6, and 10^7 cycles. The goal was to identify any trends in the specimen stiffness behavior throughout the cycling period. Figure 5-14 shows the stiffness change measured for all four fatigue tests over the duration of cyclic loading. For comparison, the stiffness values of the strength test specimens are plotted for one load cycle.

As described in Chapter 4, the static tests run at the logarithmic intervals were conducted by recording data as each specimen was loaded from 0 to 16.5 kips (8.5 kips for Specimen 4) at a rate of 100 pounds per second. A linear regression curve was fit to a subset of the data points between 1 and 15.5 kips (1 and 7.5 kips for Specimen 4) to eliminate bias from non-linearities at the extremes of the data sets. These plots can be found in Section A.2 of Appendix A. The slope of the regression line (units of kips/in.) was taken as the stiffness value corresponding to that specific cycle count.

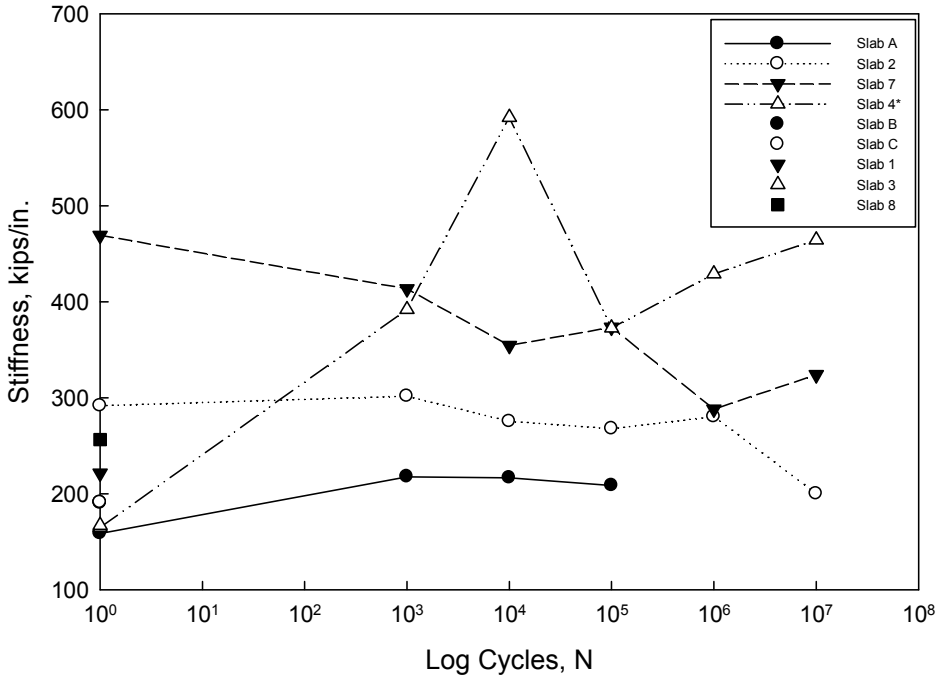

Figure 5-14. Specimen Stiffness throughout Duration of Fatigue Loading

Figure 5-14 shows there is no consistency of trend between the different test specimens. Though there is an offset of more than 100 kips/in. between the two specimens, the stiffness of Specimens 2 and 7 appear to have generally similar trends with stiffness

gradually decreasing over the duration of cyclic loading. The stiffness of Specimen A was considerably lower compared to the I-81 specimens. This can be attributed to the increased deflection across the joints that are being held open with the jacking struts thereby increasing midspan deflection. The curve stops at 10^5 cycles since the specimen failed at 280,000 cycles (more details are discussed in Section 5.2.2). The response of Specimen 4 shows much greater variability, however, this may be an artifact of the lower cyclic fatigue loading level (0.5 to 8.5 kips). Therefore, the regression curves for the midspan deflection plots of this specimen do not pertain to the same load increment as the other three fatigue-tested specimens (1 to 15.5 kips). As expected, this curve's behavior is different than the other specimens.

The stiffness values of the strength-tested specimens are also included in Figure 5-14. The strength test specimens were only loaded once, from 0 kips to failure; therefore, they are each represented as a single point at cycle 1. The stiffness values were taken from a linear regression curve from the applied load versus midspan deflection plots. However, to make it comparable to the stiffness values of the fatigue specimens, the linear regression curve pertained to data between 1 and 15.5 kips. Ranging from 167 to 256 kips/in., these five points do not seem to be any more consistent than the fatigue specimens' stiffness curves. It may be worth noting that the Specimens C and B (cast specimens) have the same stiffness value of 190 kips/in. even though Specimen B had its joint open by the screw jacks.

There are several possible reasons for the absence of a clear trend in the stiffness results A large variation in stiffness between the specimens is present at cycle 1 where the data in not affected by cyclic loading. Since this was the first time the specimens are loaded, there may be some setting-in of the specimens and fixtures (roller supports). The initial specimen loading may have caused seating of the rollers to their supports (see Figure 3-12). Also, since the specimens have the joint discontinuities there may be some permanent "setting in" deformations due to slippage and nonlinearity of the concrete face contact at the joints. There could also have been some debris in the I-81 joints that may have influenced the nonlinearity of the concrete face contact. Perhaps taking the static baseline reading after 2 or 3 cycles would have made the initial stiffness more consistent

and comparable between the specimens. Another possible cause may be related to differences in how the strength and fatigue specimens were loaded. The fatigue specimens were loaded by a computer-controlled actuator at a consistent rate of 100 pounds per second. On the other hand, the strength specimens were loaded with a manually controlled actuator with a number of starts and stops in load application. It was not possible to manually load at a constant rate for these specimens.

Examining the applied load versus midspan deflection plots at each logarithmic measurement point shows that the specimen behavior is inconsistent during loading. For example, all of the plots for Specimen A display a step-like behavior in the curves (see Appendix A). Specimen 2 does not display this behavior until after 10^4 cycles and Specimen 7 doesn't display it until after 10^5 cycles. As a consistent way to compare stiffness for each specimen, a linear regression curve was fit on all plots. The R-squared values of the regression curves are listed in Table 5-2. These values are an indication of how close the generated curve is to representing the actual data points with $R^2 = 1$ indicating a perfect fit. With the exception of Specimen 4, the regression curves in general seem to be satisfactory in representing the specimen behavior during the 1 to 15.5-kip load interval. Figures 5-15 and 5-16 show the applied load versus midspan deflection for Specimens 2 and 7, respectively, at 10^5cycles. It is evident from these plots that the behavior of the specimens was not consistent. Refer to Section A.2 in Appendix A for the entire set of applied load versus midspan deflection plots with regression curves.

Table 5-2. R-Squared Values of Load versus Displacement Linear Regression Curves

Specimen Identification	Number of Cycles					
	10^0	10^3	10^4	10^5	10^6	10^7
Specimen A	0.988	0.943	0.971	0.986	-	-
Specimen 2	0.903	0.947	0.907	0.976	0.963	0.959
Specimen 7	0.961	0.974	0.930	0.880	0.972	0.921
Specimen 4*	0.924	0.924	0.858	0.920	0.747	0.880
Specimen B	0.992	-	-	-	-	-
Specimen C	0.961	-	-	-	-	-
Specimen 1	0.983	-	-	-	-	-
Specimen 3	0.969	-	-	-	-	-
Specimen 8	0.984	-	-	-	-	-

*The R-squared values for Specimen 4 are based on an 8 kip load range

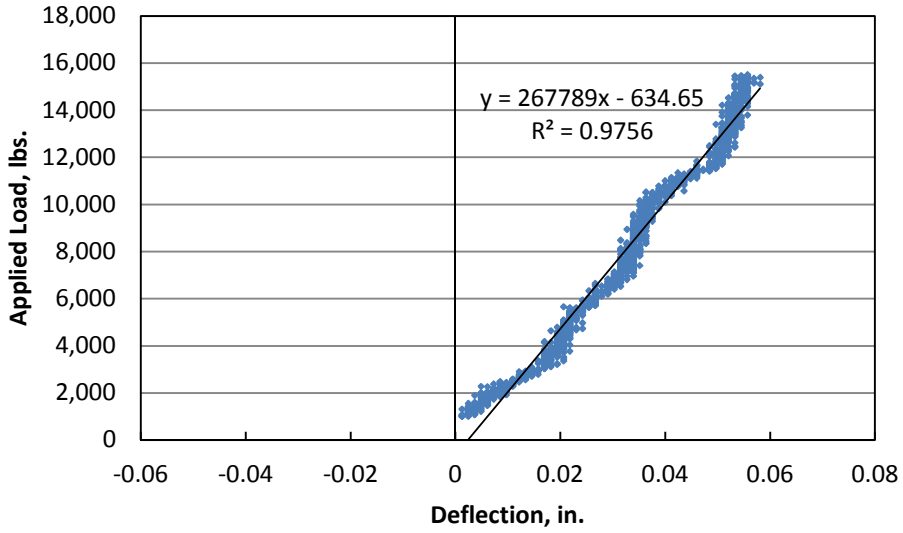

Figure 5-15. Applied Load versus Midspan Deflection for Specimen 2 after 10^5 Cycles

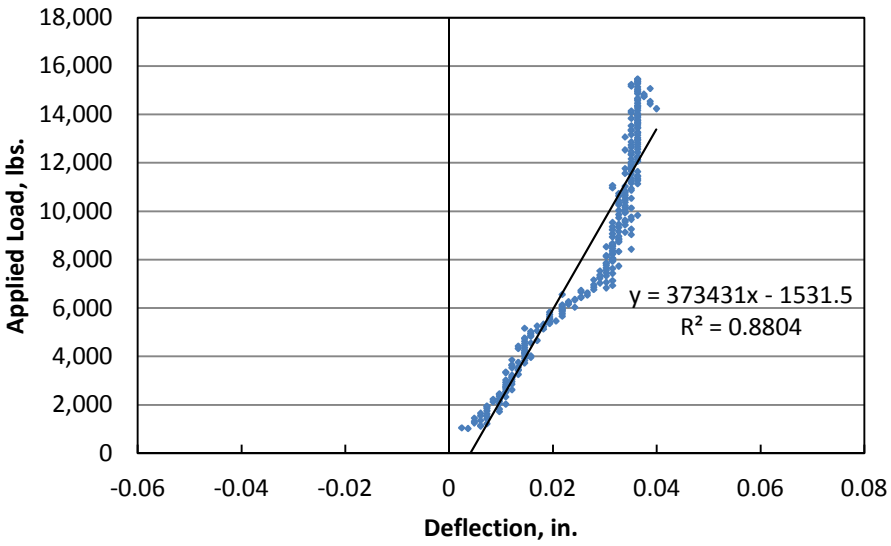

Figure 5-16. Applied Load versus Midspan Deflection for Specimen 7 after 10^5 Cycles

5.2.1 I-81 Specimens

The three I-81 specimen specimens that were fatigue tested are specimens 2, 4, and 7. Specimen 4 was tested first at a load range of 8 kips (0.5 to 8.5 kips). Testing was halted after no failure was observed at 10^7 cycles which was the practical time limit for testing under this project. The load range was increased to 16 kip (0.5 to 16.5 kips) for specimens 2 and 7. Despite this increase, there was still no observed fatigue failure at 10^7 cycles. It is important to note that the loading cycles applied in the laboratory are in addition to the loading cycles applied by trucks during17 years of bridge service. Using the AASHTO LRFD Bridge Design Specifications (2010), the number of cycles due to traffic loading can be estimated. Using AADT = 14,000 (Annual Average Daily Traffic, value provided by VDOT's 2009 Average Daily Traffic Volume report) and p = 0.20 (for rural interstate, Table C3.6.1.4.2-1):

$$Total\ Service\ Cycles = 14000 \times 0.20 \times (3\ Axles) \times (365\ days) \times (17\ years)$$
$$= 52\ Million\ Cycles$$

Any reference in this report to loading cycles of Specimens 2, 4, and 7, are in addition to the 52 million cycles that the specimens already experienced in the field. Since the stress range produced by wheel loads in the field is not known, it is difficult to determine how much fatigue damage was caused by the field loading.

The differential vertical displacement readings between the two opposing sides of the joint under the cyclic load cycle were less than the LVDT resolution. It can therefore be implied that there was no shear deformation occurring across the joint. Plots of the joint displacement readings are presented in Appendix A (Section A.2). Without vertical joint displacement, the contribution of shear to the stress range in the reinforcing bars is essentially zero and the stress range can be predicted by the axial stress range in the bar due to bending. This bar condition is similar to the bar condition of the tests by Hanson et al (1976), where there was no construction joint present in their test specimens.

The crack opening displacement across the joints was monitored using DEMEC gages that were mounted on the side faces of the specimens (Sides A and B). The readings were taken at the maximum16.5-kip load during the static stiffness tests. Figure 5-17 shows the location the LVDT's and the DEMEC gages on the side face of the specimens and also labels the joints and sides. Each joint was monitored with four pairs of DEMEC points, two pairs on each side (top and bottom).

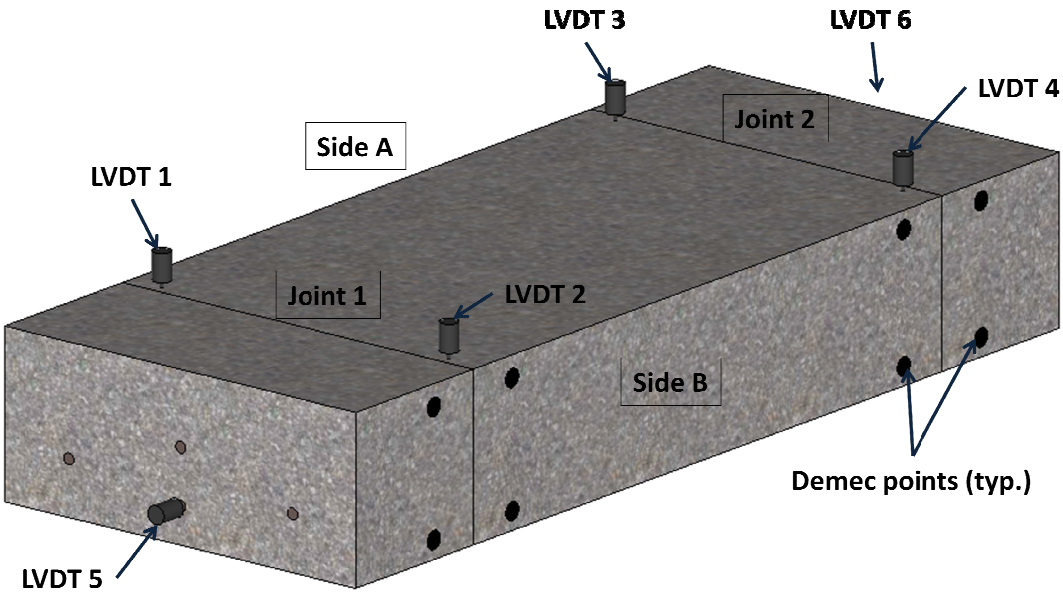

Figure 5-17. Typical I-81 Slab Specimens with LVDT and DEMEC Gage Locations

The displacement of the joints relative to their vertical planes was recorded at the same logarithmic intervals as the static stiffness tests. Since there were two DEMEC pairs on each joint for each side, a line could be created based on both DEMEC reading displacements for each log cycle relative to the unloaded condition. Figures 5-18 to 21 show the joint displacement at the different log intervals for Specimen 7 (see Appendix A for Specimens 2 and 4). The vertical axis of these plots represents the depth of the slab, with zero being the bottom of the slab, and the joint is represented by the vertical line that intersects the horizontal axis at zero. Based on the assumption that plane sections remain plane, the horizontal displacement measured at both DEMEC points was connected with a straight line that is extrapolated to the specimen surfaces. Although the joint behavior for Specimens 2 and 7 is not entirely consistent, the general trend is that the crack opening displacement gradually increases as a function of cycle count. In Figure 5-21, the curves for 10^6 and 10^7cycles are not available since the DEMEC points at Joint 2 had become loose. Also, there seems to have been in error in the process of setting up and recording data for Joint 1 on Side A (Figure 5-18) since there is an unexpected shift after 10^3 cycles. Here, it seems that one of the top DEMEC points was bumped and/or loosened.

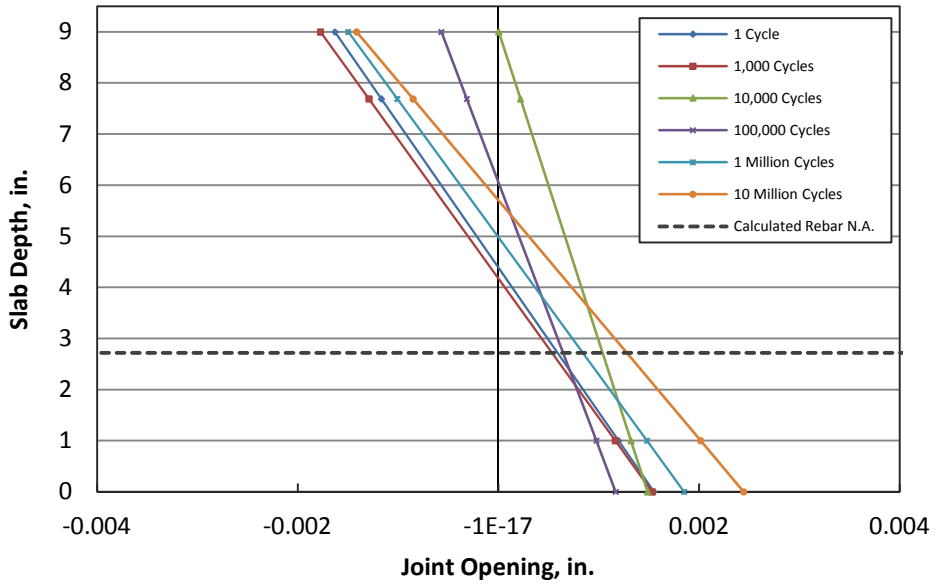

Figure 5-18. Opening of Joint 1 (Specimen 7, Side A)

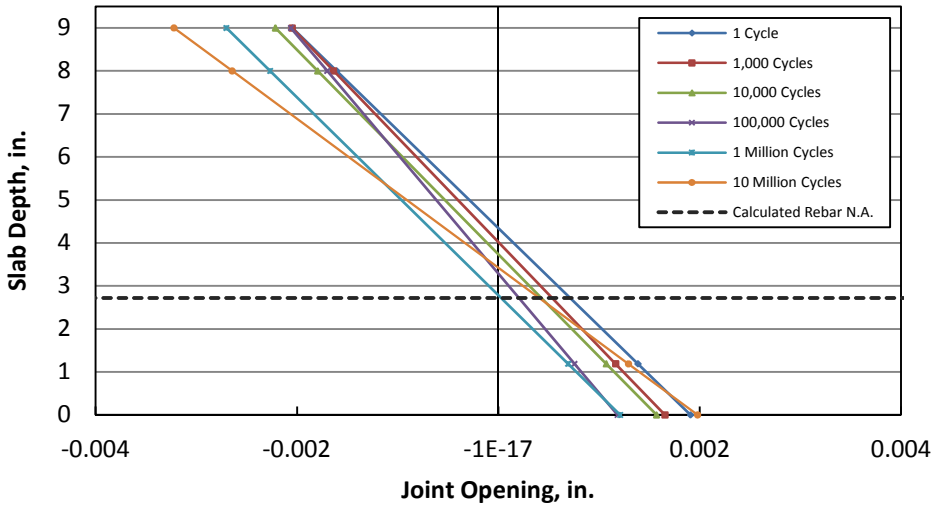

Figure 5-19. Opening of Joint 1 (Specimen 7, Side B)

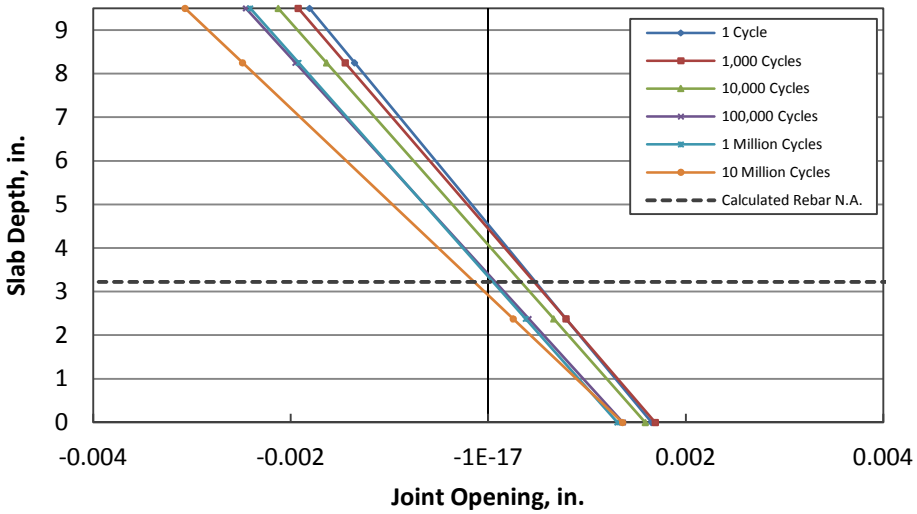

Figure 5-20. Opening of Joint 2 (Specimen 7, Side A)

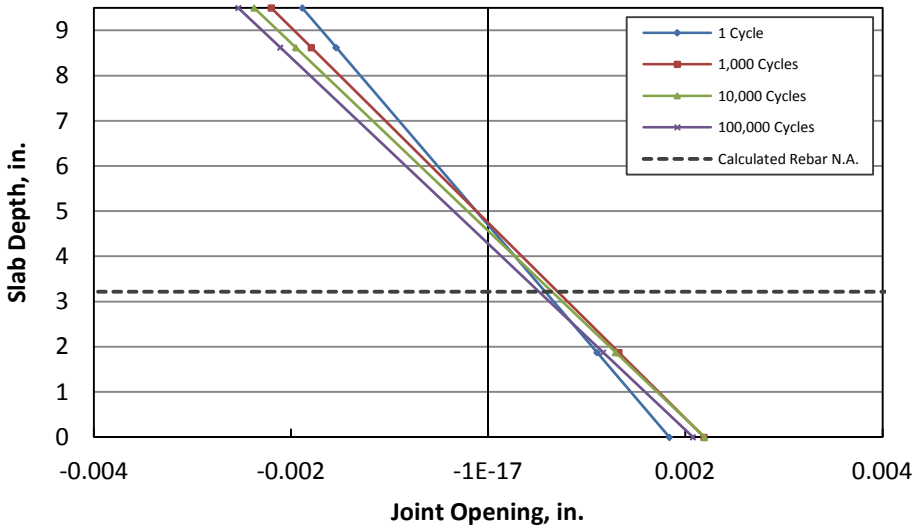

Figure 5-21. Opening of Joint 2 (Specimen 7, Side B)

5.2.2 Cast Specimen with Jacking System

After the jacking system was designed, there were two untested cast specimens remaining for the jacking system implementation. One was used for a strength test (Specimen B, see Section 5.1.2) and the other for a fatigue test (Specimen A). It would have been ideal to also use the jacking setup to open the joints of the two alternate I-81 specimens, but these did not have enough end block length to anchor the jacking strut system. The test

procedures and setup for Specimen A were the same as for the I-81 specimens with the exception that the jacking system was used to open the joints and LVDT's were used instead of DEMEC points to measure joint opening displacement. Figure 5-22 shows Specimen A with the location of the LVDT's and the sides and joints labeled. Due to limited instrumentation availability, only Joint 1 was monitored with LVDT's for horizontal joint displacement.

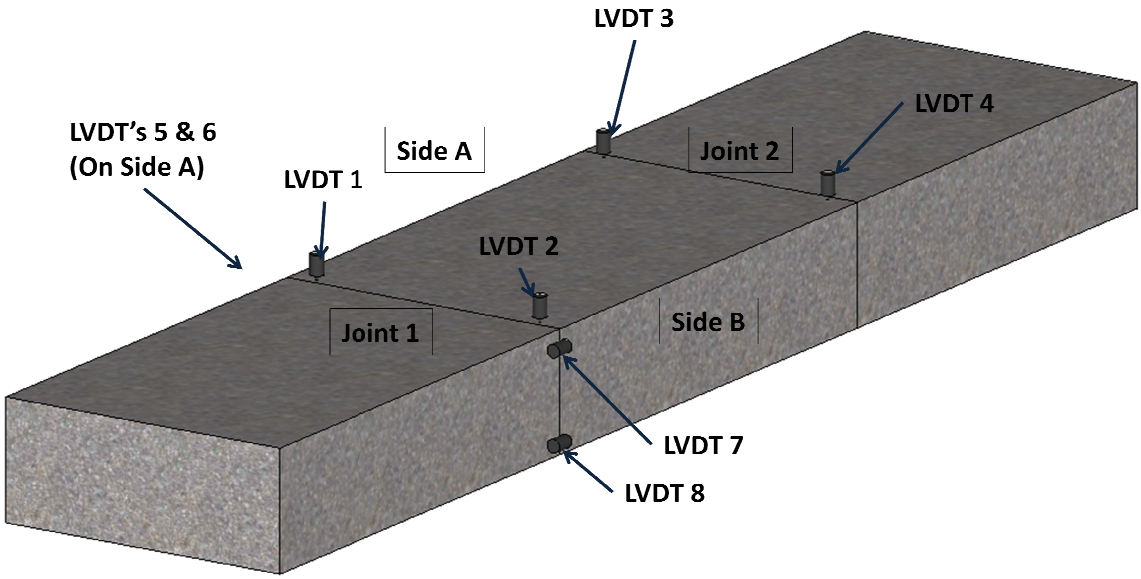

Figure 5-22. Cast Specimen with LVDT Locations

Similar to Specimen B (strength test with jacking setup), the joints were jacked open before testing using the jacking struts on both sides of the specimen. Since Specimen B was opened by applying a 20 kip load on each jacking strut, the same procedure was followed for Specimen A. However, the jacking struts were only jacked up to 18 kips each. The jacks were turned manually and they became difficult to turn beyond 18 kips. Since the joints were already opened at the 18 kip load, this was considered sufficient. Figure 5-23 shows that the jacking force was maintained within 1.5 kips of the original load throughout the duration of fatigue cycling. This indicates there was no appreciable slip of the anchor blocks used to transfer the jacking force to the specimens. The small loss in jacking force could be due to local slippage of the rebars on the faces of the construction joint. Jack A was the jacking strut set up on Side A of the specimen. Similarly, Jack B was located on Side B.

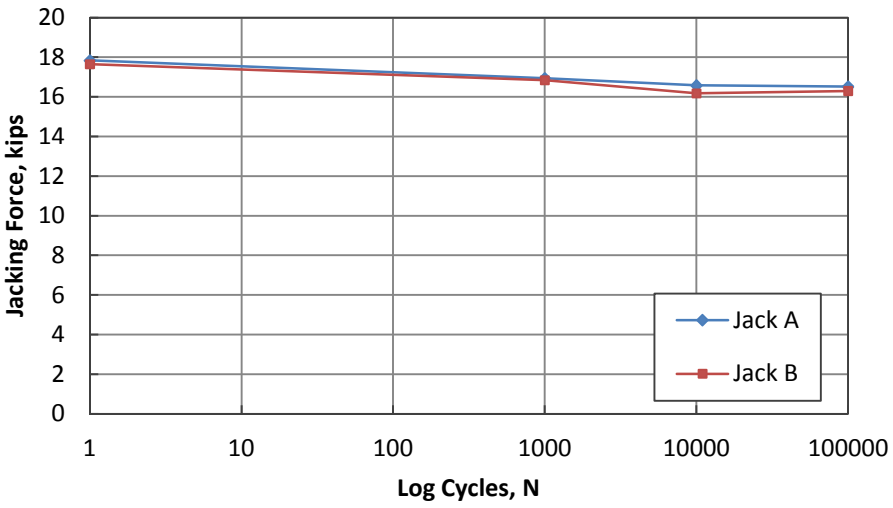

Figure 5-23. Jacking Force Maintained by Jacking Strut Throughout Fatigue Loading

The opening of the joints was monitored while the joints were opened with the screw jacks. Note that LVDT's were used for Specimen A instead DEMEC gages. Figure 5-24 shows the displacement based on the four LVDT's set up at Joint 1. The displacement of the two LVDT's on each side was plotted with the jack force of the jacking strut on the same side of the specimen. For example, the displacement read by LVDT's 7 and 8 was plotted with the jacking force of Jack B. Due to instrumentation availability, only Joint 1 was monitored with LVDT's set up horizontally across the joint.

Although the cast specimens were virtually identical and the jacking setup for Specimens A and B was the same (centerline of jacking struts at mid-height of specimens), there was a difference in the joint behavior during the jacking process. When Specimen B was jacked, the joints behaved in a linear manner (see Figures 5-8 and 5-9 in Section 5.1.2). However, Figure 5-24 displays nonlinear behavior at the top of Joint 1. This implies that the single reinforcing bar crossing the top of the joint may have yielded during the jacking process. The cross-section of the joint had four bars crossing the joint, three near the bottom and one near the top, causing the bar neutral axis to be closer to the bottom of the specimen. Since the jacking force was applied at mid-height, the resulting eccentricity caused a higher tensile stress for the top bar. Figure 5-25 shows a representative stress-strain curve for a Grade 60 No. 5 bar from a tensile test. The yield stress shown is 67.5 ksi, which is higher than the specified yield stress for Grade 60 steel (60 ksi).

The calculations in Section E.4 reveal that the top bar indeed yielded when the specimen was jacked to 36 kips (18 kips per jack), and with a P-delta analysis the strain of the top bar is quantified at 0.00293 in./in., which is less the strain value corresponding to the onset of strain hardening (0.01196 in./in.). The bending caused by application of the cyclic loading puts the top of the specimen in compression, thereby reducing the total tensile stress in the top bar. For that reason, the fatigue loading did not adversely affect the bar. The bar stress and strain cycled elastically along a line parallel to the original linear portion of the bar's stress strain curve.

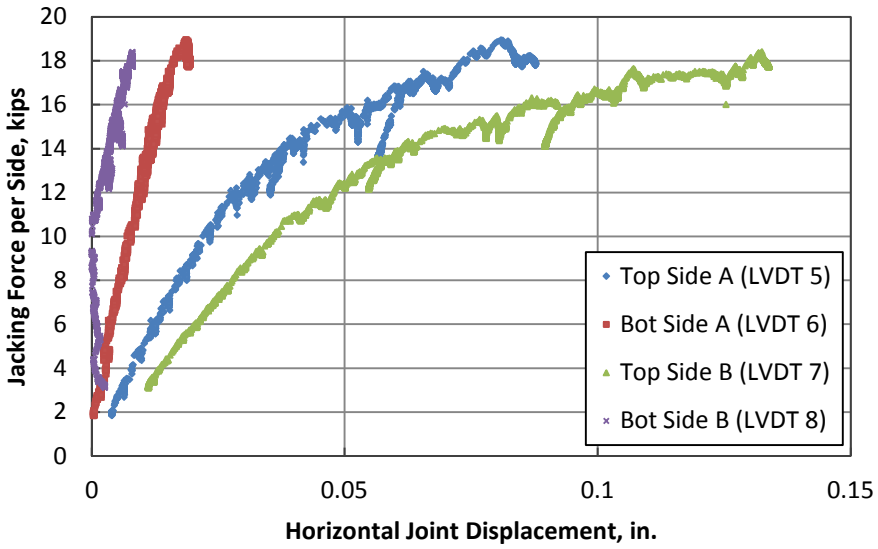

Figure 5-24. Joint Opening LVDT Readings at Joint 1 during Jacking

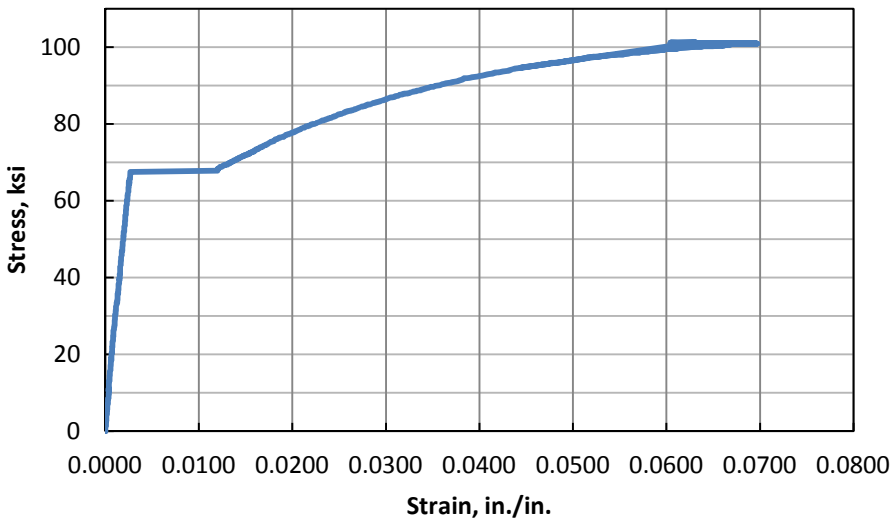

Figure 5-25. Representative Stress-Strain Curve of Grade 60 No. 5 Reinforcing Bars

The horizontal joint deflections of Joint 1 at logarithmic intervals are shown in Figures 5-26 and 5-27. The deflection magnitude is significantly larger compared to the I-81 specimens. This may be attributable to the fact that the joint was open and there was greater unbonded length of the rebars in the vicinity of the joint. The general trend in joint deflection is an increase in deflection from 1 to 10^4 cycles, but the deflections less at 10^5 cycles. In addition, the first load cycle deflection curve for Side A shifted to the right. This could be due to the setting in of fixtures and/or the specimen itself, or a shift the bottom LVDT.

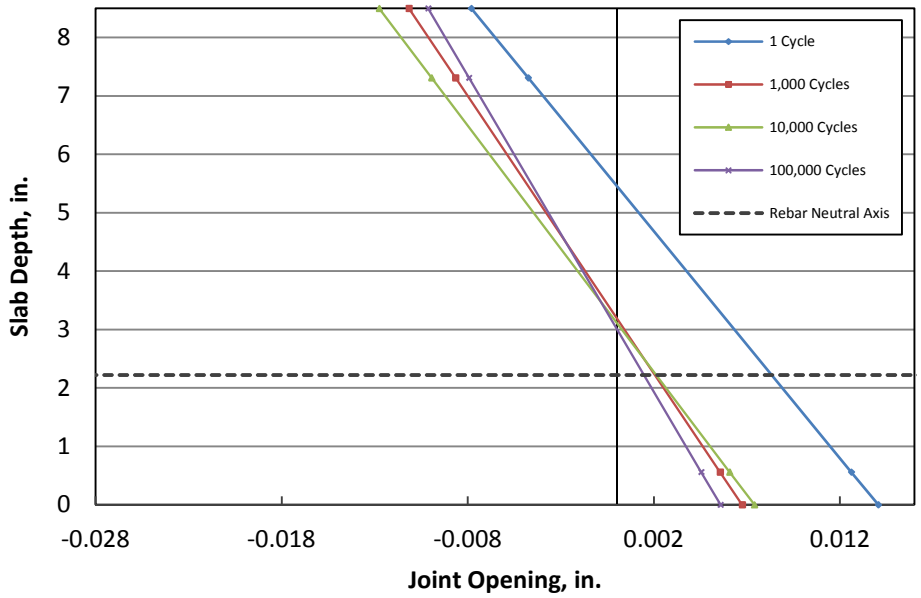

Figure 5-26. Opening of Joint 1 (Specimen A, Side A)

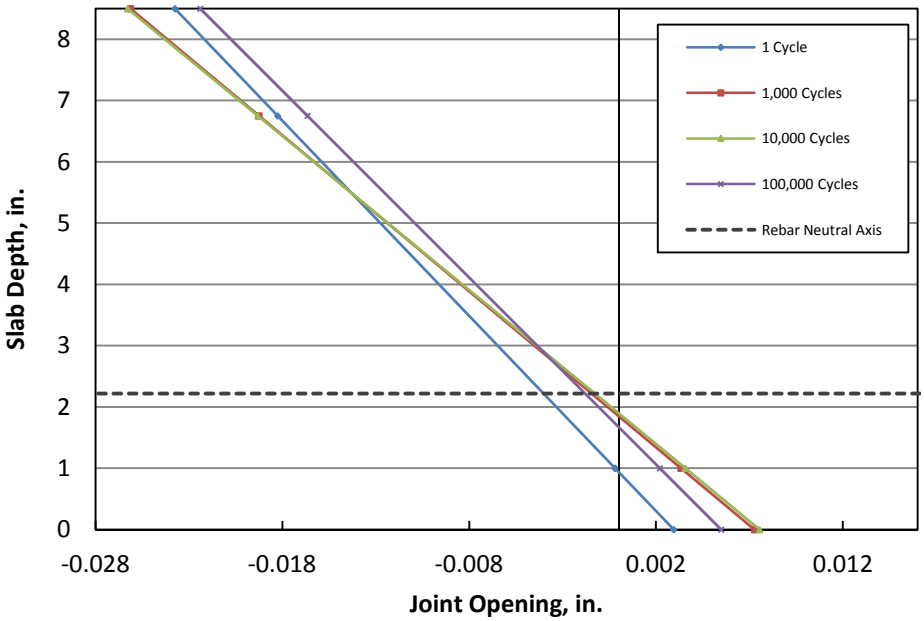

Figure 5-27. Opening of Joint 1 (Specimen A, Side B)

Unlike the I-81 specimens, there were significant vertical deflections across the joints for Specimen A. Figure 5-28 shows the average change in vertical deflections across both joints measured at different cycle counts. There appears to be larger deflections during the first load cycle. However, after examining all the data for Specimen A, there appears

to be a consistent nonlinear behavior during the first load cycle where the deflection does not return to zero after unloading. This could be caused by the supports and the specimen setting in when first loaded. This nonlinearity did not repeat after the first cycle.

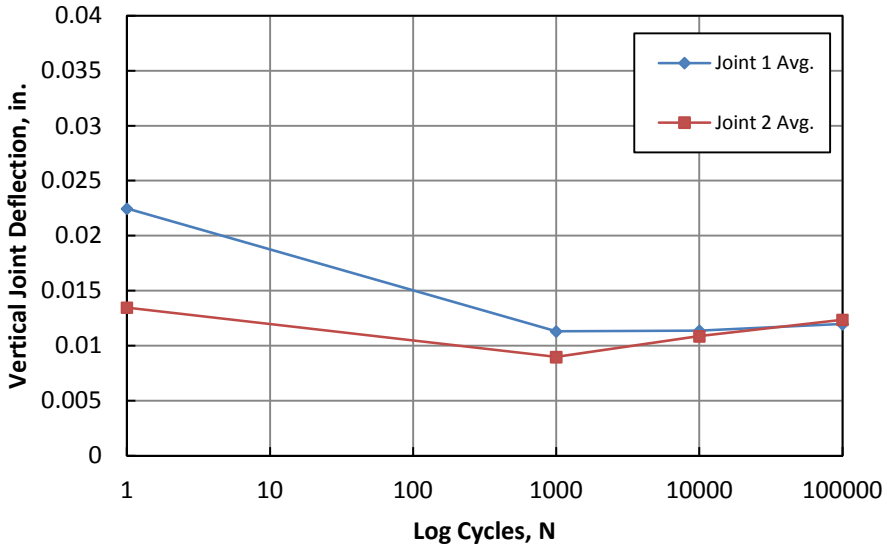

Figure 5-28. Vertical Deflection Across Joints Throughout Fatigue Loading

The top reinforcing bar in Specimen A failed in fatigue after 282,000 cycles under a load range of 16 kips. The differential vertical joint deflections (shear deformations across the joint) are expected to add significant stress in the reinforcing steel beyond the primary axial stress due to bending and jacking. This stress component is not present when there is no vertical joint displacement (shear deformations) as was the case for the I-81 slab specimens. Since the fatigue failure occurred with the open joint scenario and shear deformations present, the stress component due to the shear deformations seems to be critical.

The top bar across Joint 2 failed while the bottom bars did not fail. This caused the specimen's end section to tilt outward since only the bottom bars were carrying moment across the joint. Figure 5-29 shows the end section on the left and the closure pour section on the right after the top bar failed. Part of the failed top bar can be seen inside the joint. After this photograph was taken, the bottom three bars were cut to completely open the joint and expose the fracture face of the failed bar for examination. The opened

joint revealed that the failure plane of the failed bar did not coincide with the plane of the joint. The bar extended 0.67 in. out from the face of the specimen's end section.

In the I-81 closure pour the 3 by 3-ft. section failed all of the reinforcing bars across the joints while the Specimen A test only failed the top bar. This is predictable based on differences between the test specimen and field boundary conditions. The test specimen does not have the end block rotational constraint provided by the continuous slab in the I-81 bridge. Therefore, when one bar fails the test specimen end block rotates and is unstable. The constraint of the I-81 slab kept the joint in relative position allowing other bars to eventually fail. In addition, Specimen A was never exposed to an outdoor environment, water, or de-icing salts prior to testing. So if there was any corrosion in the bars, it was insignificant compared to the I-81 closure pour. Here, the rebars experienced significant section loss because of corrosion, which in turn increased the stresses on the other bars.

Figure 5-29. Opened Joint after Fatigue Failure, Closure Pour Section on Right Side

A close up photograph of the fracture face of the failed rebar is shown in Figure 5-30 with evident fatigue damage. The smooth portion, which takes up the top two-thirds of

the rebar face, is the fatigue crack, while the rough-surfaced bottom third is the overload region. The crack does not seem to have started at the location of the transverse lugs which is where Helgason et al. (1976) observed all of the fatigue cracks originating for their tensile-loaded fatigue specimens. Instead, it seems to have originated at the top of the rebar. This confirms that the stress range for the rebars across an open joint is not a pure tensile stress. Since fatigue cracks originate at locations of highest stress, the top of the rebar seems to be the location of highest stress. As the cycles increased, the fatigue crack propagated from its origin at the top down towards the bottom. Failure occurred when the remaining section of the rebar (rough region) could not withstand stresses due to the cyclic application of a truck wheel load. Some traces of corrosion can be seen on the fracture face but this occurred when the failed specimen was exposed to moisture after the failure. There were no traces of corrosion when the failure surface was first examined.

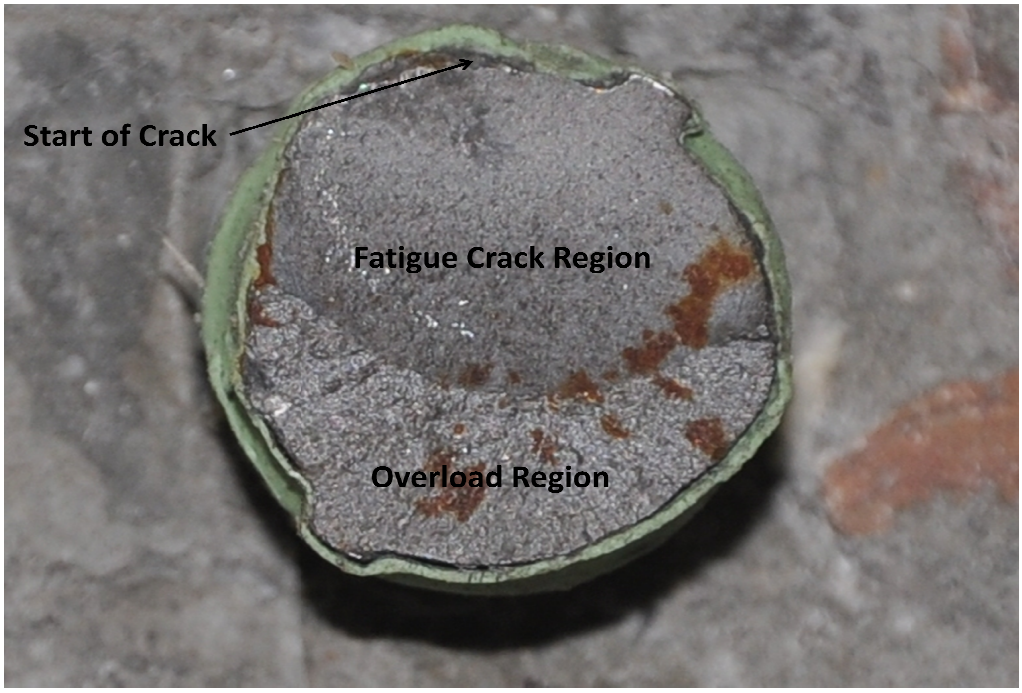

Figure 5-30. Bar Fracture Face with Evident Fatigue Damage

Shear across a construction joint is transferred by the dowel action of the reinforcing bars crossing the joint (Park and Paulay, 1975). There are three different mechanics of dowel action of reinforcing bars across a construction joint: flexure, shear, and kinking. These

are shown in Figure 5-31, where "kinking" is the major source of dowel action for rebars across a construction joint (Paulay, et al., 1974).

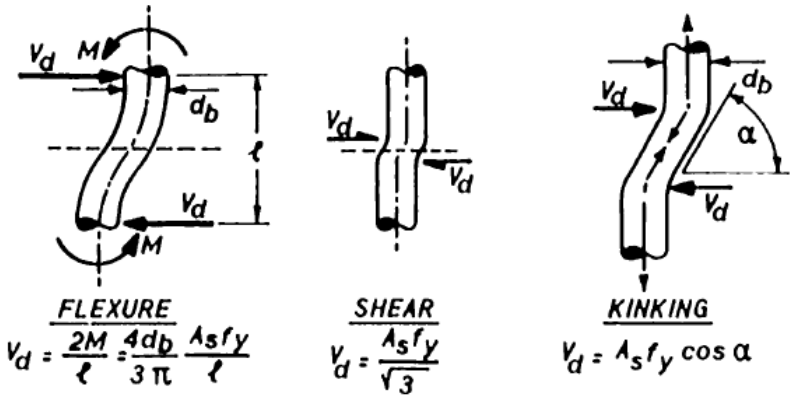

Figure 5-31. Mechanisms of Reinforcing Steel Dowel Action across Construction Joint (Paulay, et al., 1974)

Based on statistical analysis of their tests, Helgason et al (1976) arrived at the following equations to predict fatigue life of reinforcing bars under axial load:

$$logN = 6.9690 - 0.0383 f_r \quad (5\text{-}1)$$

$$logN = 6.9690 \pm 0.3586 - 0.0383 f_r \quad (5\text{-}2)$$

The curves these equations represent can be seen in Figure 2-1. Here N is the number of cycles at failure and f_r is the stress range. Equation 5-1 is a linear regression of the non-threshold portion of the S-N plots, while Equation 5-2 represents the tolerance limits where there is 95% probability of occurrence. Using the latter and N = 282,000 cycles, the stress range was bounded between 30.3 and 49.0 ksi (39.7 ksi mean).

These equations were developed from test data where the bars were embedded in beam-type concrete specimens that loaded the bars primarily in tension. The bar that failed in Specimen A was loaded in a combination of axial load due to jacking, axial stress due to slab bending and local bending stresses as shown by Park & Pauley. The failure initiated at the top of the bar. Theoretically the shear stress is zero at this location, therefore it is reasonable to ignore the contribution of shear to the driving stress range. This leaves the slab global flexure, local bar bending, and jacking-induced stresses as the contributing

components to the total stress range in the bar (see Figure 5-32). Note that this total stress range value is a change in stress from the high tensile stress already present in the top bar due to the sustained jacking force of 36 kips.

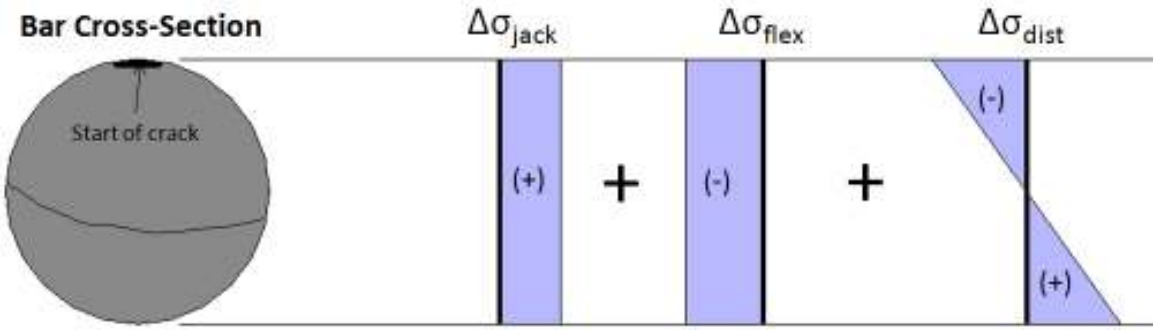

Figure 5-32. Components Affecting Stress Range at Location Where Crack Originated

The jacking and flexural stress components can easily be calculated. However, it is difficult to determine the local bending (distortion) stress component since the dowel action mechanism is uncertain. Section E.6 provides calculations to determine the local bending stress component based on the following relationship:

$$f_r = \Delta\sigma_{bend} + \Delta\sigma_{dist} - \Delta\sigma_{jack} \quad (5\text{-}3)$$

As anticipated, the local bending stress component was the primary driving factor since it contributes 84 percent of the total stress range. This confirms that an open joint with measurable shear deformations are critical for fatigue in a closure pour scenario. Since this is the result of one specimen, additional testing would be ideal for confirmation of the current results.

CHAPTER 6: CONCULSIONS & RECOMMENDATIONS

6.1 Conclusions

This testing program investigated a problem that has not been studied in the literature. The particular design of the I-81 closure joint does not provide any shear transfer between the concrete on either side of the joint. The joints were located between the supporting bridge girders and there was no bearing support at the joint. Therefore, all shear and moment across the joint was being carried by the reinforcing steel. Under wheel loads on the bridge deck, the reinforcing bars were subjected to a combination of axial force due to bending of the slab, direct shear, and local bending caused by shear deformation across the joint. In addition, shrinkage of the closure pour section relative to the adjoining slab sections caused the joints to open introducing axial shrinkage forces in the bars. The following text summarizes the conclusions drawn from the strength and fatigue tests.

Strength tests:

- The load versus displacement behavior of the I-81 slab specimens and the new cast specimens were similar. The I-81 slab specimens failed at higher loads that can partially be explained by differences in the concrete material properties. At least for the specimens tested, it can be concluded that the I-81 bridge slabs did not have reduced strength versus the new cast specimens. This indicates there is no significant reduction in strength due to corrosion or other internal damage.
- The strength test specimens did not fail at the construction joints. The cracks that defined the failure mode appeared to initially develop as shear cracks in the closure pour concrete, followed by a transition to flexural cracks in the I-81 specimens. The shear cracks began outside of the load patch and spread underneath the load patch as they propagated up in the specimens. Although the slab specimens were tested in one-way bending, the failure pattern is similar to what is observed taking a slice through a punching shear failure in a two-way slab test.

- Based on observation of the failure mode of the strength tests, it can be concluded that the critical failure plane was not the construction joint. A strength failure initiated by a wheel overload would be expected to result in a typical punching shear failure in the closure pour section. The 3 ft square section that failed in the I-81 bridge deck failed at the construction joints and a transverse crack across the closure pour. This mode differs from that observed in the strength tests. Therefore, it appears unlikely that the I-81 slab failure was caused by strength if the reinforcing steel was undamaged or mildly damaged.
- The most likely cause of failure in the I-81 deck was degradation of the reinforcing bars across the construction joint. Observations of the failure indicated severe section loss due to corrosion in some bars and relatively new, shear-type failures of other bars. The fact that the deck lasted 17 years indicates that degradation of the bars was probably a gradual process. It is known that corrosion is a time dependent degradation process. The strength tests indicate that shear-type failure of the bars is unlikely. Therefore, the reasonable conclusion is that some of the reinforcing bars failed by fatigue. Unfortunately the fracture surfaces were too damaged by contact and surface corrosion to verify this conclusion using fractography.
- There was no measurable shear displacement across the construction joints in the strength tests that did not have the joints jacked open. The test with the clearly open joint did experience shear deformation across the joint. Since the loading configuration was the same for both tests, this indicates that there was shear transfer between the concrete faces of the joint due to friction or interface contact in the un-jacked specimens. This makes it difficult to determine stress in the reinforcing steel since the proportions of shear force carried by the steel bars and the concrete is not known.

Fatigue tests:

- The first I-81 slab specimen test that was cycled under an 8 kip simulated wheel load did not experience failure after 10^7 load cycles. The slab specimens were tested in one-way bending compared to the two-way bending expected in the I-81

bridge deck. Under an actual wheel load on the bridge deck the slab specimen strip would be subjected to only a portion of the wheel load. Using an equivalent slab width, it was determined that the required wheel load required for the test specimens was about 5 kips. Therefore, the 5 kip load can be considered approximately equivalent to the AASHTO 16 kip wheel load on the bridge slab. However, the test load was set at half the AASHTO wheel load, 8 kips, for testing purposes.

- The load was increased to 16 kips (full wheel load) for the second and third tests of the I-81 slab specimens. Again, no failures occurred after 10^7 load cycles. Considering the proportions of the test specimens relative to the deck slab, 16 kips can be considered to be an artificially high wheel load.
- No differential shear deflection was observed across the construction joint in the three I-81 slab specimen tests. Lack of such deformation indicates that the effects of direct shear and local bending on the reinforcing bars are minimal. The calculated axial stress range in the top reinforcing bar due to bending across the joint is 8.68 ksi for both the 8 kip and 16 kip wheel loads. This value is below the 21.3 ksi fatigue threshold predicted in the literature.
- The new cast slab fatigue specimen had the construction joint jacked open to preclude any interface contact between the concrete. In this condition, about 0.01 in. of differential displacement was observed under the 16 kip wheel load. Under these test conditions, a 16 kip simulated wheel load caused fatigue failure of one of the reinforcing bars after 282,000 load cycles. Based on the mean prediction from the data in the literature, 282,000 cycles indicates a stress range of 39.7 ksi. Since the stress range due to primary bending across the joint is 8.68 ksi, it can be estimated that local bending effects accounted for 84 percent of the mean stress range in the reinforcing bar that failed.
- Openness of the construction joint appears to be the critical factor influencing fatigue life of the joint. The specimens from the I-81 bridge did not experience fatigue failure even though the joints were not tightly closed. There was enough frictional and interface contact to allow the concrete to carry shear forces across the joint. When concrete contact was prevented by jacking open the new

specimen, fatigue failure was observed in the test. Joint openness, for the purpose of shear transfer across the joint, is difficult to measure. Even vertical faces of the construction joint have some roughness and interface contact.

- Differential vertical displacement of the construction joint is an indirect measure of the openness of the joint and the ability of the concrete to provide shear transfer. The specimens with no measurable vertical displacement across the joint (less than 0.0007 in.) did not experience fatigue failure. The specimen with measurable vertical displacement across the joint (0.01 in) did experience fatigue failure.

Measurement of vertical differential deflection across the construction joint appears to be a viable means to assess fatigue vulnerability of construction joints in the field. This can be easily measured using a steel plate with a dial indicator mounted on a magnetic base. The indicator can be placed to span across the joint. A vehicle can then be positioned to place a wheel load adjacent to the gage location. No deflection indicates a low potential for fatigue. A vertical deflection across the joint within the resolution of the dial indicator indicates that fatigue is a possible concern for the future. Unfortunately, the scope of this research program was insufficient to establish a more accurate deflection threshold for fatigue.

6.2 Recommendations

The results of this research study present the need for further research of the influence of fatigue in the bars crossing construction joints. Unfortunately, it was only possible to implement the ideal conditions for fatigue failure (open joint) to one test specimen. While the resulting fatigue failure of the test specimen indicates the possibility of a fatigue failure in a bridge deck with a closure pour scenario—given the right conditions—a definitive conclusion cannot be drawn without additional testing. Future research could involve testing similar specimens with the joints opened to different degrees. This would determine the critical joint width where the magnitude of the shear deformations would become significant. A statistical analysis of the data could result in a formula for design.

A field testing program to monitor joint deflection under wheel loads can be implemented based on the conclusions drawn from the test results. This program could incorporate the procedure described in the final conclusion of the fatigue tests in the previous section. A significant differential joint deflection would indicate the possibility of fatigue damage of the reinforcing bars.

REFERENCES

[1] Sprinkel, M. M., Weyers, R., Blevins, C., Ramniceanu, A., and Weyers, S. A. (2010). "Failure and Repair of Deck Closure Pour on Interstate 81." *Transportation Research Record: Journal of the Transportation Research Board*, 2150(-1), 119-128.

[2] Dowling, N. E. (2007). *Mechanical Behavior of Materials : Engineering Methods for Deformation, Fracture, and Fatigue*, Pearson/Prentice Hall, Upper Saddle River, N.J.

[3] Helgason, T., and Hanson, J. "Investigation of Design Factors Affecting Fatigue Strength of Reinforcing Bars-Statistical Analysis." *Proc., Abeles Symposium on Fatigue of Concrete*, ACI Publications SP-41, 107-138.

[4] Wight, J. K., and MacGregor, J. G. (2009). *Reinforced Concrete: Mechanics and Design*, Prentice Hall, Upper Saddle River, N.J.

[5] Helgason, T., Hanson, J. M., Somes, N. F., Corley, W. G., and Hognestad, E. (1976). "Fatigue Strength of High-Yield Reinforcing Bars." *NCHRP Report*(164).

[6] Rabbat, B. G., and Corley, W. G. (1984). "Long-Time Fatigue Properties of High Yield Reinforcing Bars." *Materials and Structures*, 17(1), 35-38.

[7] Corley, W. G., Hanson, J. M., and Helgason, T. (1978). "Design of Reinforced Concrete for Fatigue." *Journal of the Structural Division*, P. C. Association, ed., American Society of Civil Engineers, 921-932.

[8] MacGregor, J. G., Jhamb, I. C., and Nuttall, N. "Fatigue Strength of Hot Rolled Deformed Reinforcing Bars." ACI.

[9] Abbas, E. K. (2011). "Corrosion Assessment for Failed Bridge Deck Closure Pour." Virginia Polytechnic Institute and State University.

[10] AASHTO (2010). *AASHTO LRFD Bridge Design Specifications*, American Association of State Highway and Transportation Officials, Washington, D.C.

[11] Gilbert, R. I. (1992). "Shrinkage Cracking in Fully Restrained Concrete Members." *ACI Structural Journal*, 89(2).

[12] ACI "Building Code Requirements for Structural Concrete (ACI 318-08) and Commentary." American Concrete Institute.

[13] Park, R., and Paulay, T. (1975). *Reinforced Concrete Structures*, John Wiley & Sons Inc.

[14] Paulay, T., Park, R., and Phillips, M. H. (1974). "Horizontal Construction Joints in Cast-in-Place Reinforced Concrete." *ACI Special Publication SP-42: Shear in Reinforced Concrete*, 2, 599-611.

APPENDIX A- Individual Specimen Test Results

A.1 Strength Tests

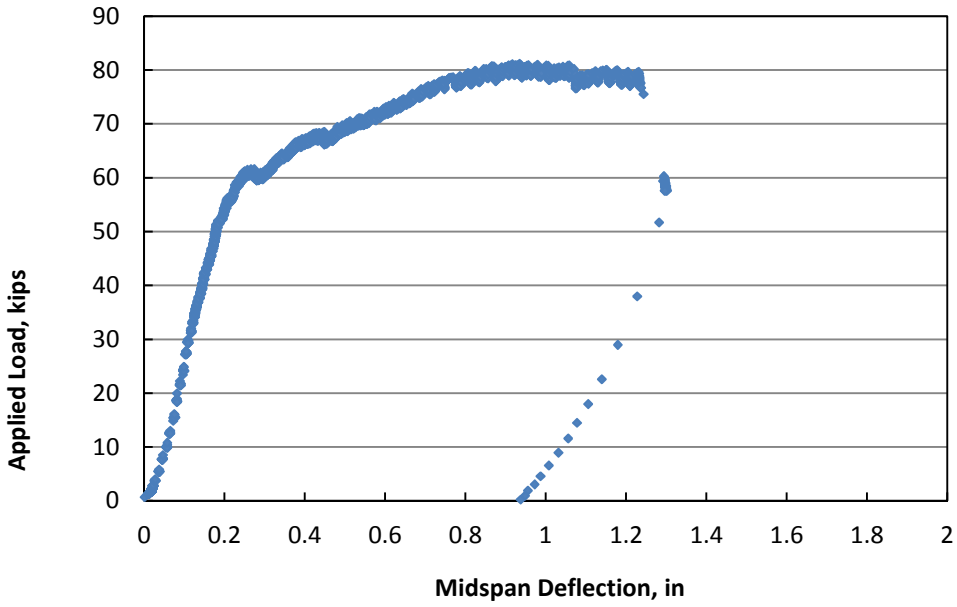

Figure A-1. Specimen 1 Applied Load versus Midspan Deflection

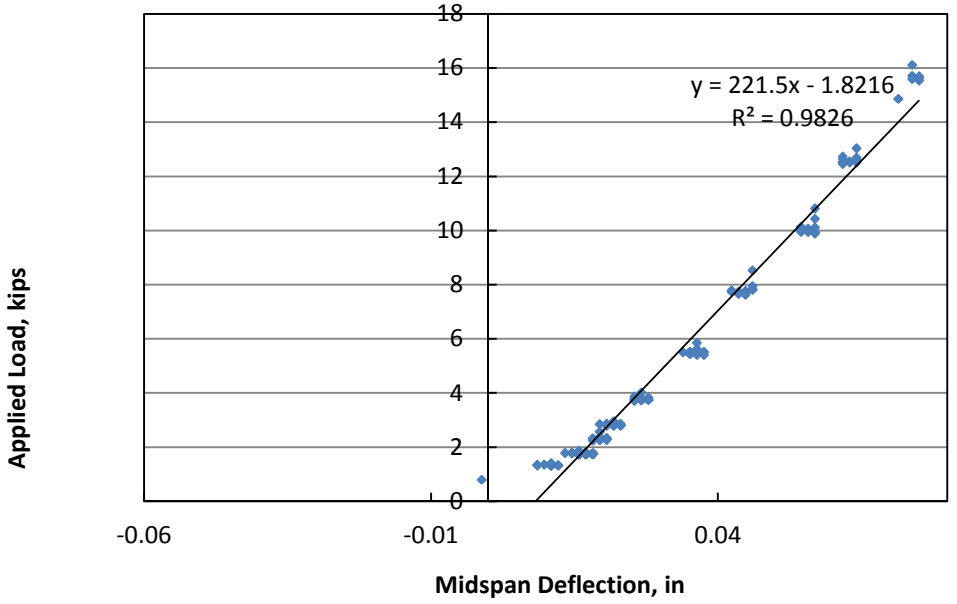

Figure A-2. Specimen 1 Stiffness from Applied Load versus Midspan Deflection

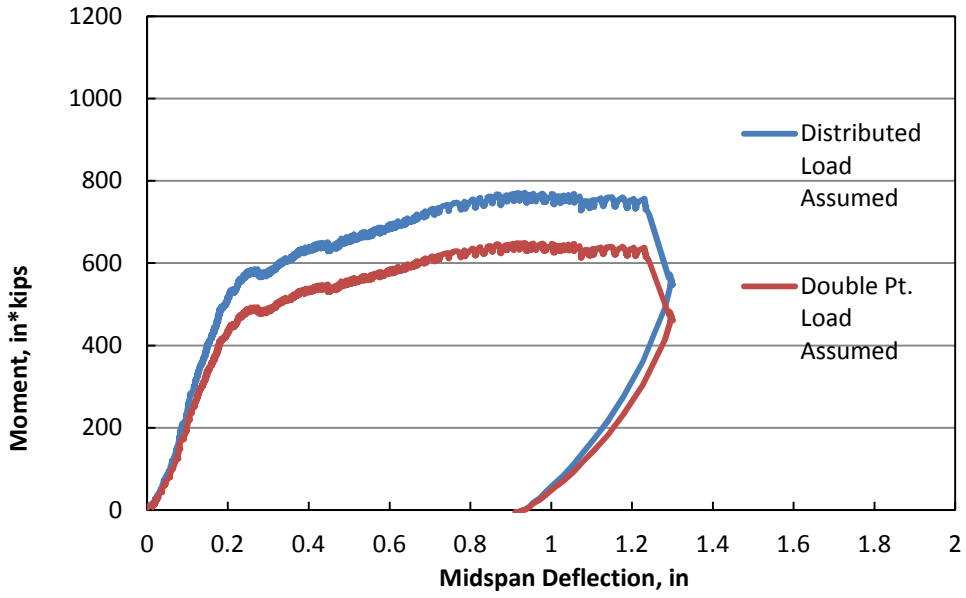

Figure A-3. Specimen 1 Bounded Moment at Midspan versus Midspan Deflection

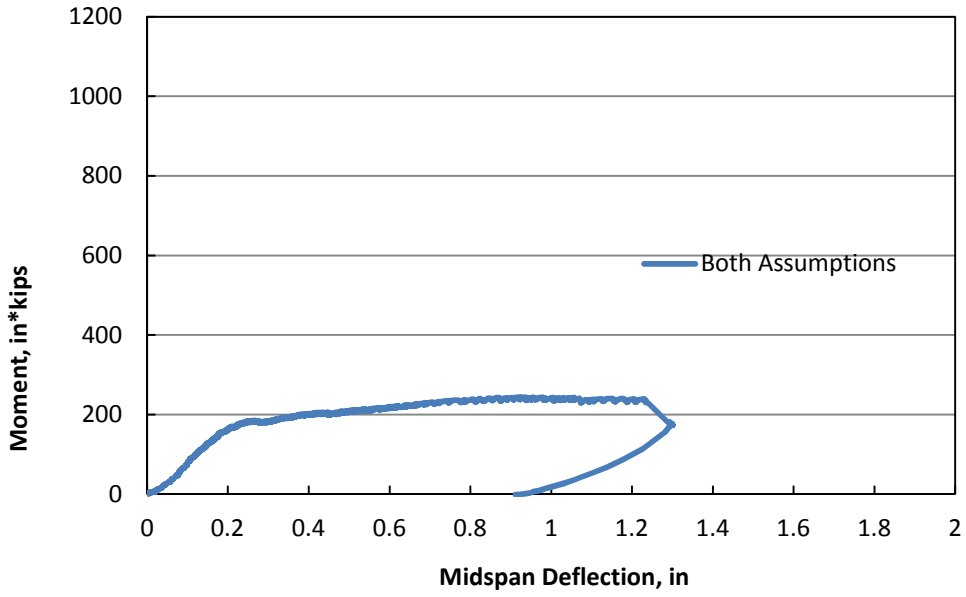

Figure A-4. Specimen 1 Bounded Moment at Joints versus Midspan Deflection

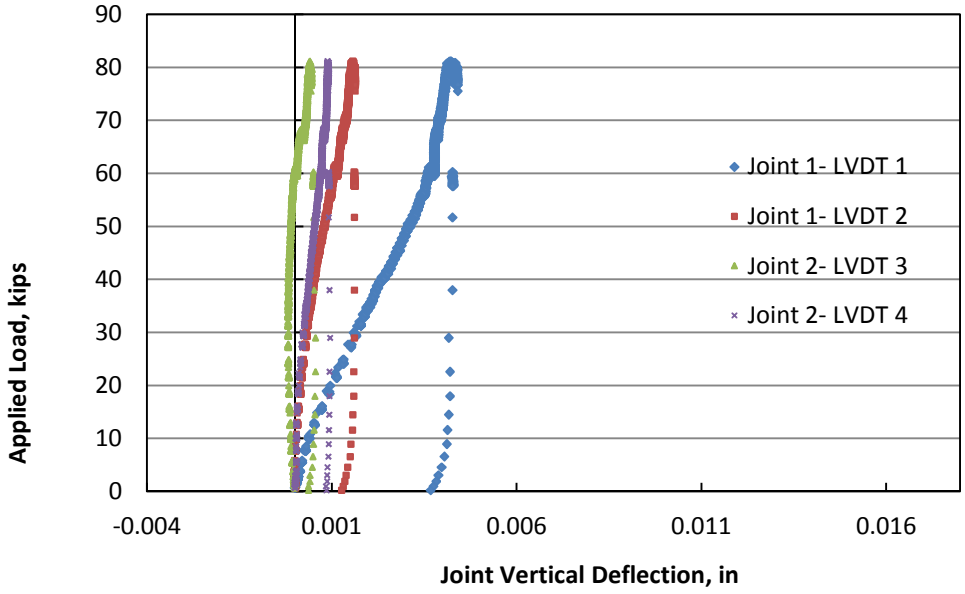

Figure A-5. Specimen 1 Vertical Joint Differential Deflection

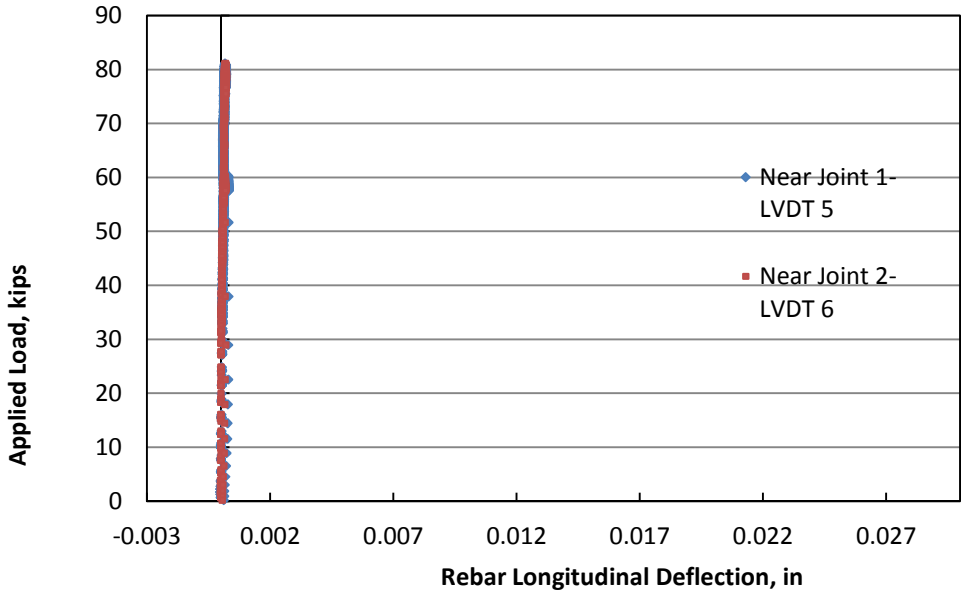

Figure A-6. Specimen 1 Bottom-Most Longitudinal Rebar Slip

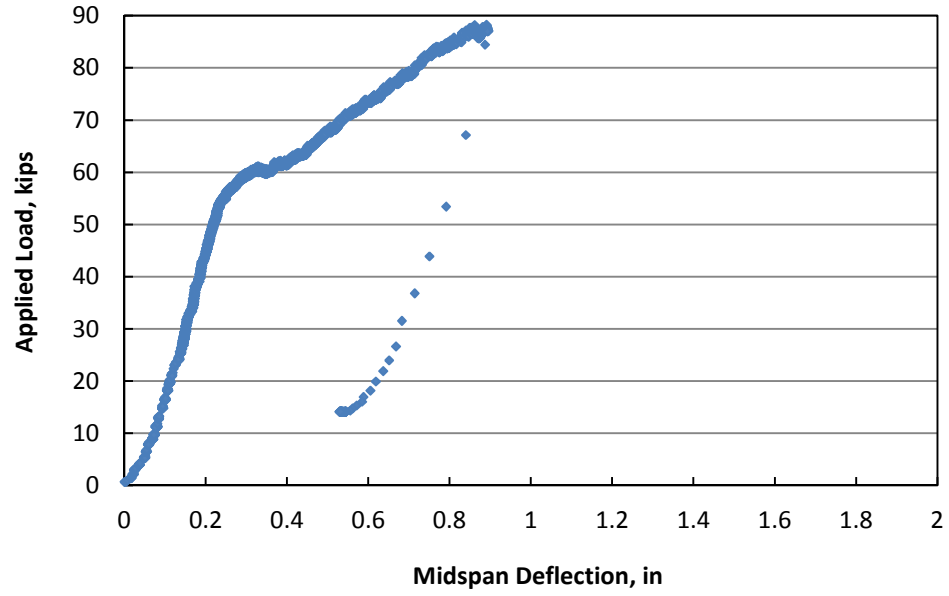

Figure A-7. Specimen 3 Applied Load versus Midspan Deflection

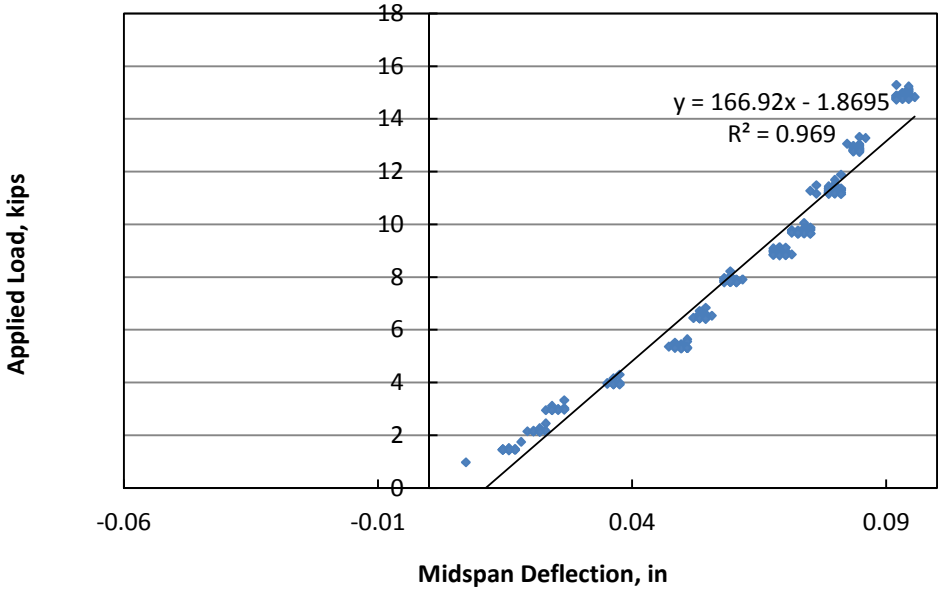

Figure A-8. Specimen 3 Stiffness from Applied Load versus Midspan Deflection

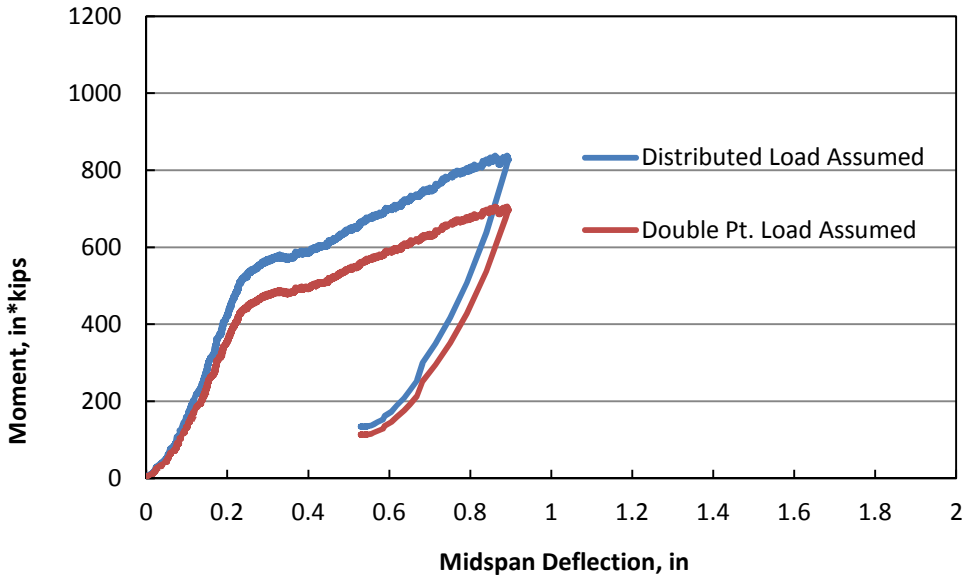

Figure A-9. Specimen 3 Bounded Moment at Midspan versus Midspan Deflection

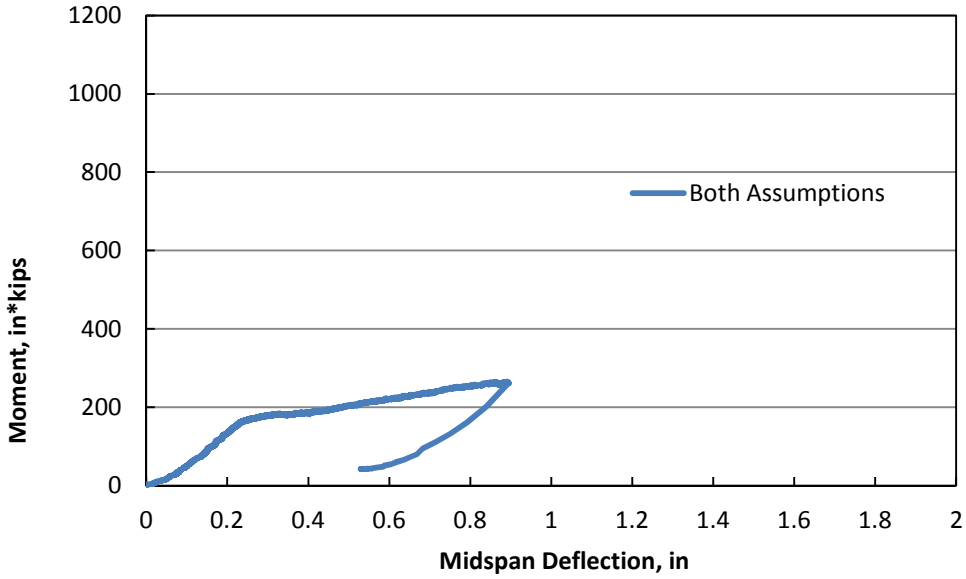

Figure A-10. Specimen 3 Bounded Moment at Joints versus Midspan Deflection

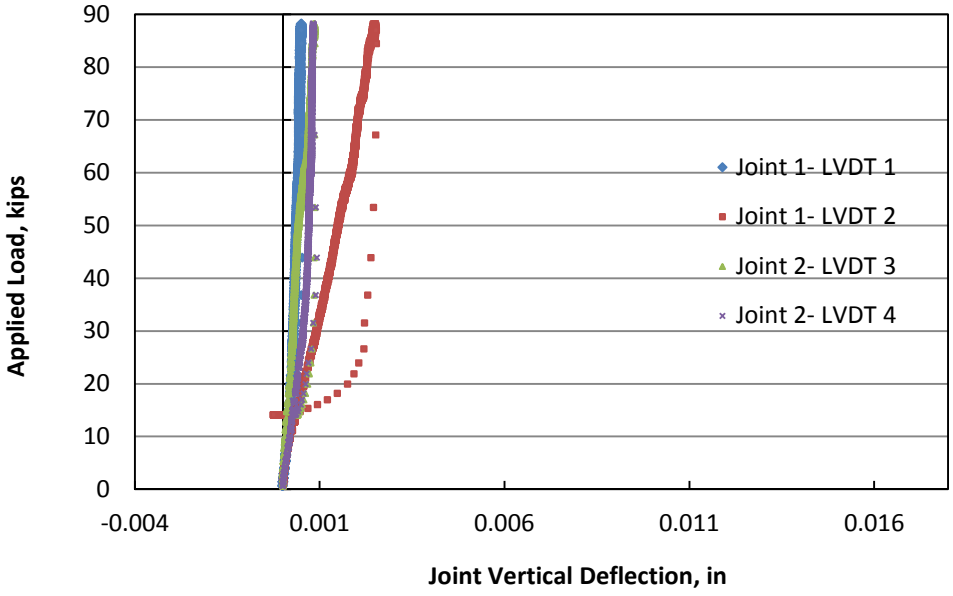

Figure A-11. Specimen 3 Vertical Joint Differential Deflection

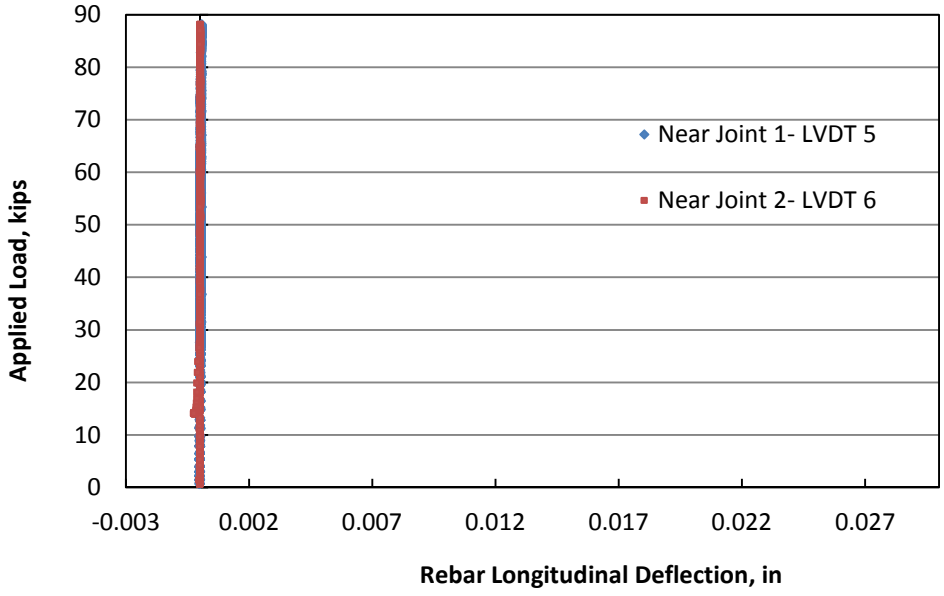

Figure A-12. Specimen 3 Bottom-Most Longitudinal Rebar Slip

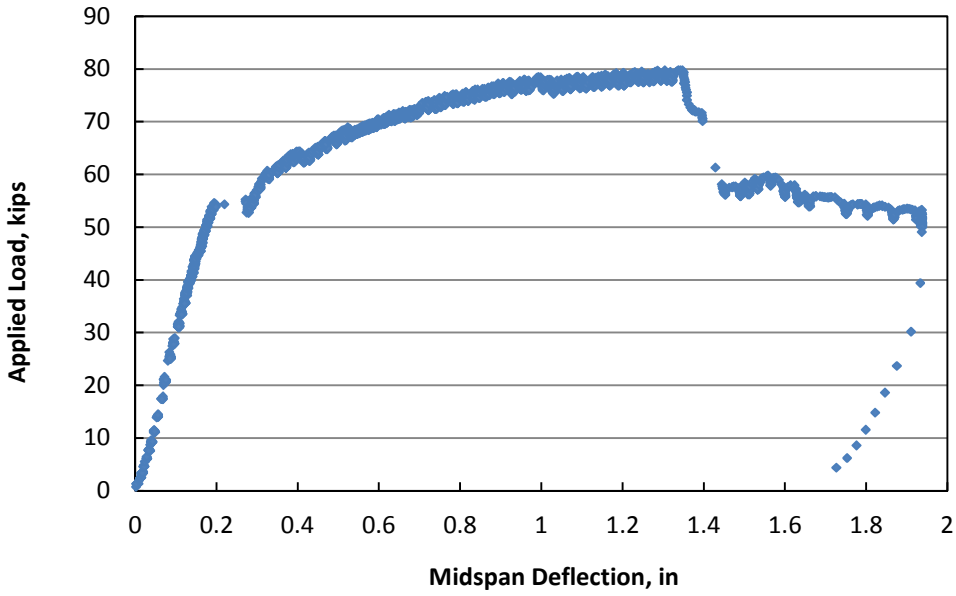

Figure A-13. Specimen 8 Applied Load versus Midspan Deflection

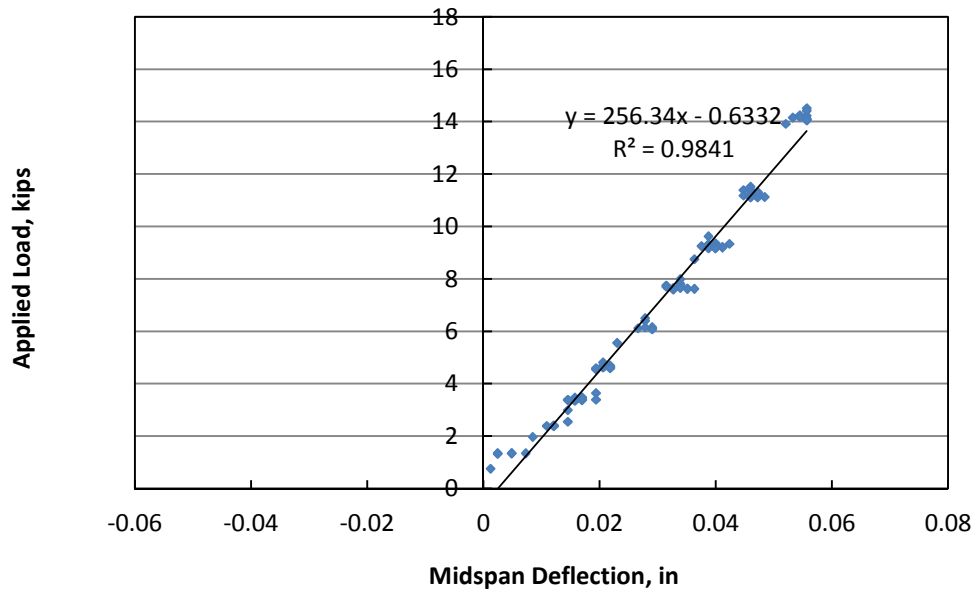

Figure A-14. Specimen 8 Stiffness from Applied Load versus Midspan Deflection

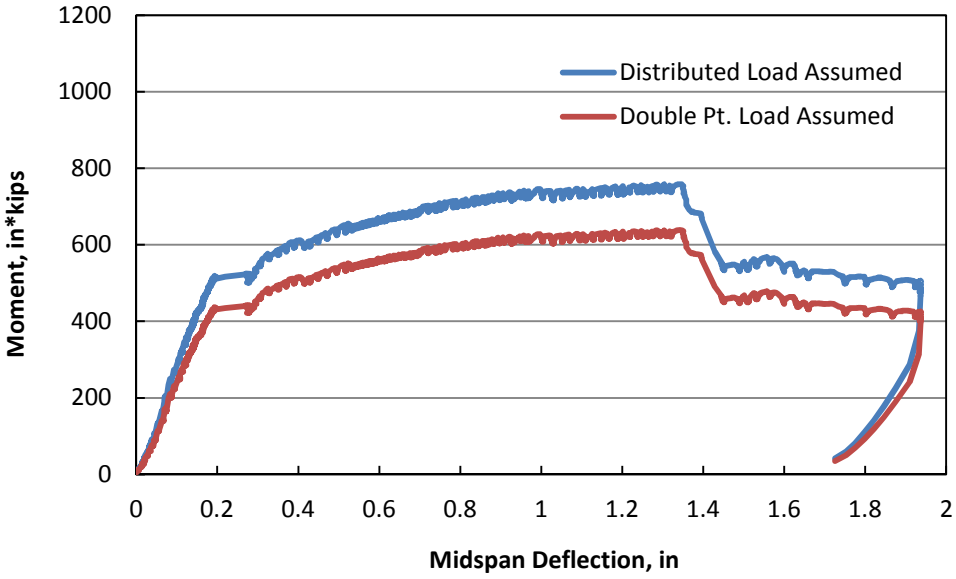

Figure A-15. Specimen 8 Bounded Moment at Midspan versus Midspan Deflection

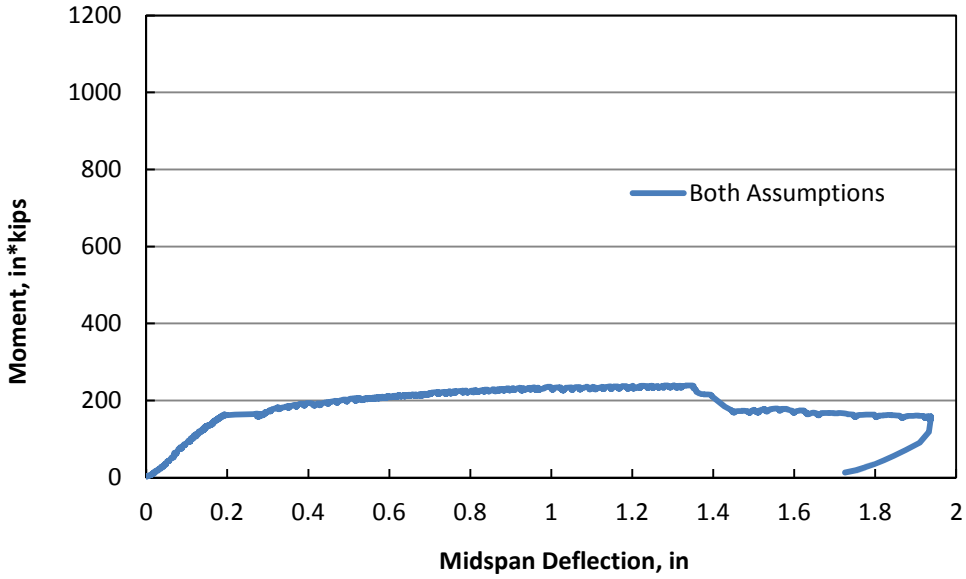

Figure A-16. Specimen 8 Bounded Moment at Joints versus Midspan Deflection

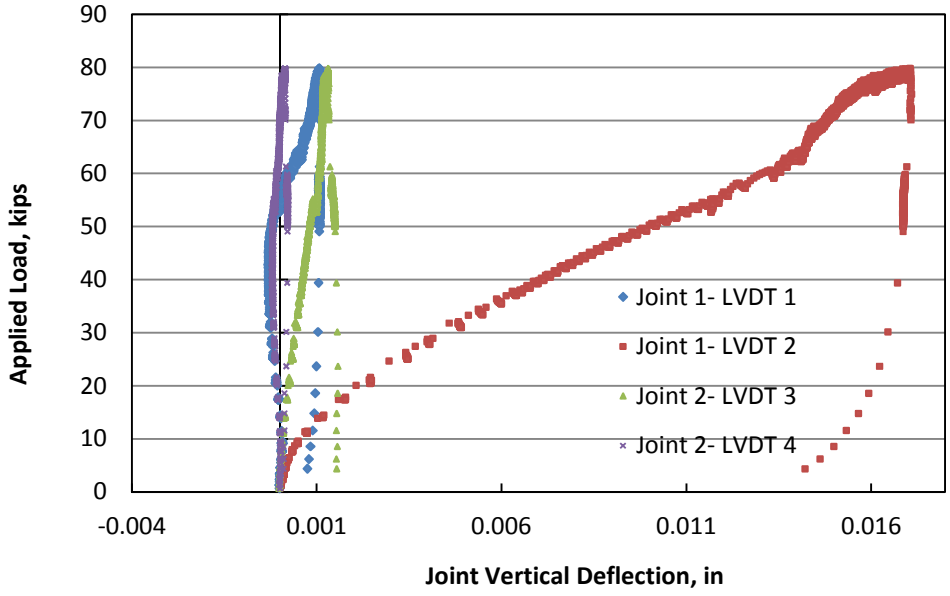

Figure A-17. Specimen 8 Vertical Joint Differential Deflection

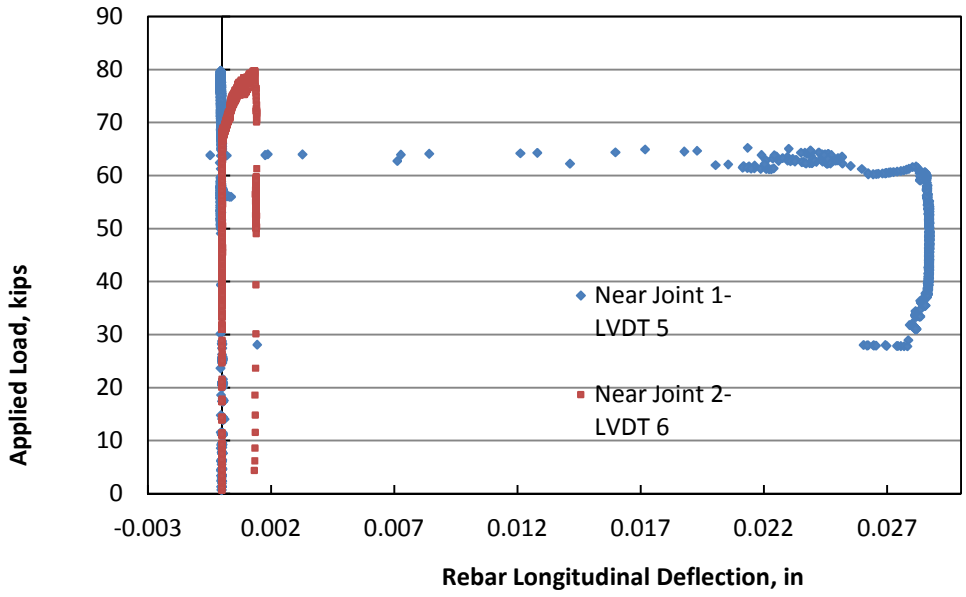

Figure A-18. Specimen 3 Bottom-Most Longitudinal Rebar Slip

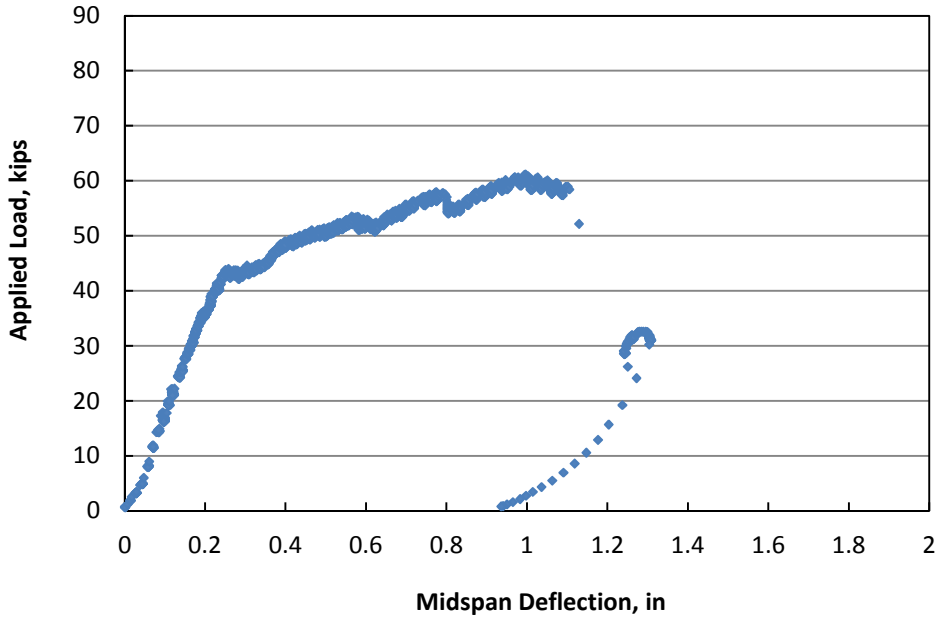

Figure A-19. Specimen C Applied Load versus Midspan Deflection

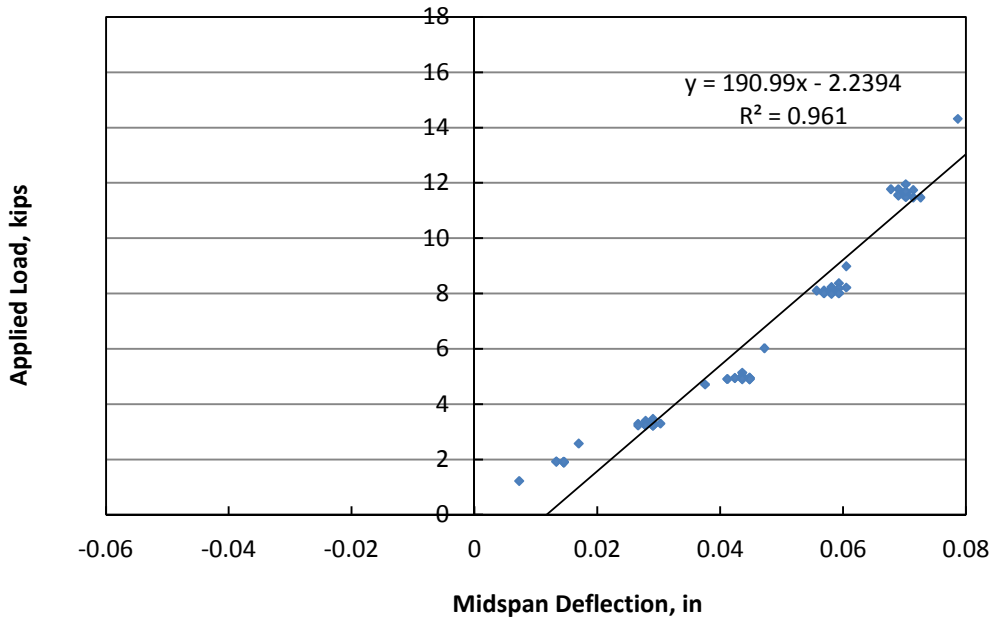

Figure A-20. Specimen C Stiffness from Applied Load versus Midspan Deflection

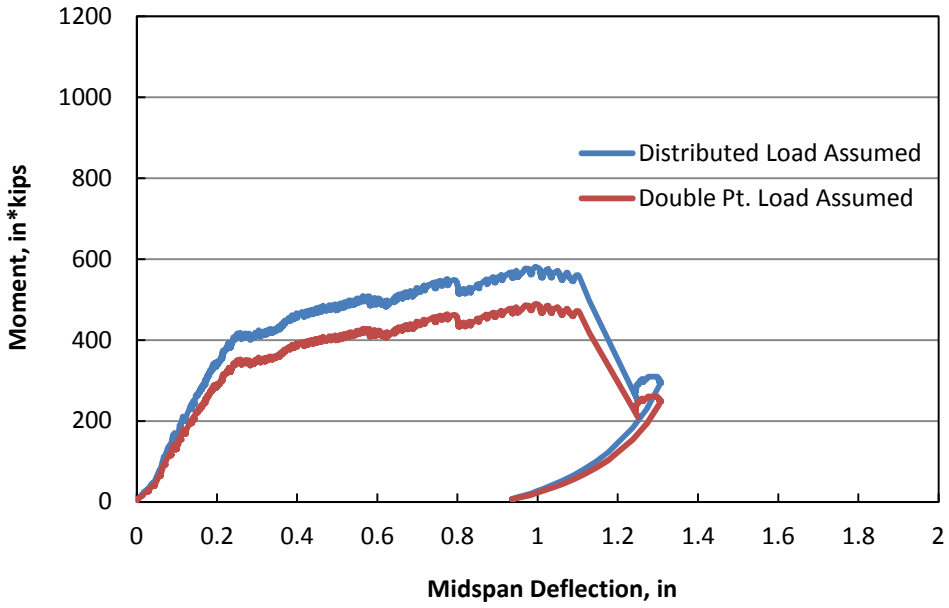

Figure A-21. Specimen C Bounded Moment at Midspan versus Midspan Deflection

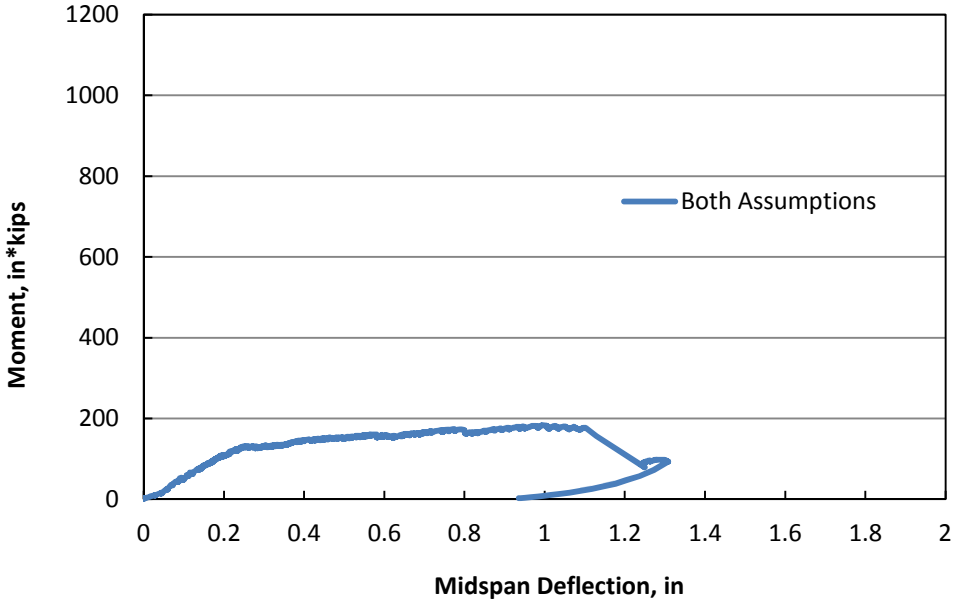

Figure A-22. Specimen C Bounded Moment at Joints versus Midspan Deflection

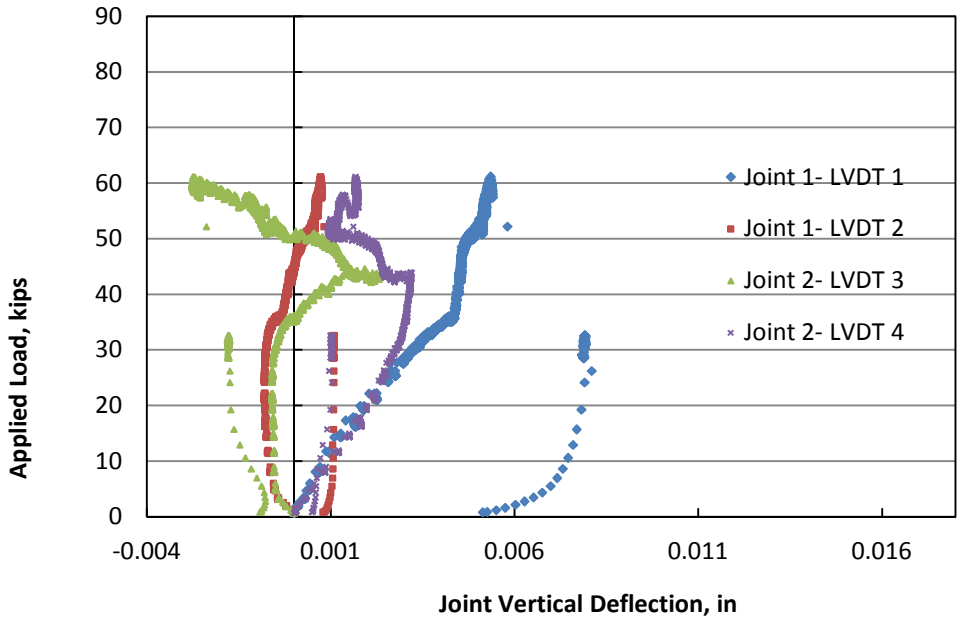

Figure A-23. Specimen C Vertical Joint Differential Deflection

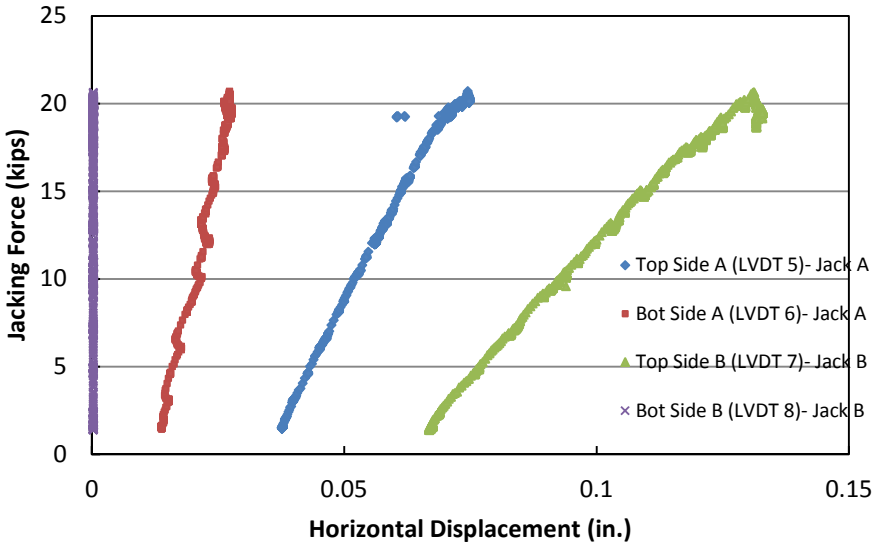

Figure A-24. Specimen B Jacking Before Testing- Joint 1

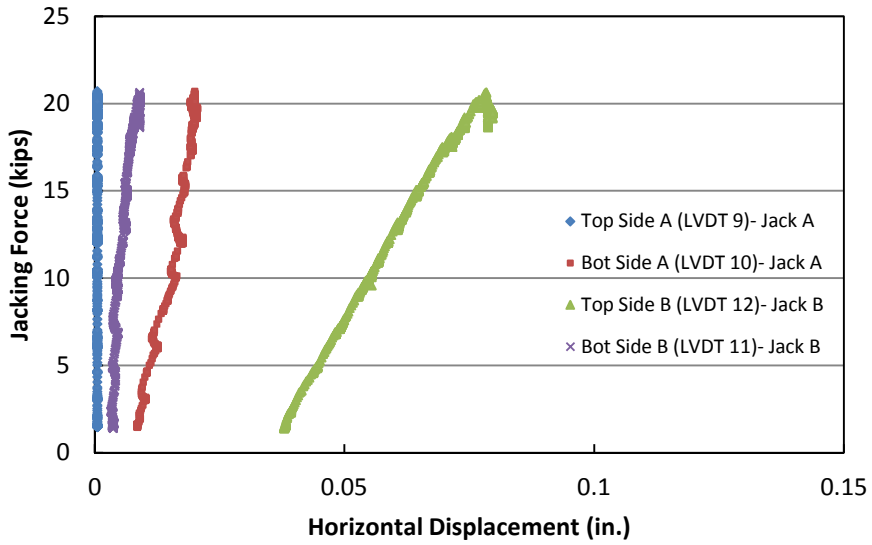

Figure A-25. Specimen B Jacking Before Testing- Joint 2

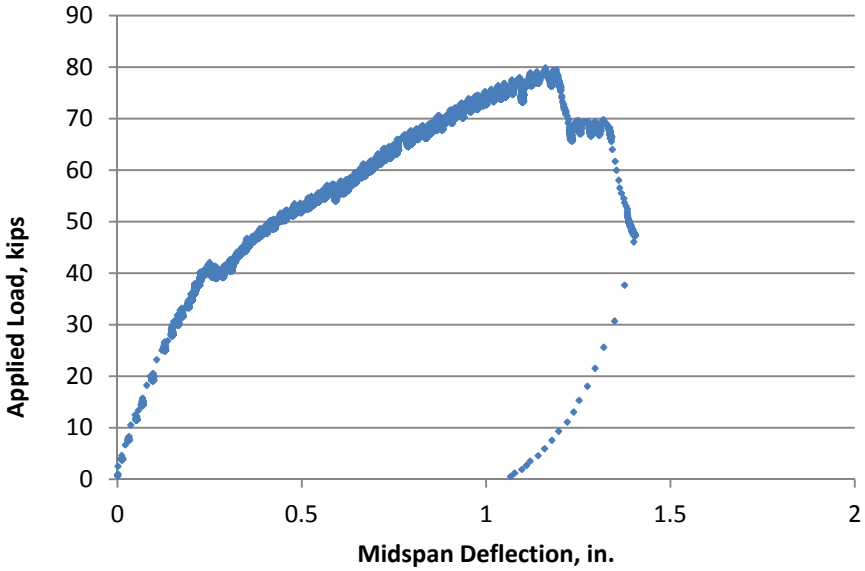

Figure A-26. Specimen B Applied Load versus Midspan Deflection

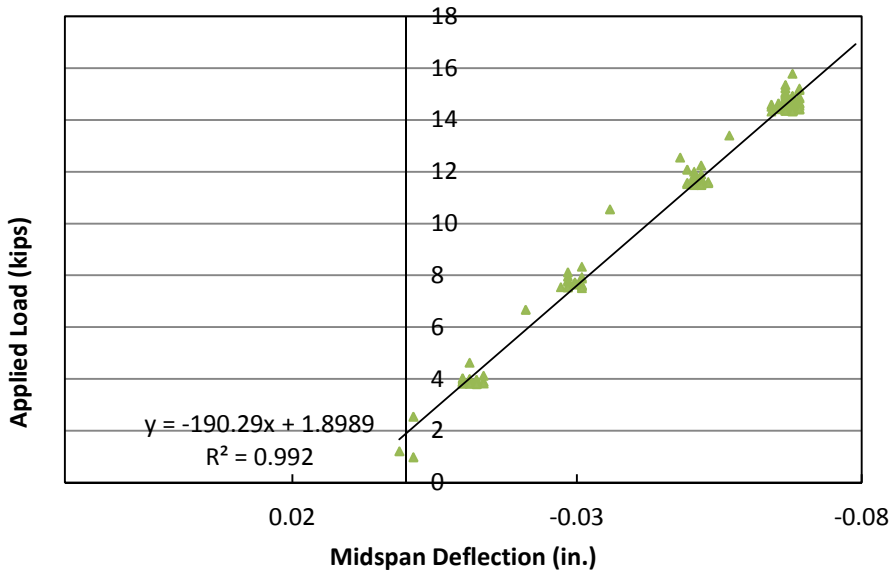

Figure A-27. Specimen B Stiffness from Applied Load versus Midspan Deflection

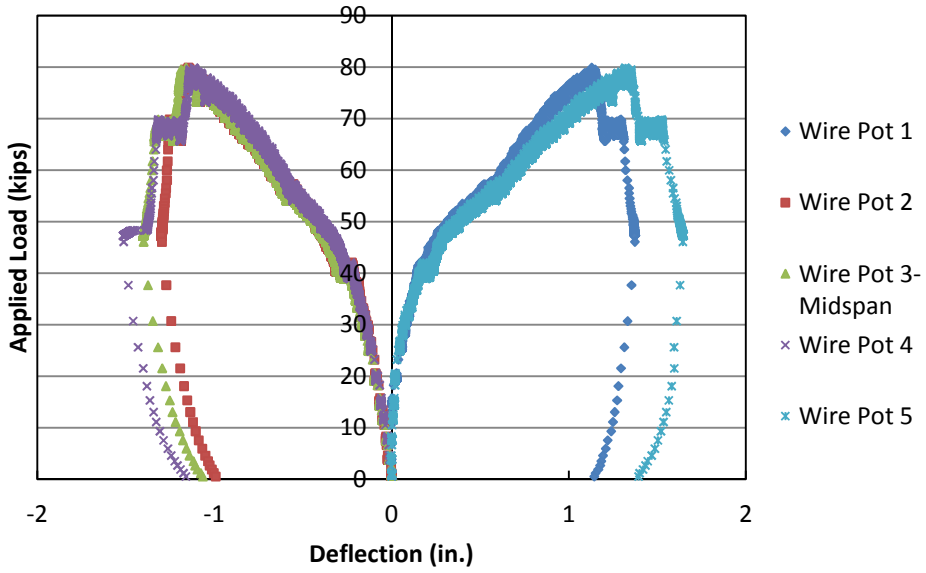

Figure A-28. Specimen B Applied Load versus Slab Deflection at Five Locations

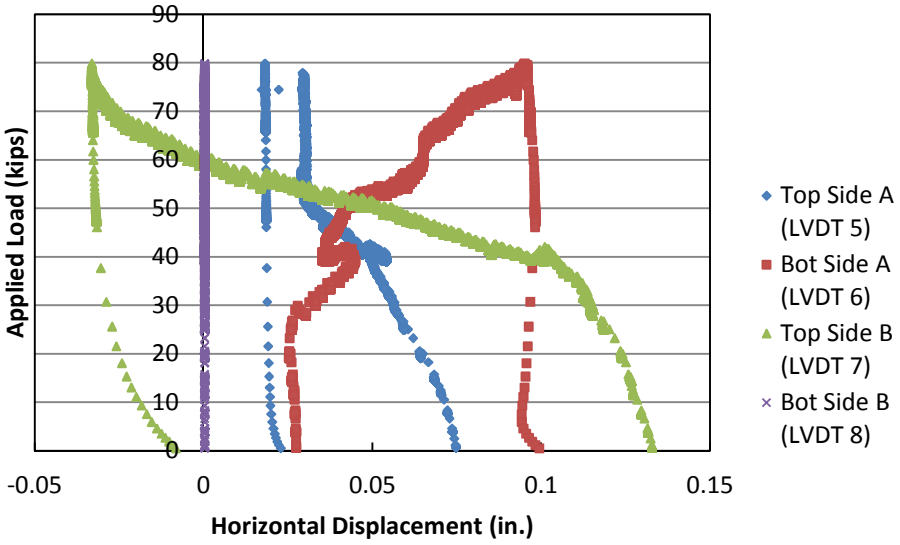

Figure A-29. Specimen B Joint 1 Horizontal Displacement

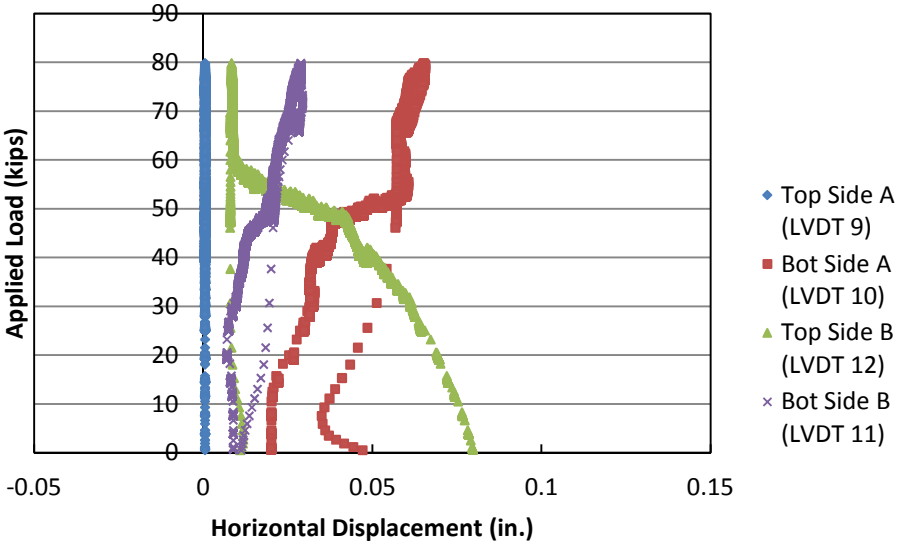

Figure A-30. Specimen B Joint 2 Horizontal Displacement

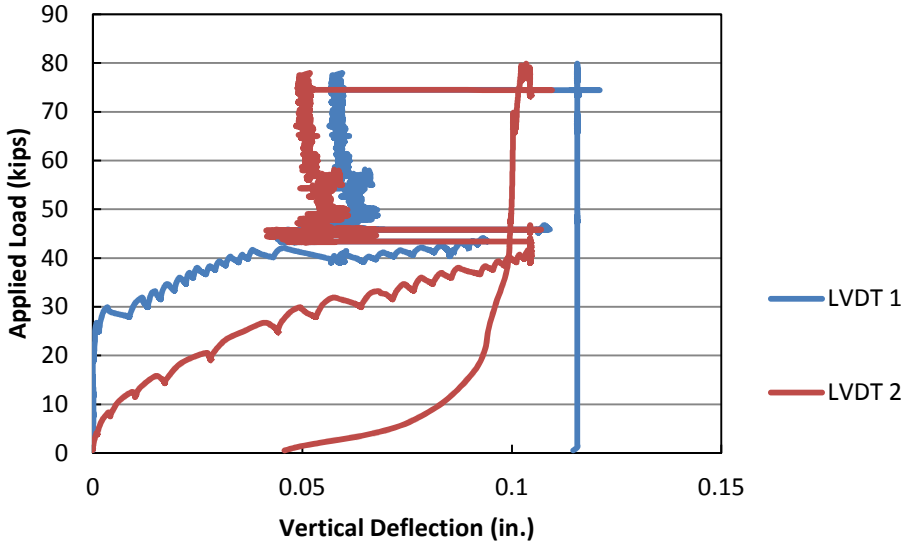

Figure A-31. Specimen B Vertical Joint Differential Deflection- Joint 1

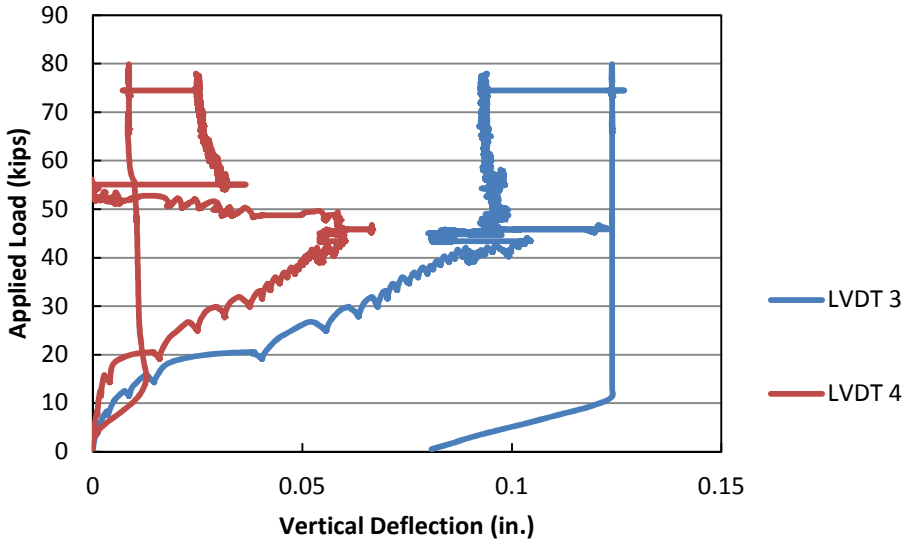

Figure A-32. Specimen B Vertical Joint Differential Deflection- Joint 2

A.2 Fatigue Tests

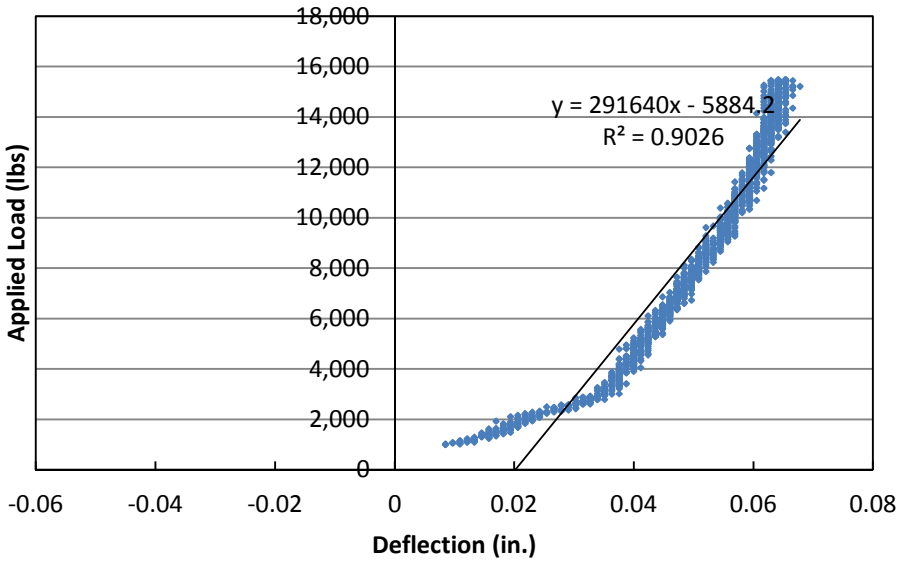

Figure A-33. Specimen 2 Stiffness at 1 Cycle

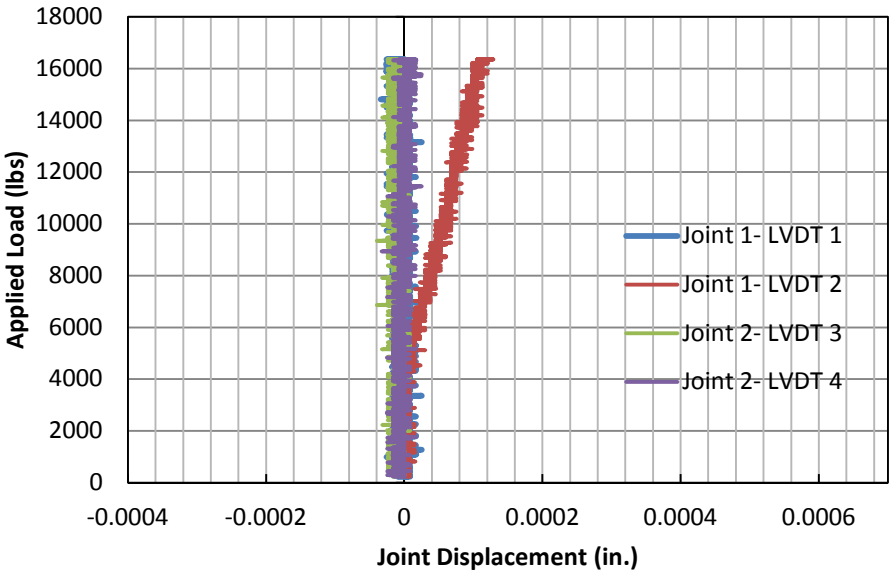

Figure A-34. Specimen 2 Vertical Joint Differential Deflection at 1 Cycle

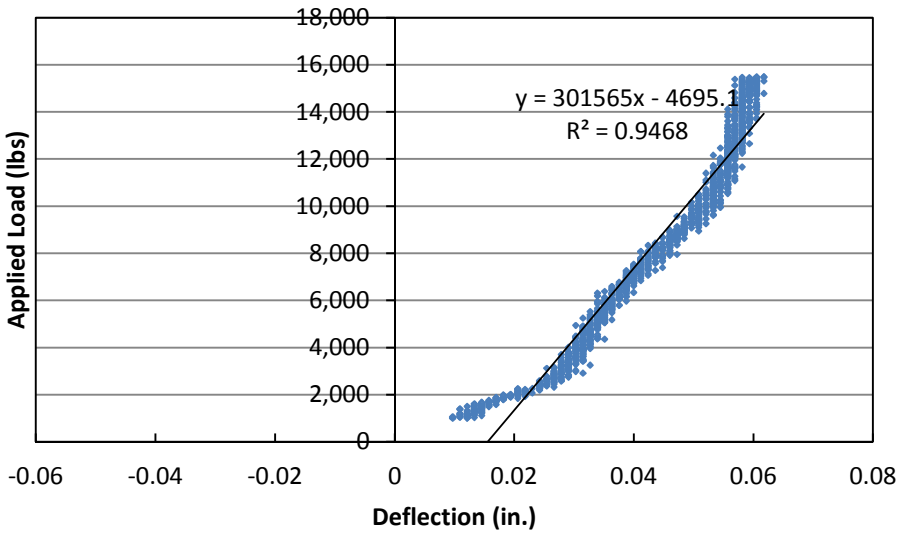

Figure A-35. Specimen 2 Stiffness at 1,000 Cycles

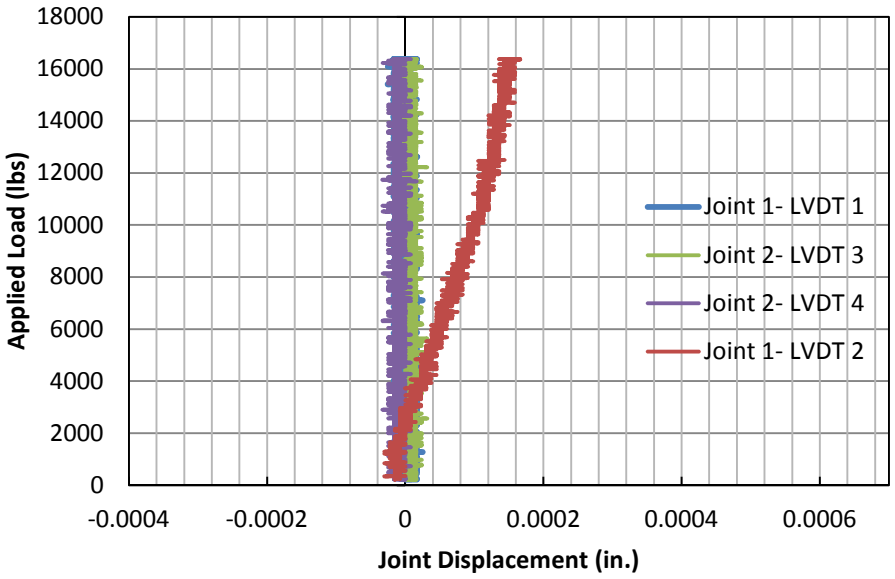

Figure A-36. Specimen 2 Vertical Joint Differential Deflection at 1,000 Cycles

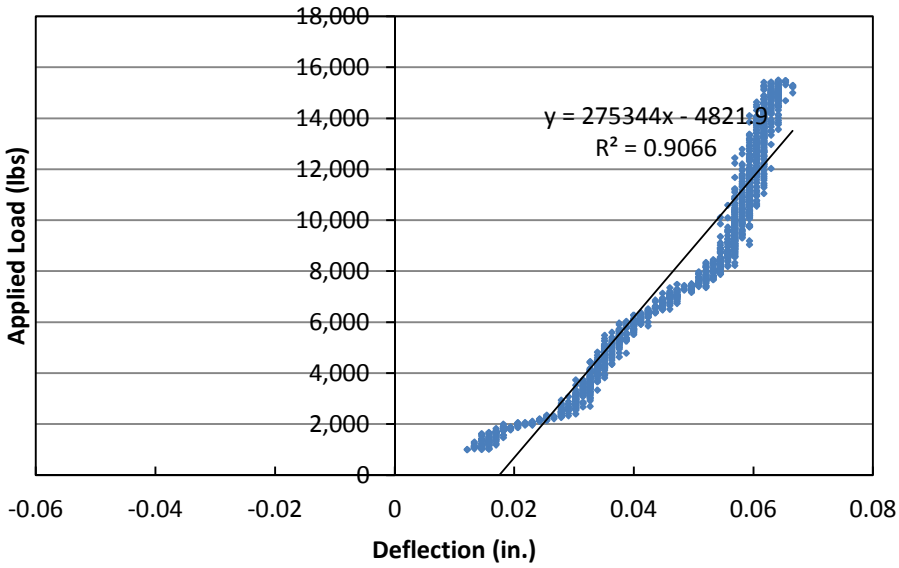

Figure A-37. Specimen 2 Stiffness at 10,000 Cycles

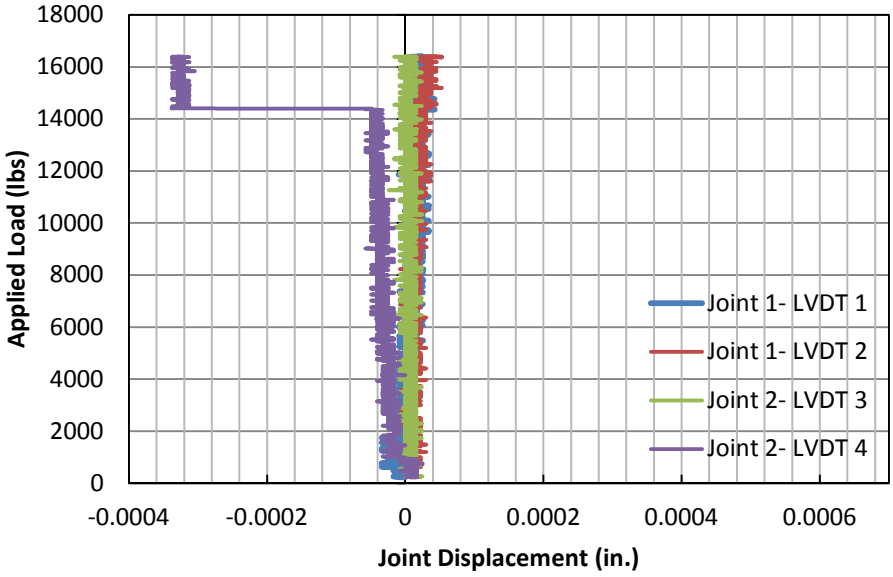

Figure A-38. Specimen 2 Vertical Joint Differential Deflection at 10,000 Cycles

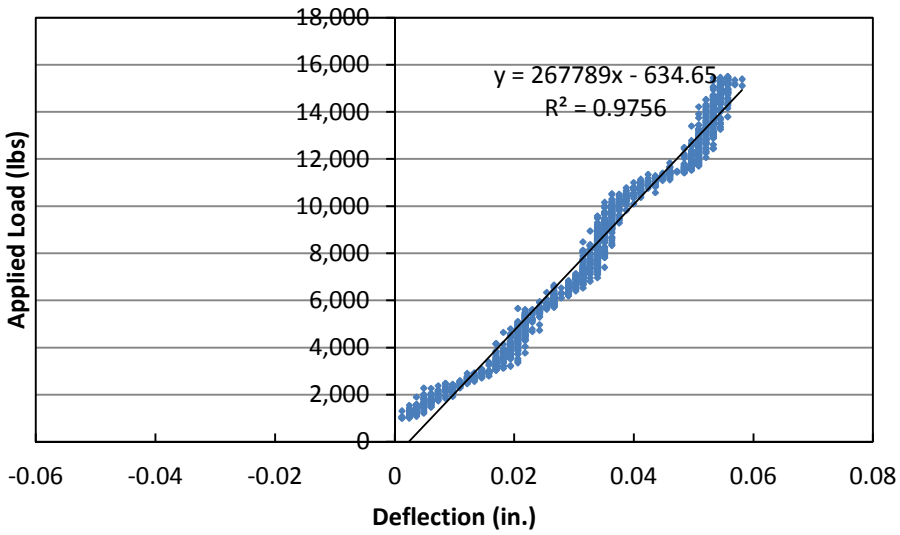

Figure A-39. Specimen 2 Stiffness at 100,000 Cycles

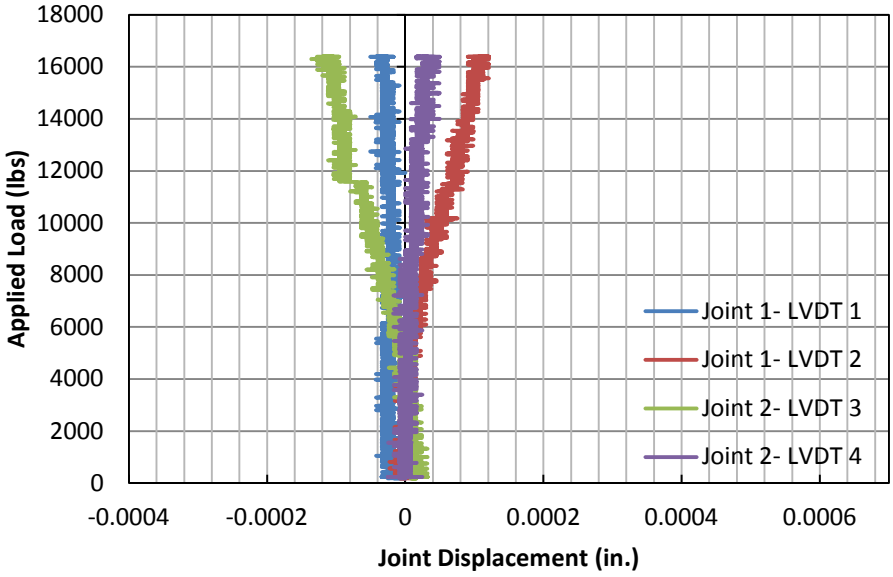

Figure A-40. Specimen 2 Vertical Joint Differential Deflection at 100,000 Cycles

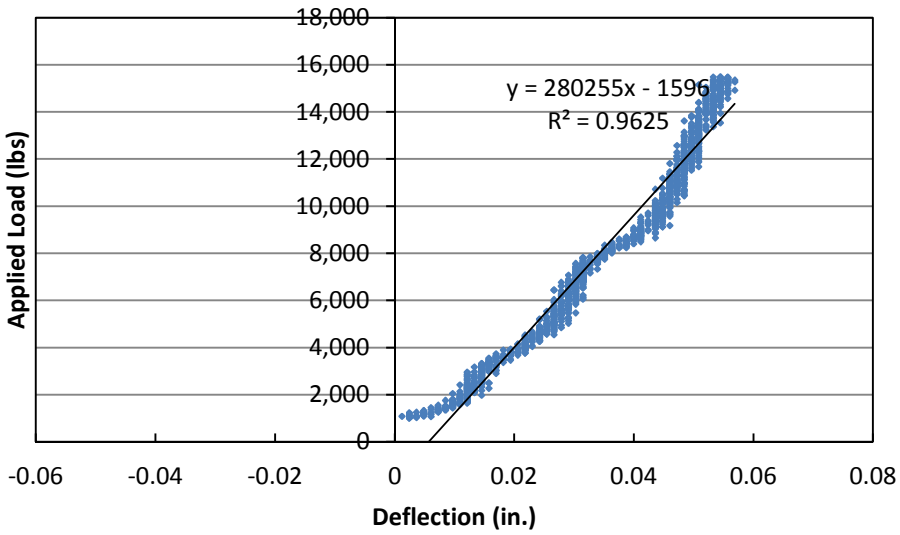

Figure A-41. Specimen 2 Stiffness at 1 Million Cycles

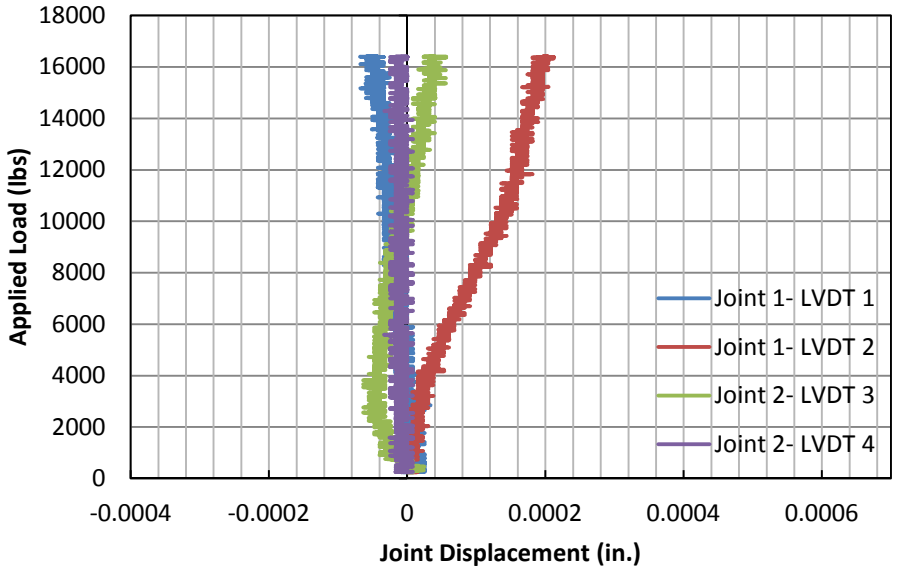

Figure A-42. Specimen 2 Vertical Joint Differential Deflection at 1 Million Cycles

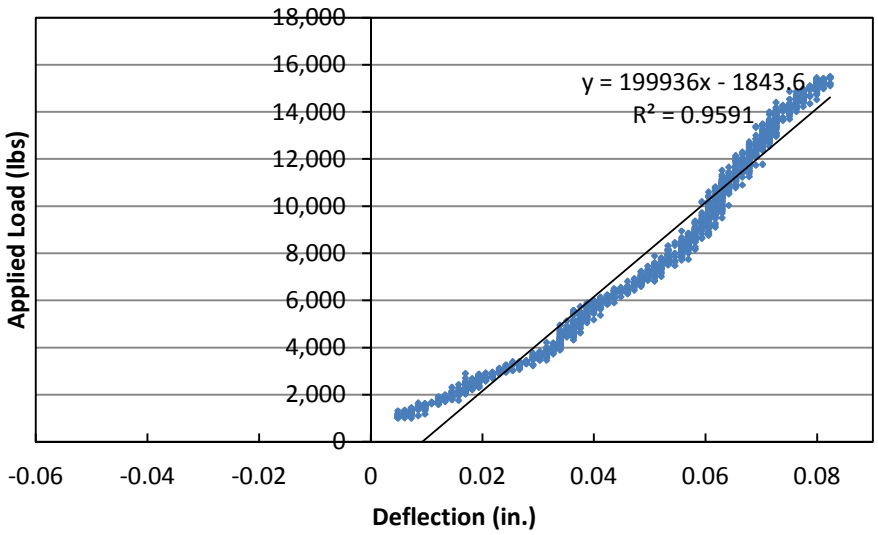

Figure A-43. Specimen 2 Stiffness at 10 Million Cycles

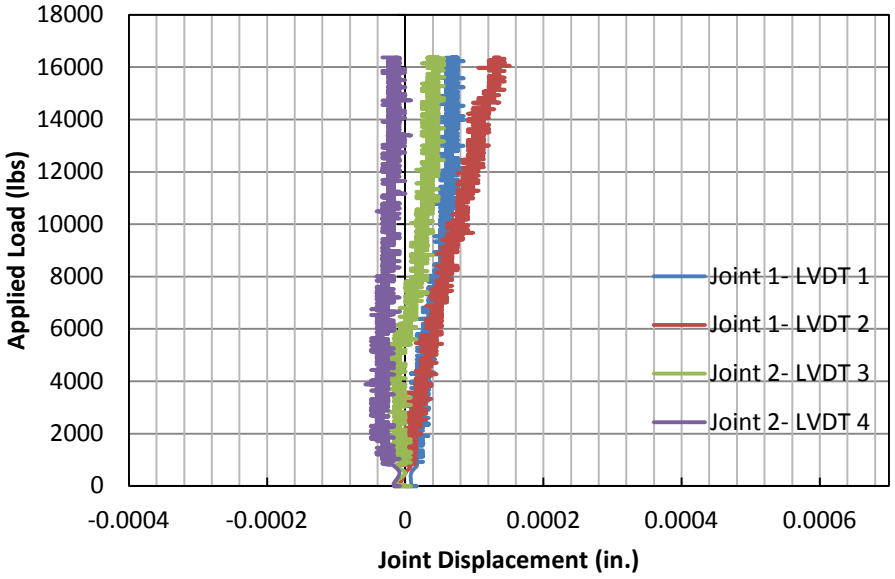

Figure A-44. Specimen 2 Vertical Joint Differential Deflection at 10 Million Cycles

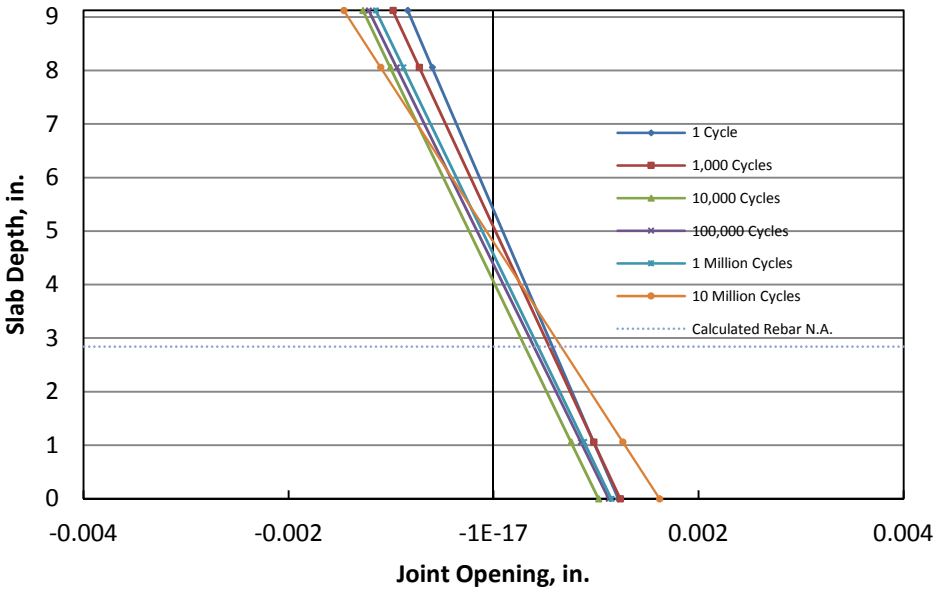

Figure A-45. Opening of Joint 1 (Specimen 2, Side A)

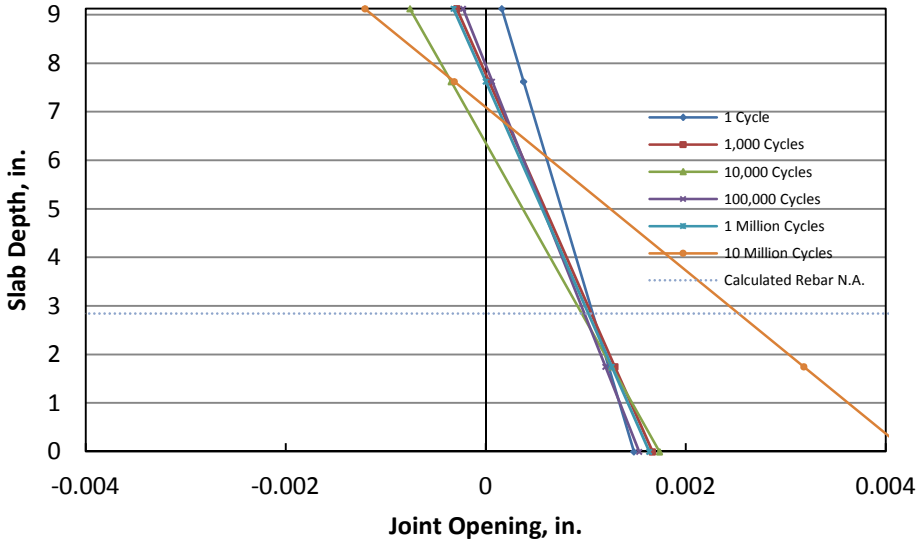

Figure A-46. Opening of Joint 1 (Specimen 2, Side B)

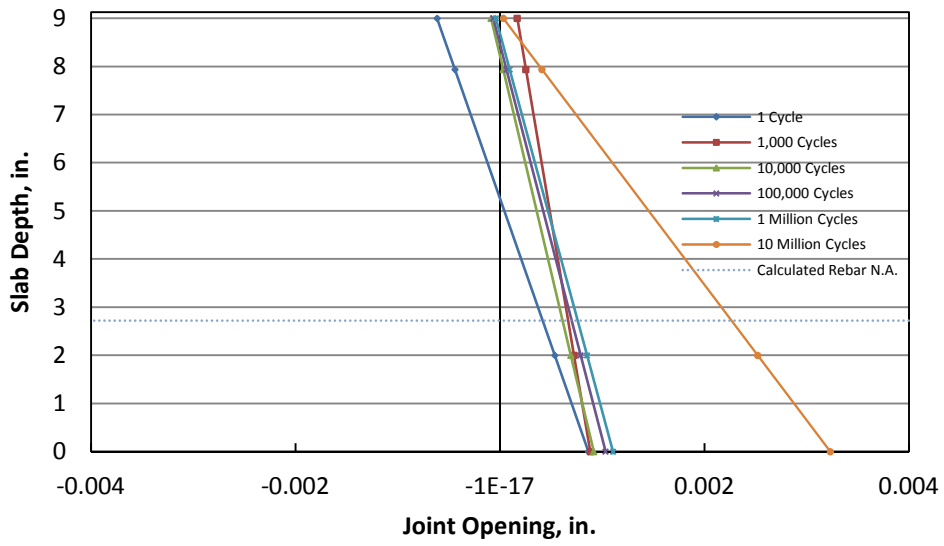

Figure A-47. Opening of Joint 2 (Specimen 2, Side A)

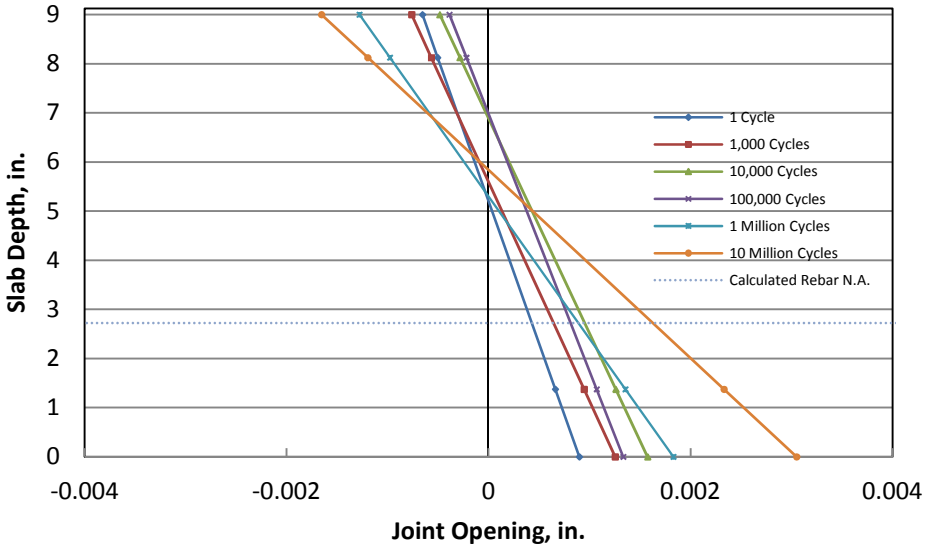

Figure A-48. Opening of Joint 2 (Specimen 2, Side B)

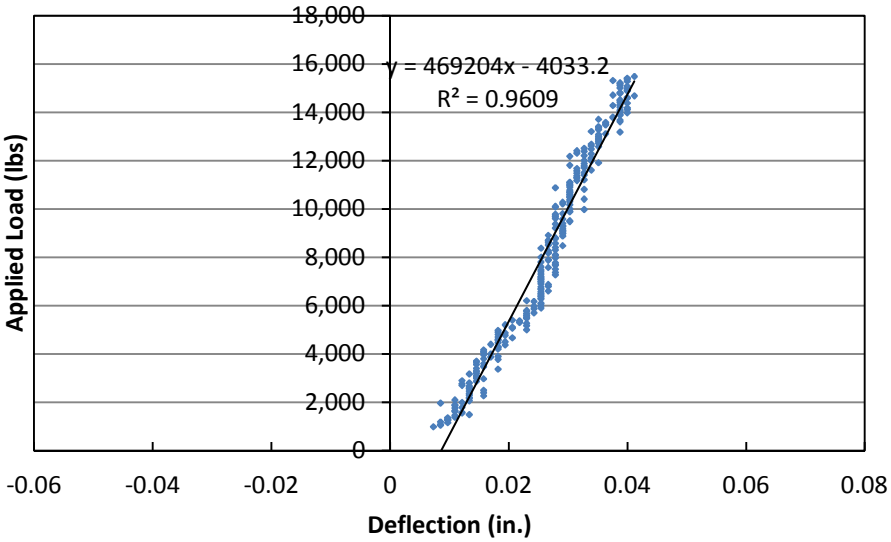

Figure A-49. Specimen 7 Stiffness at 1 Cycle

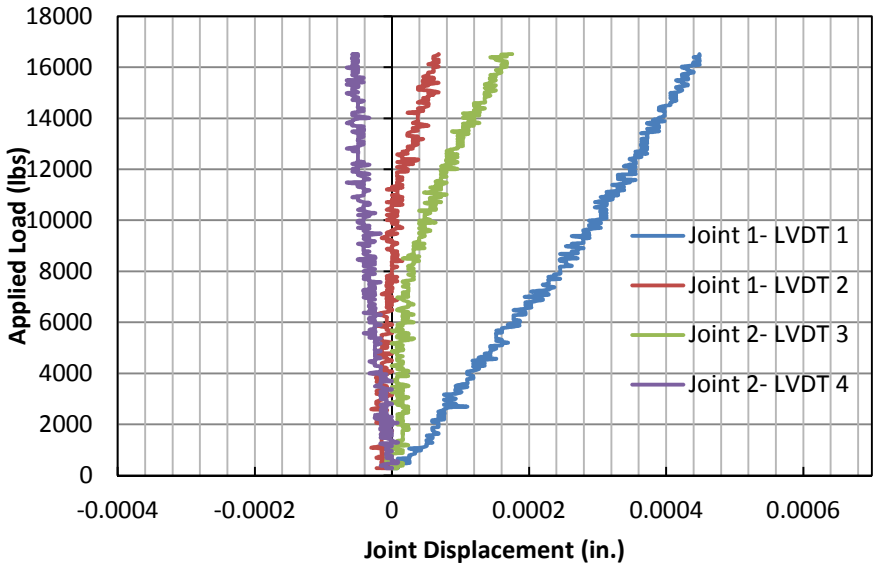

Figure A-50. Specimen 7 Vertical Joint Differential Deflection at 1 Cycle

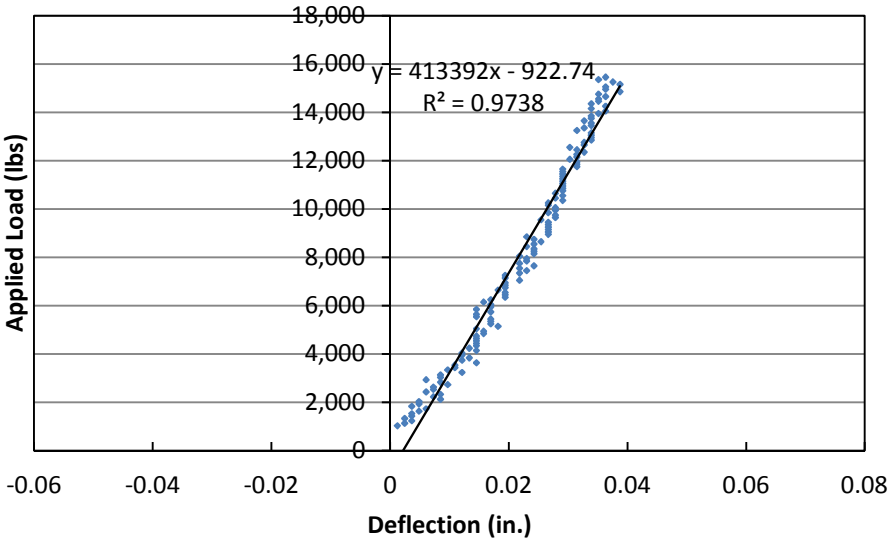

Figure A-51. Specimen 7 Stiffness at 1,000 Cycles

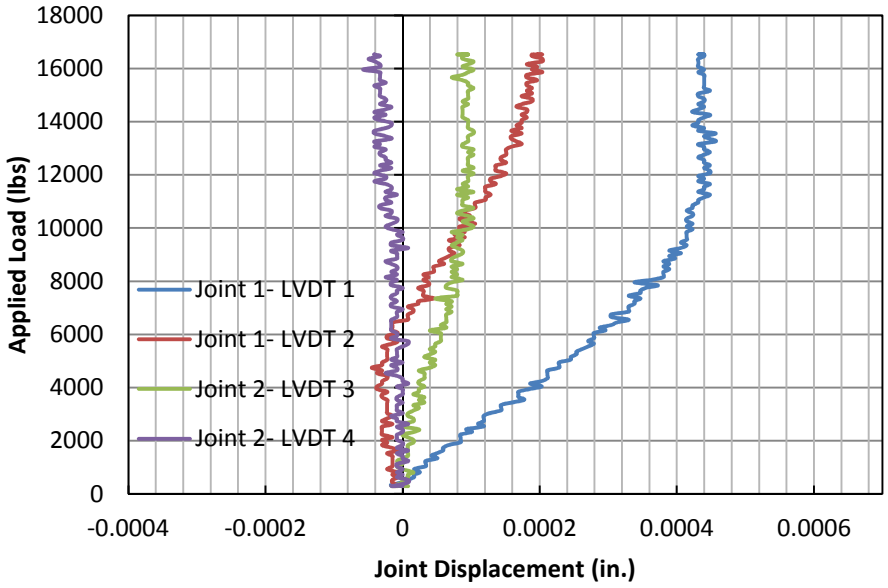

Figure A-52. Specimen 7 Vertical Joint Differential Deflection at 1,000 Cycles

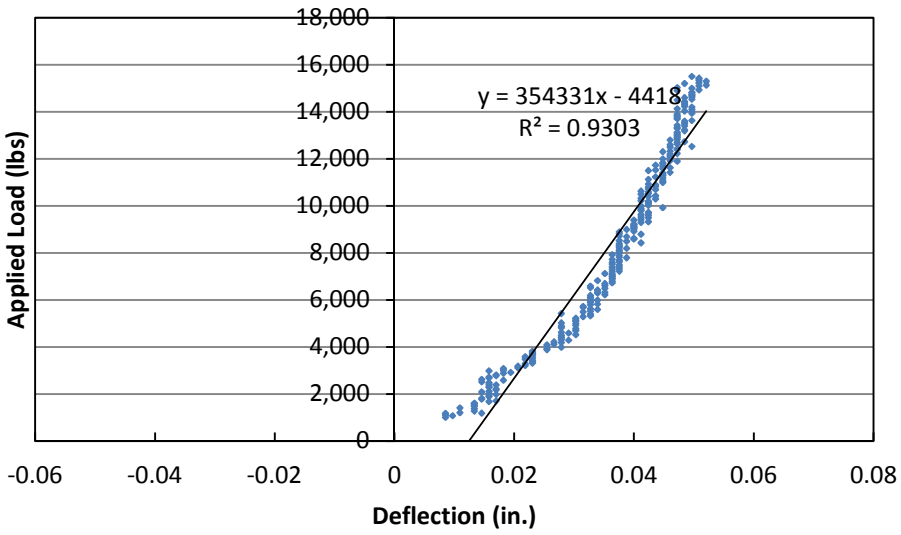

Figure A-53. Specimen 7 Stiffness at 10,000 Cycles

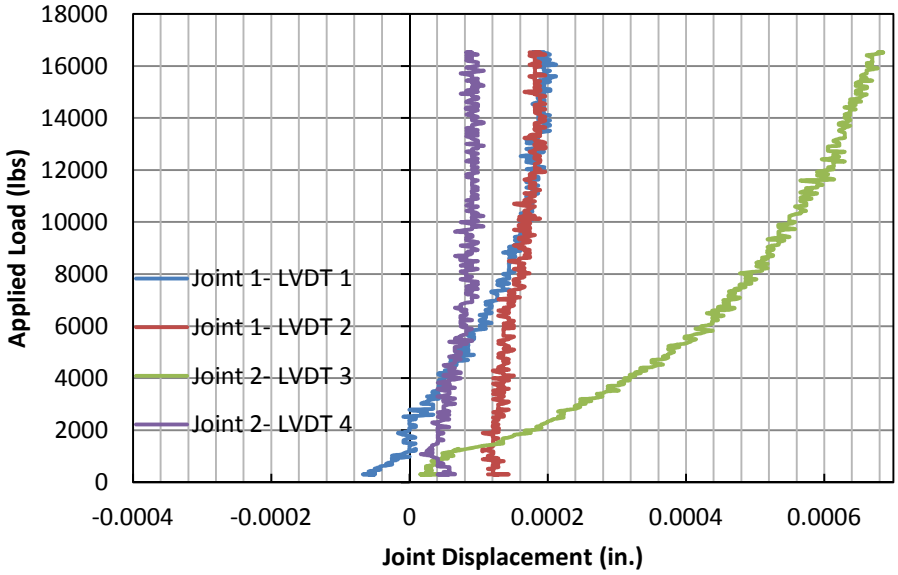

Figure A-54. Specimen 7 Vertical Joint Differential Deflection at 10,000 Cycles

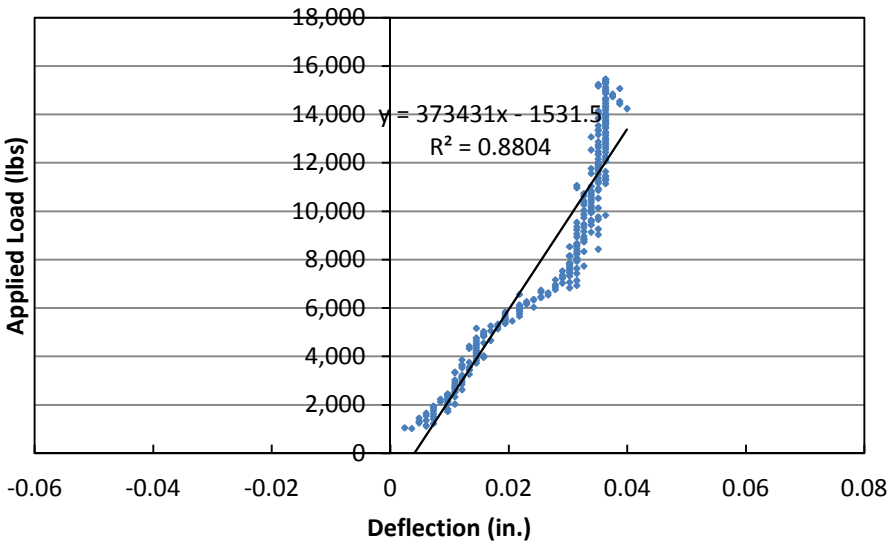

Figure A-55. Specimen 7 Stiffness at 100,000 Cycles

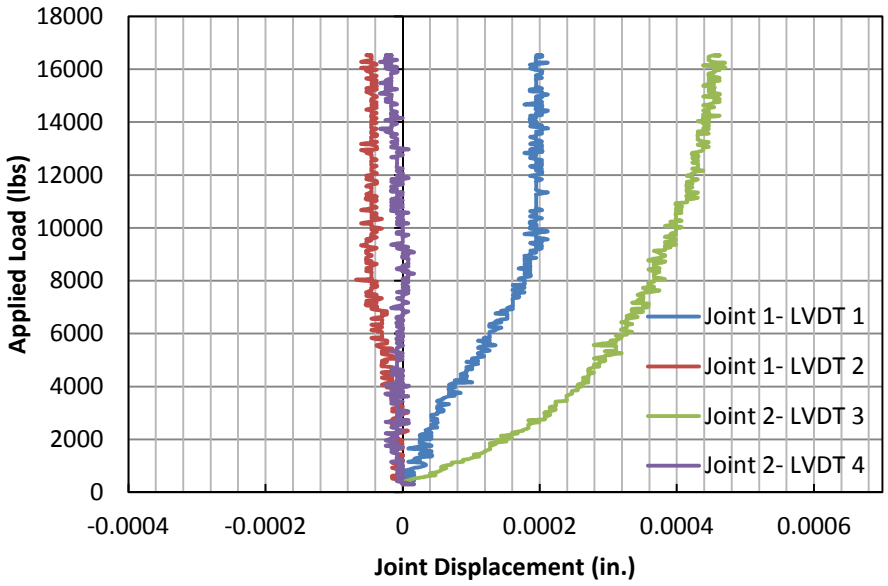

Figure A-56. Specimen 7 Vertical Joint Differential Deflection at 100,000 Cycles

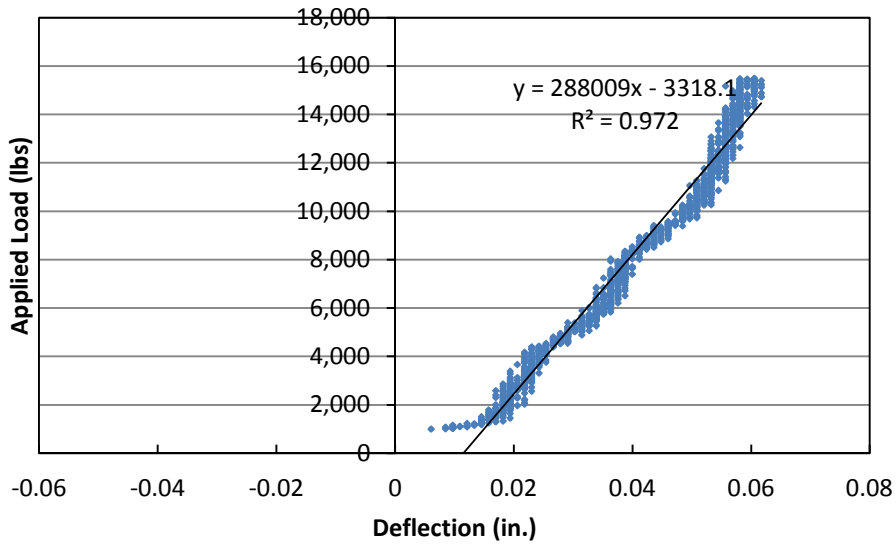

Figure A-57. Specimen 7 Stiffness at 1 Million Cycles

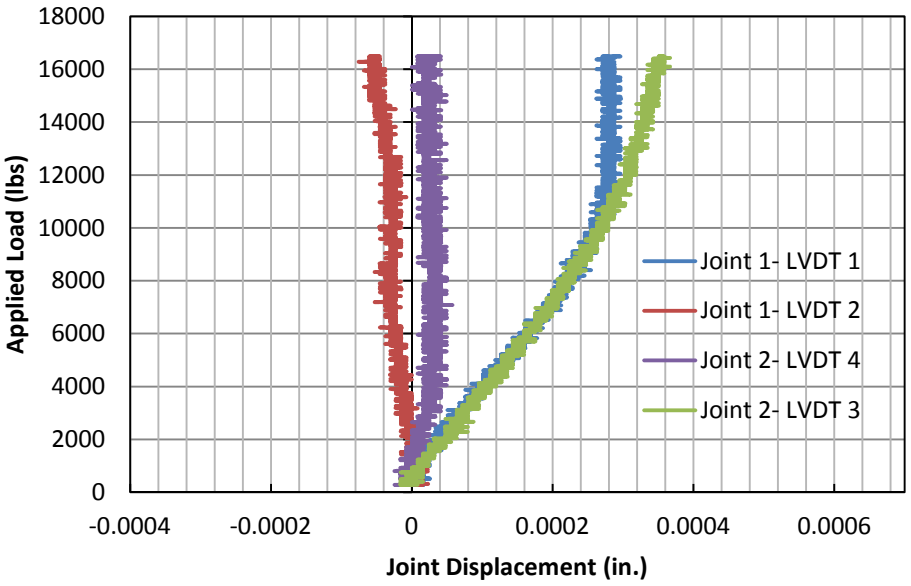

Figure A-58. Specimen 7 Vertical Joint Differential Deflection at 1 Million Cycles

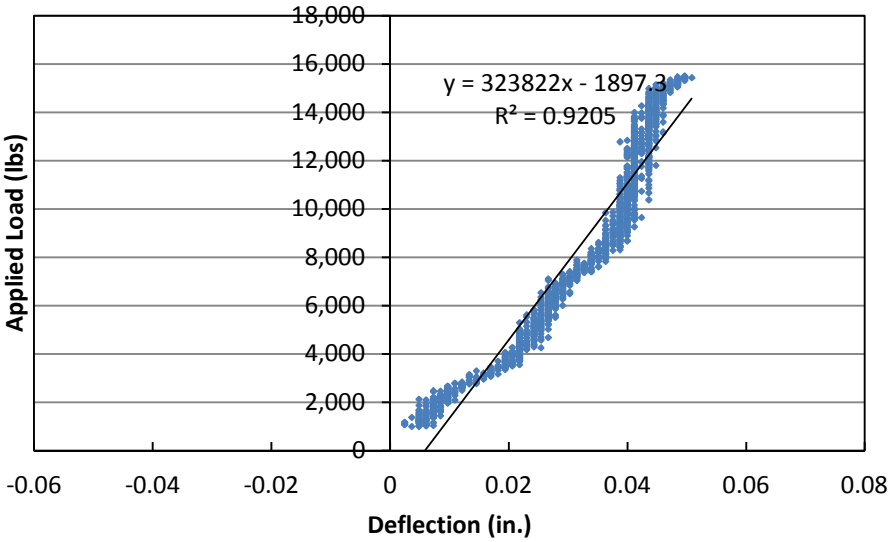

Figure A-59. Specimen 7 Stiffness at 10 Million Cycles

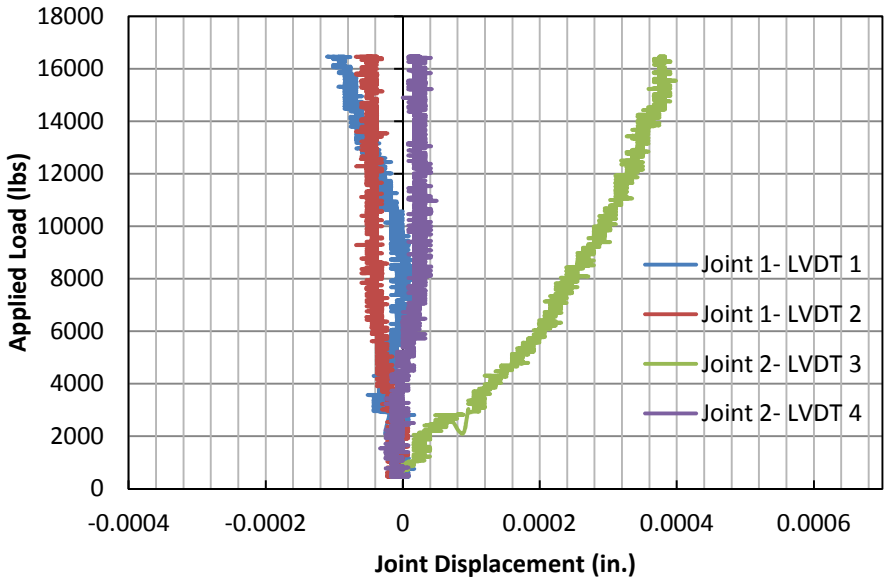

Figure A-60. Specimen 7 Vertical Joint Differential Deflection at 10 Million Cycles

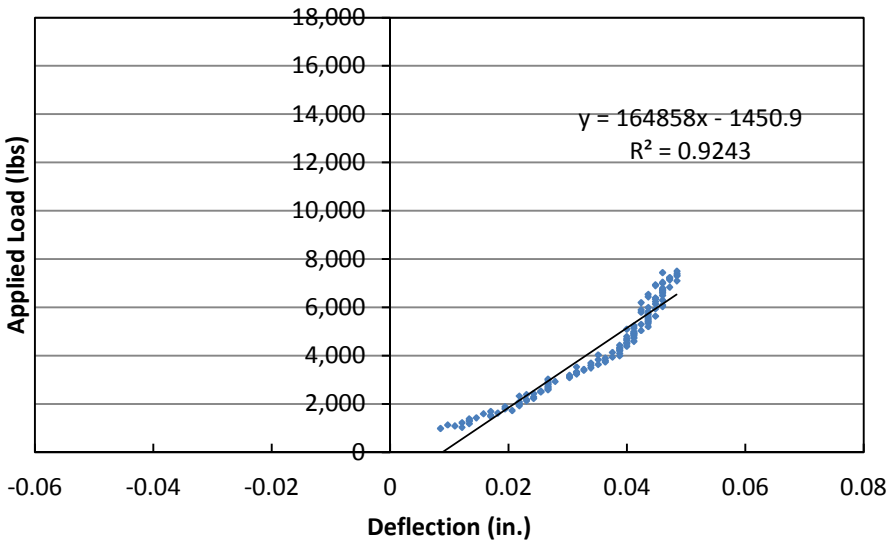

Figure A-61. Specimen 4 Stiffness at 1 Cycle

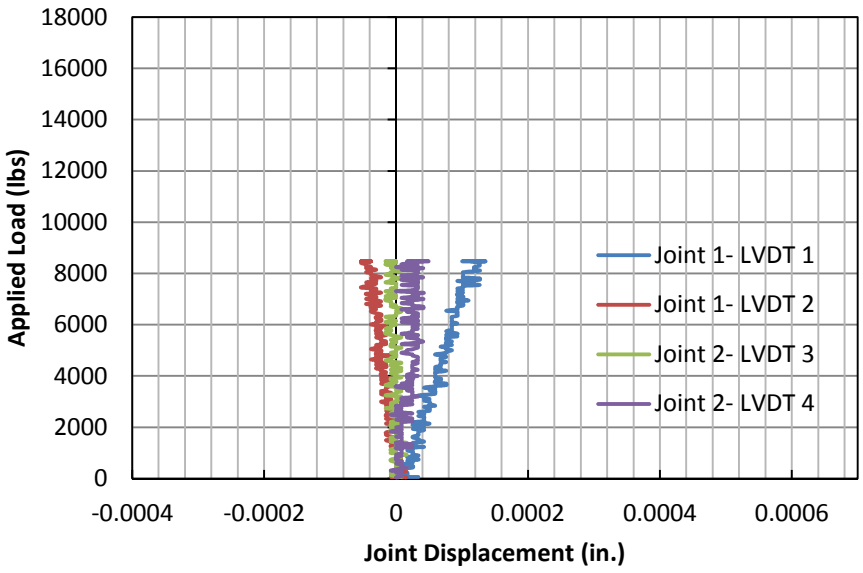

Figure A-62. Specimen 4 Vertical Joint Differential Deflection at 1 Cycle

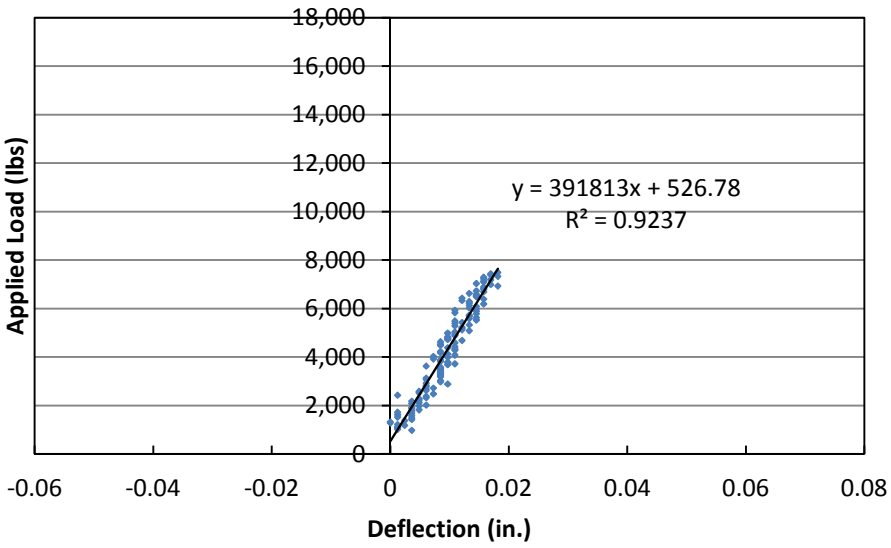

Figure A-63. Specimen 4 Stiffness at 1,000 Cycles

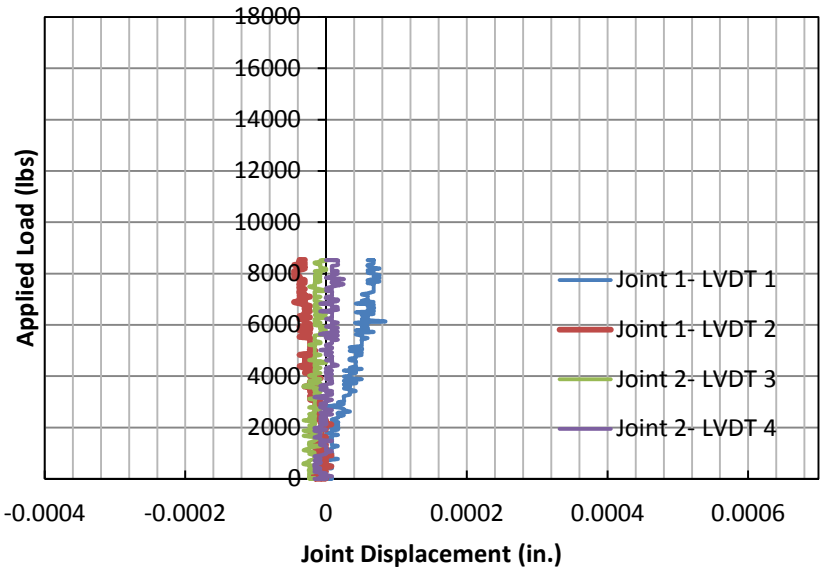

Figure A-64. Specimen 4 Vertical Joint Differential Deflection at 1,000 Cycles

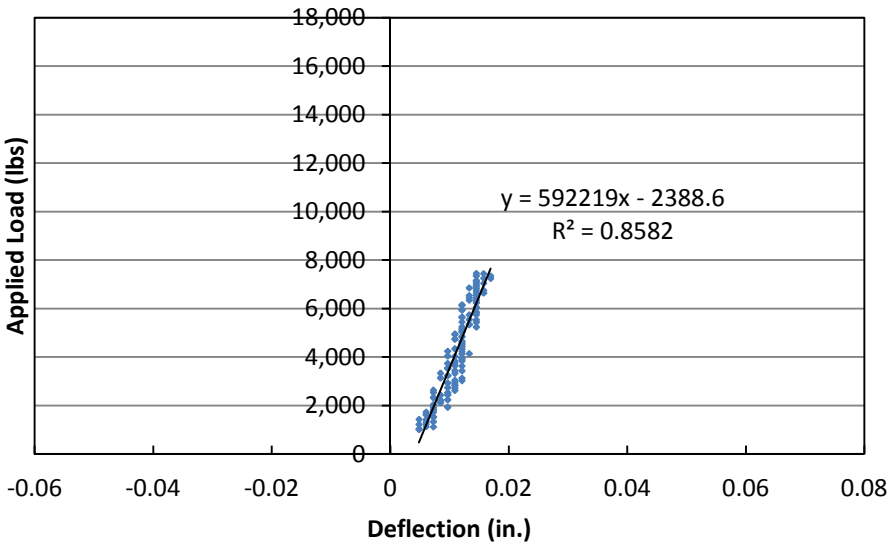

Figure A-65. Specimen 4 Stiffness at 10,000 Cycles

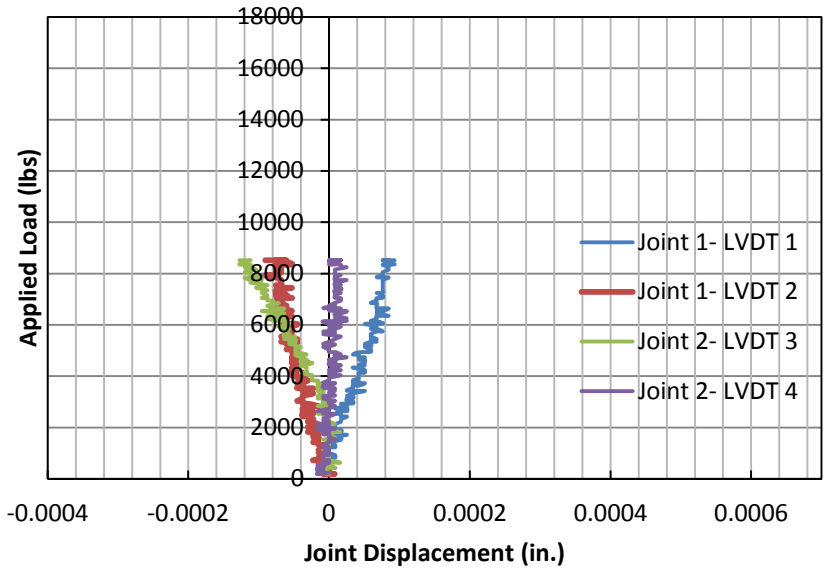

Figure A-66. Specimen 4 Vertical Joint Differential Deflection at 10,000 Cycles

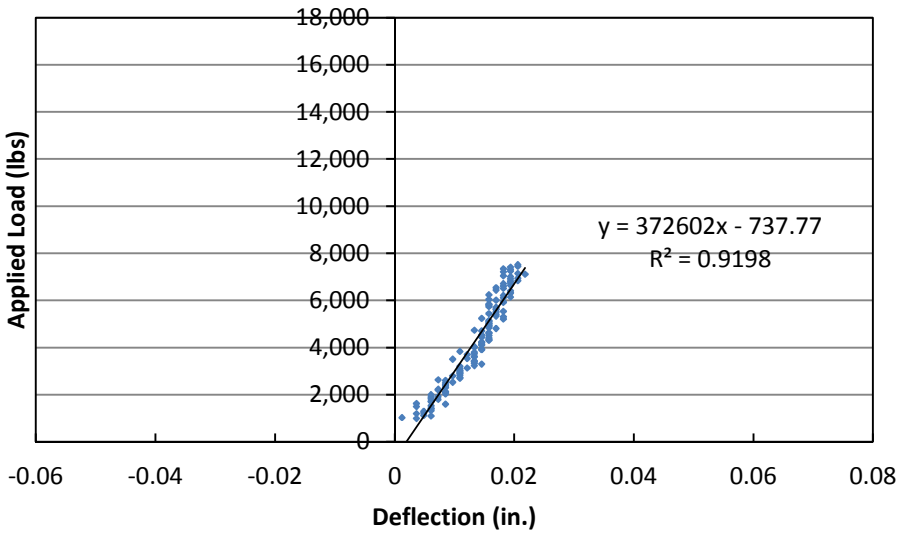

Figure A-67. Specimen 4 Stiffness at 100,000 Cycles

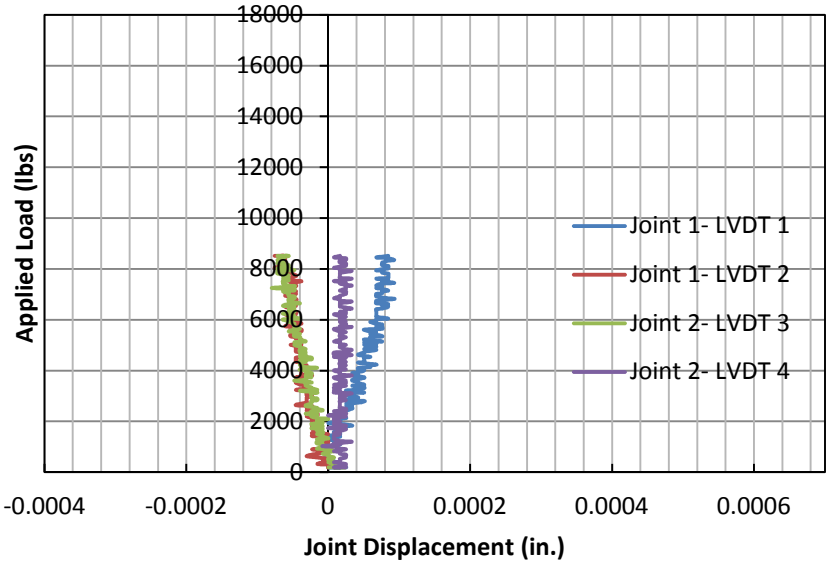

Figure A-68. Specimen 4 Vertical Joint Differential Deflection at 100,000 Cycles

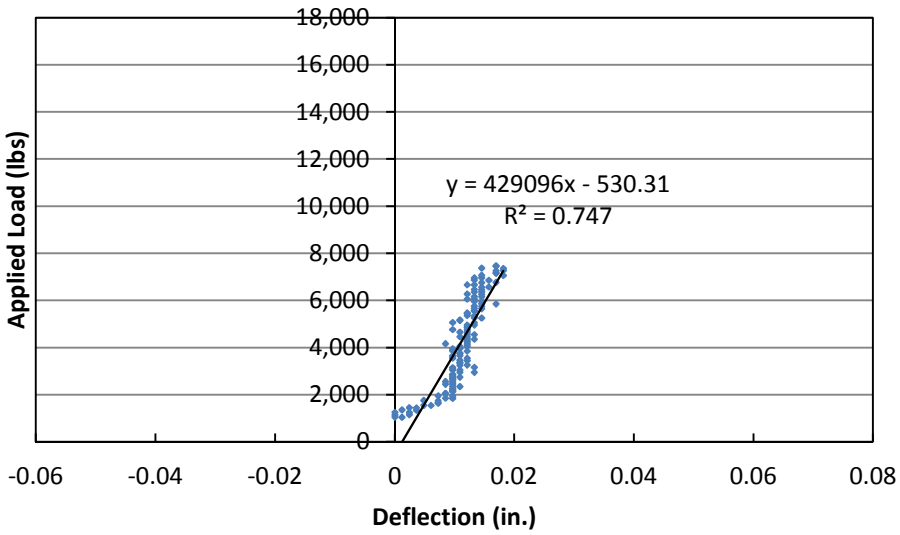

Figure A-69. Specimen 4 Stiffness at 1 Million Cycles

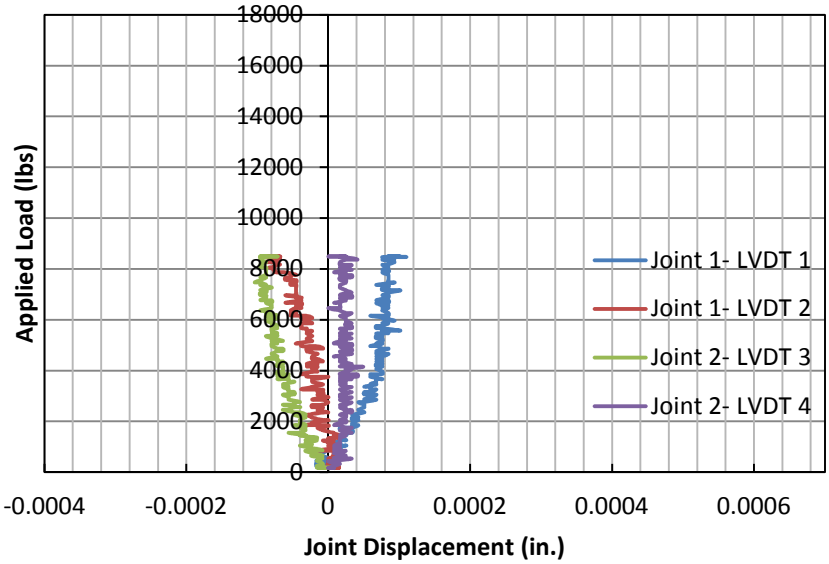

Figure A-70. Specimen 4 Vertical Joint Differential Deflection at 1 Million Cycles

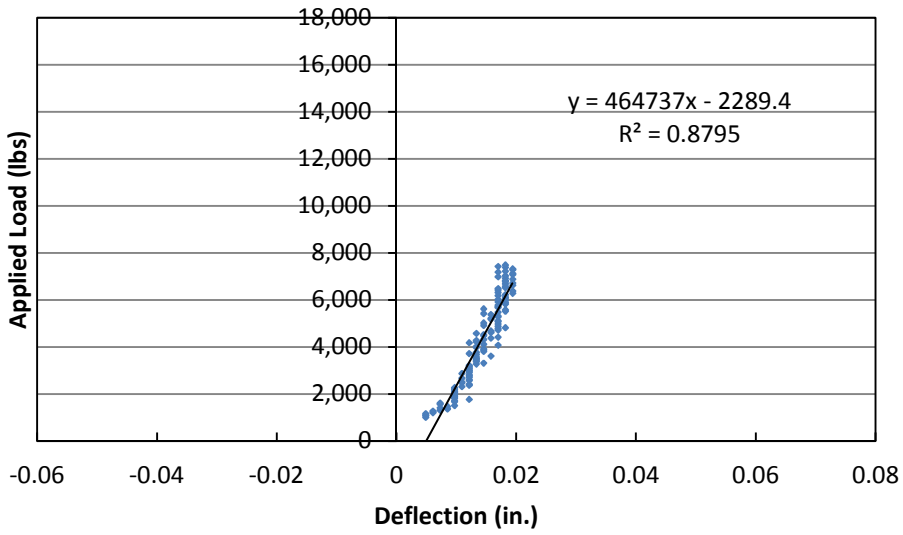

Figure A-71. Specimen 4 Stiffness at 10 Million Cycles

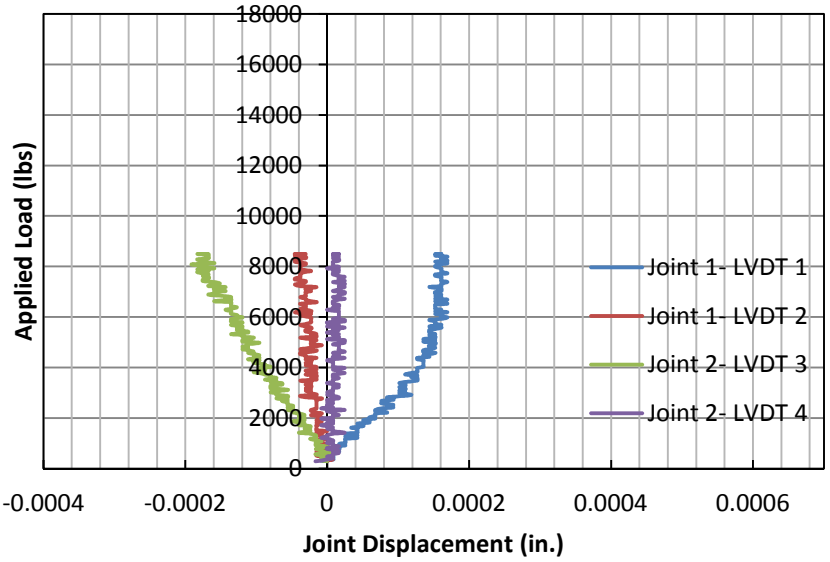

Figure A-72. Specimen 4 Vertical Joint Differential Deflection at 10 Million Cycles

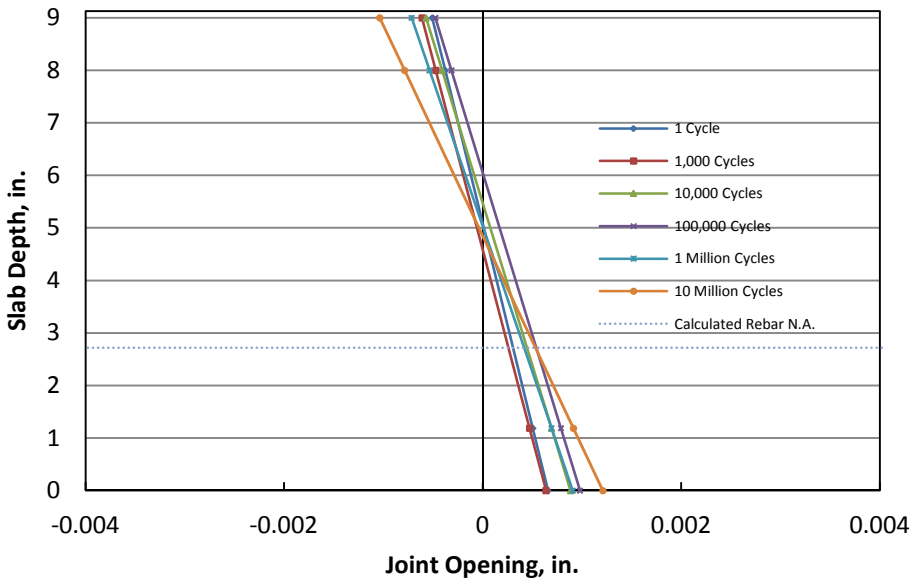

Figure A-73. Opening of Joint 1 (Specimen 4, Side A)

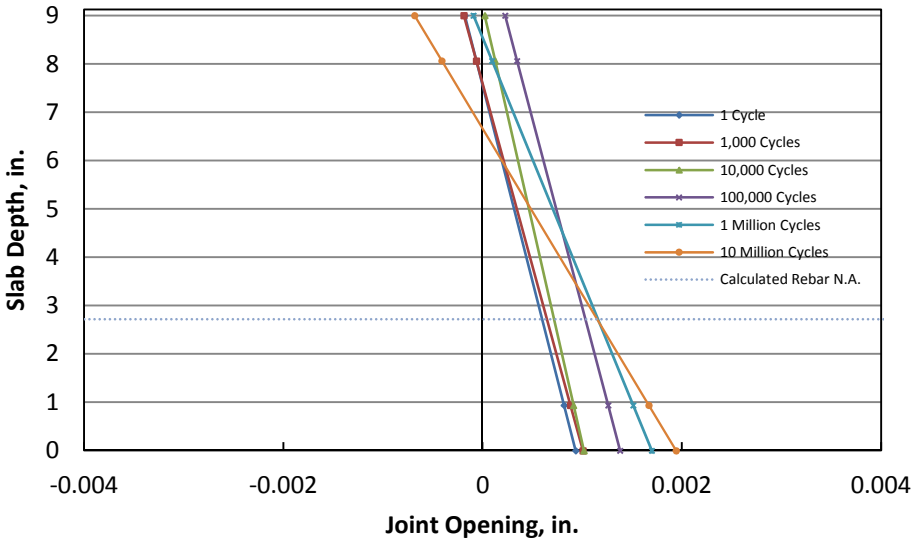

Figure A-74. Opening of Joint 1 (Specimen 4, Side B)

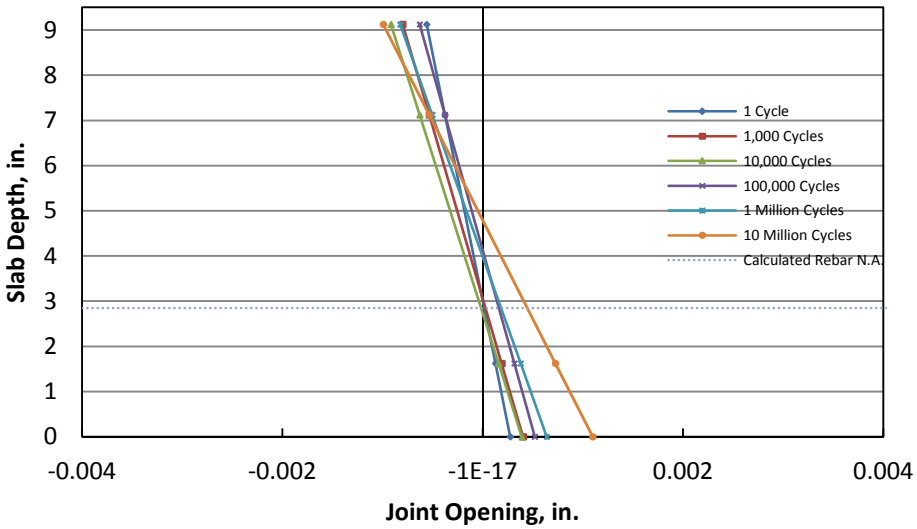

Figure A-75. Opening of Joint 2 (Specimen 4, Side A)

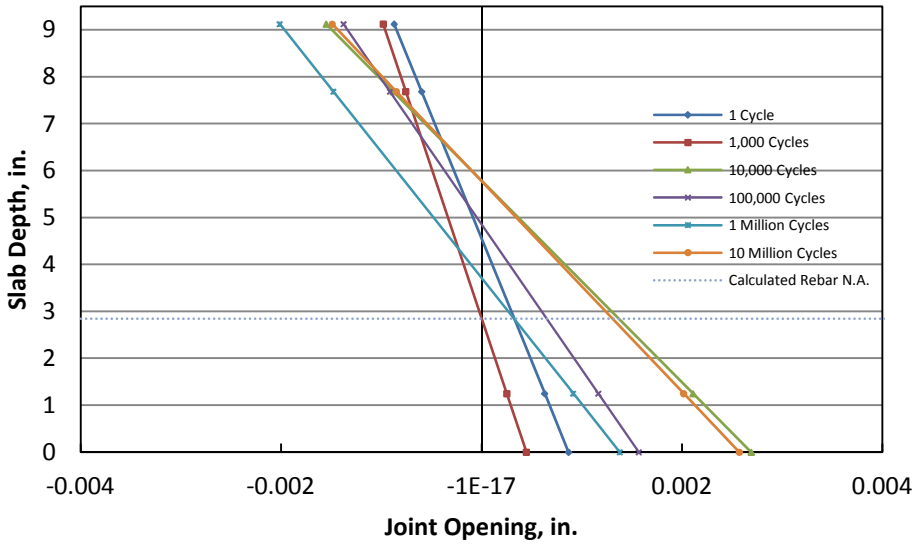

Figure A-76. Opening of Joint 2 (Specimen 4, Side B)

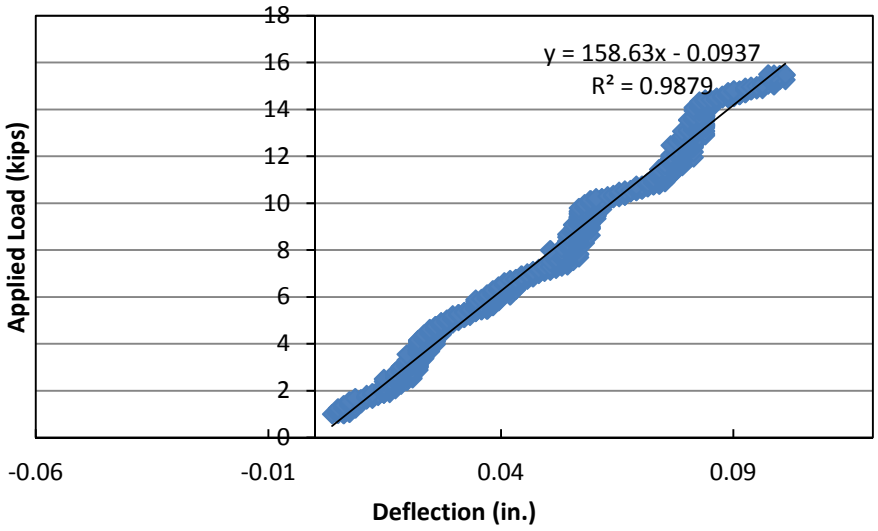

Figure A-77. Specimen A Stiffness at 1 Cycle

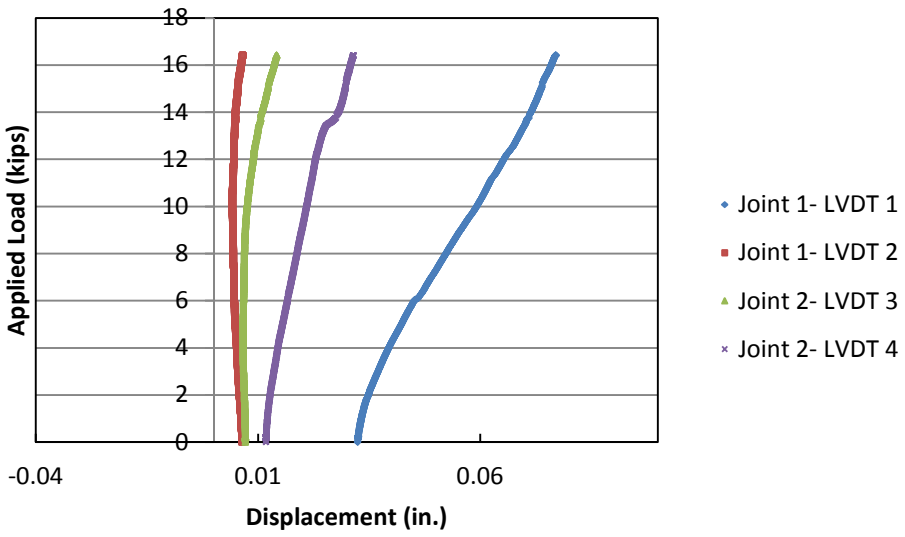

Figure A-78. Specimen A Vertical Joint Differential Deflection at 1 Cycle

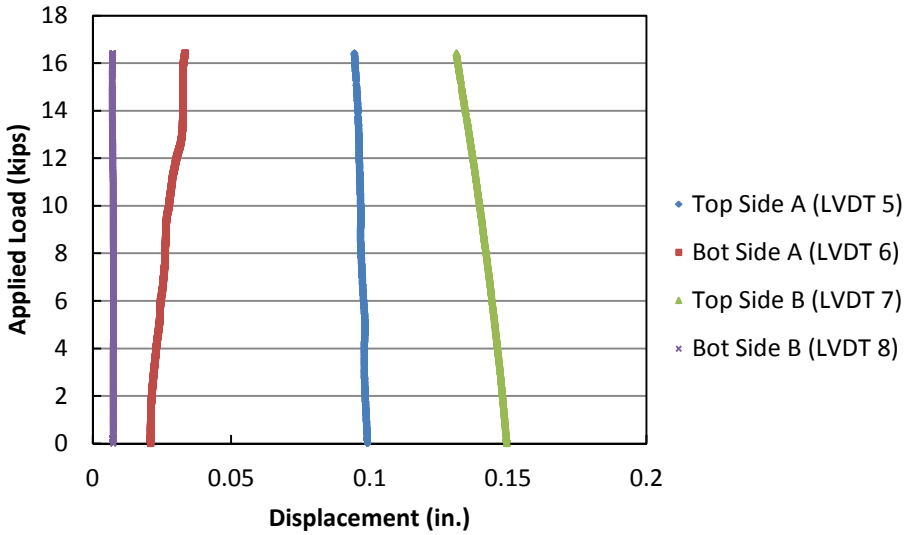

Figure A-79. Specimen A Horizontal Joint 1 Deflection at 1 Cycle

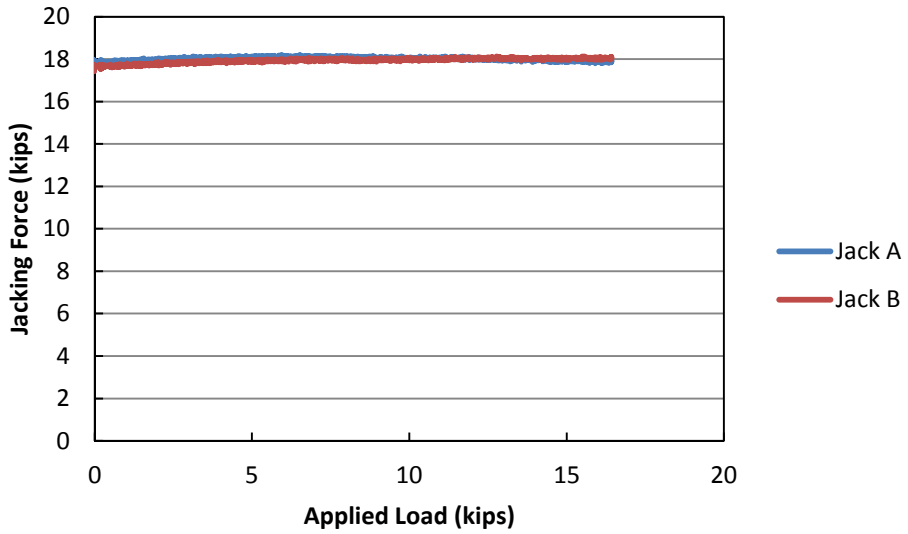

Figure A-80. Specimen A Jacking Forces During Static Test at 1 Cycle

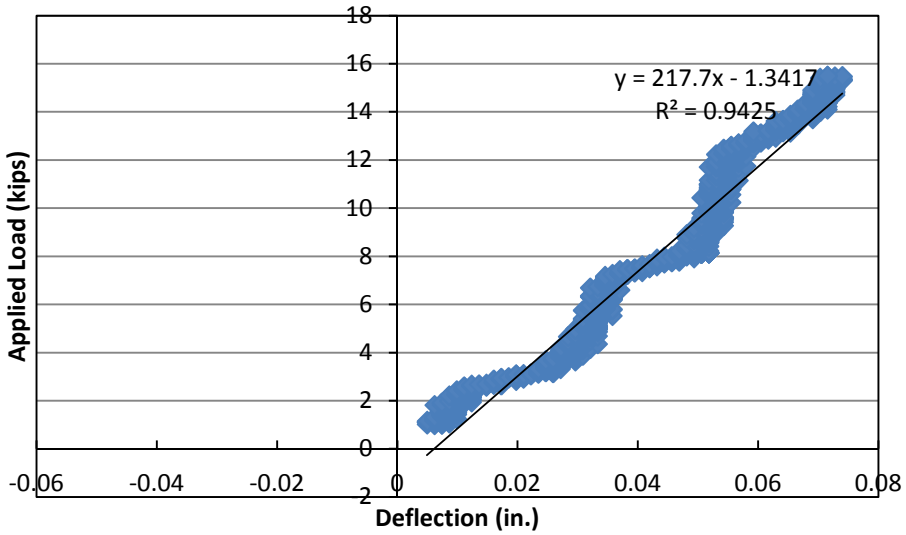

Figure A-81. Specimen A Stiffness at 1,000 Cycles

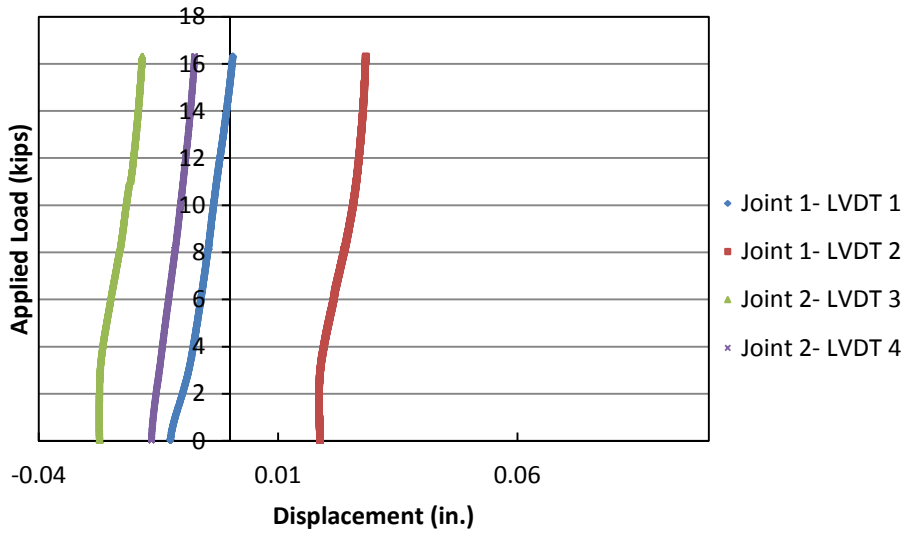

Figure A-82. Specimen A Vertical Joint Differential Deflection at 1,000 Cycles

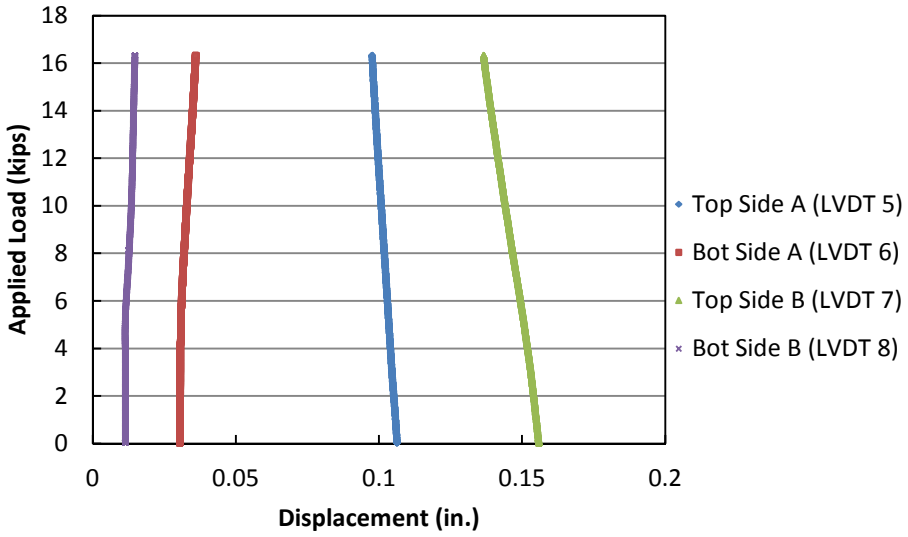

Figure A-83. Specimen A Horizontal Joint 1 Deflection at 1,000 Cycles

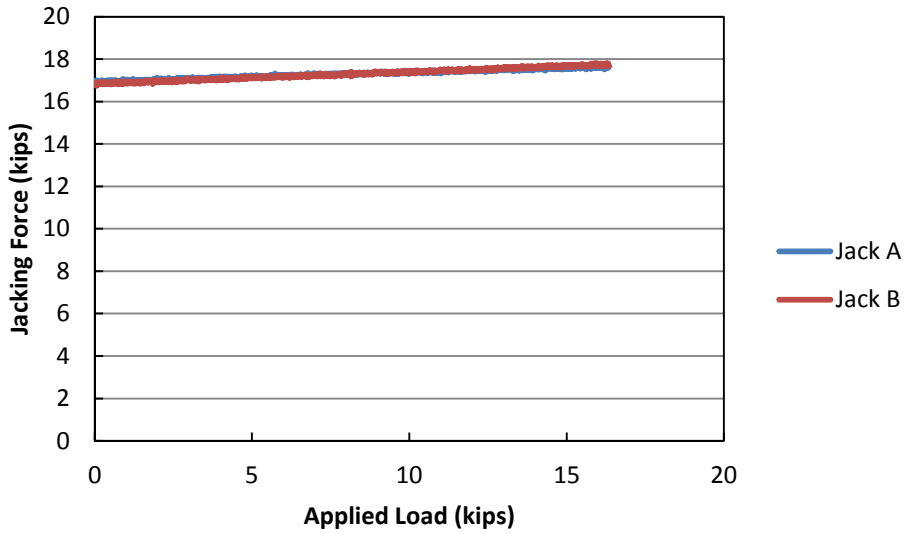

Figure A-84. Specimen A Jacking Forces During Static Test at 1,000 Cycles

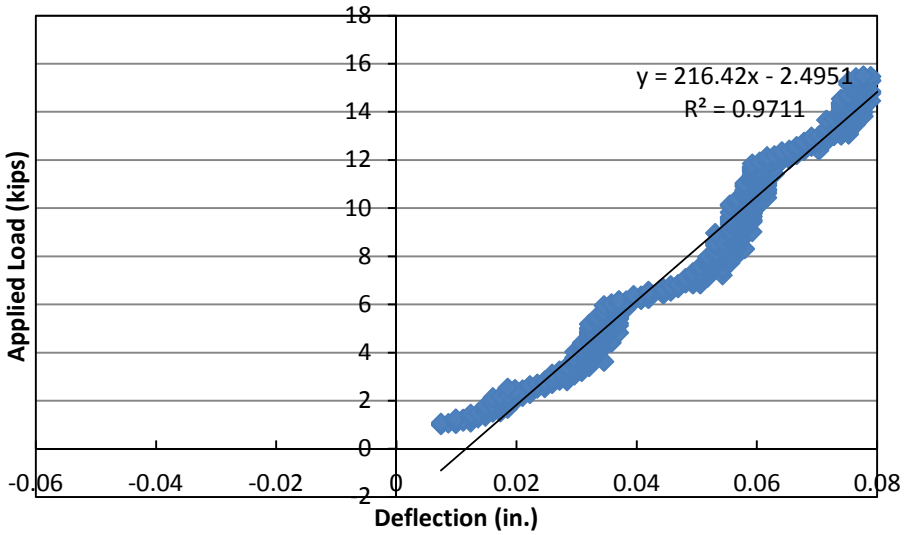

Figure A-85. Specimen A Stiffness at 10,000 Cycles

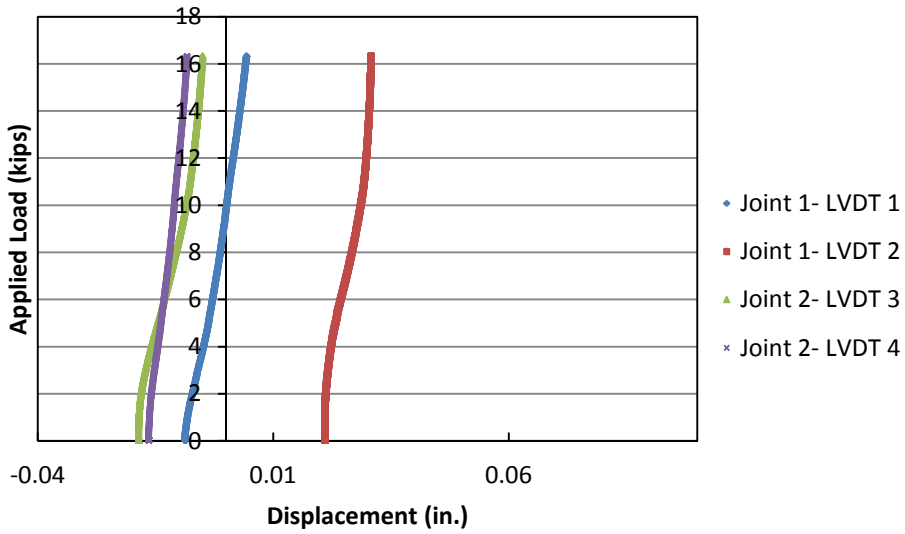

Figure A-86. Specimen A Vertical Joint Differential Deflection at 10,000 Cycles

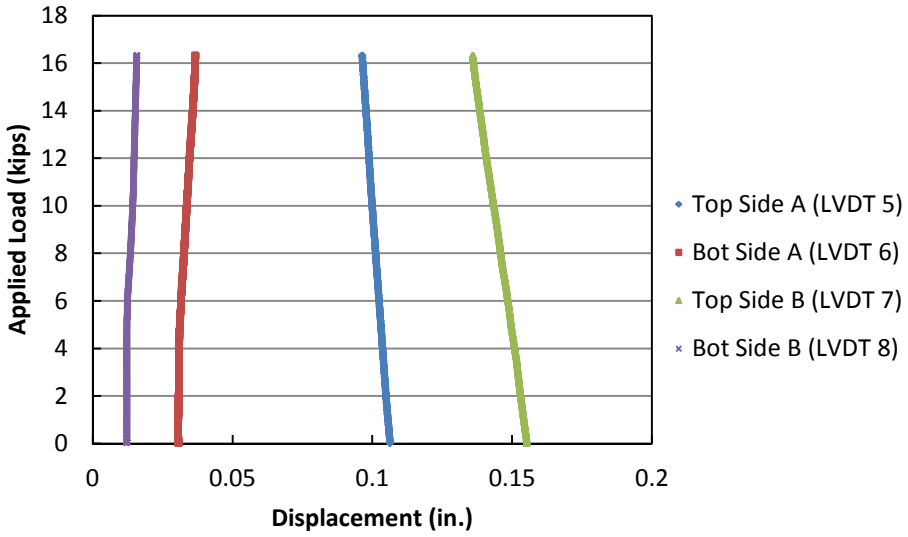

Figure A-87. Specimen A Horizontal Joint 1 Deflection at 10,000 Cycles

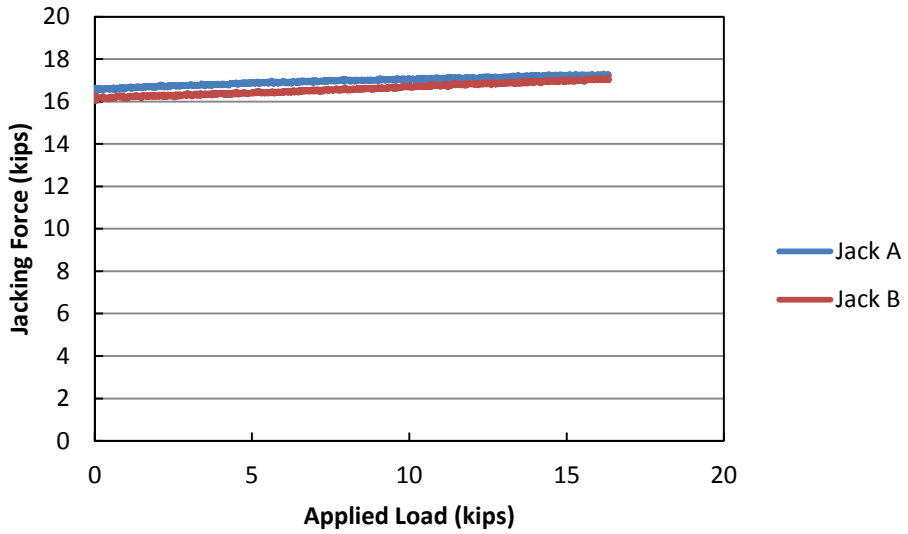

Figure A-88. Specimen A Jacking Forces During Static Test at 10,000 Cycles

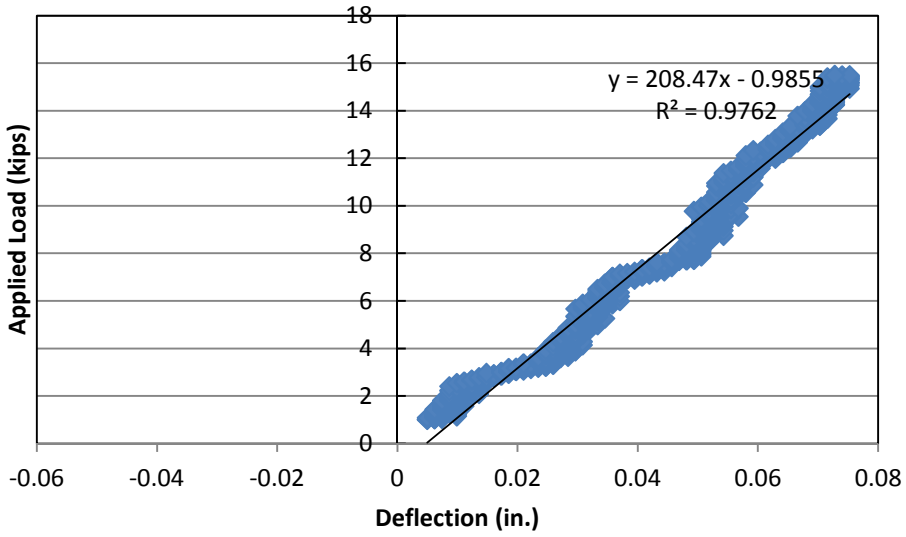

Figure A-89. Specimen A Stiffness at 100,000 Cycles

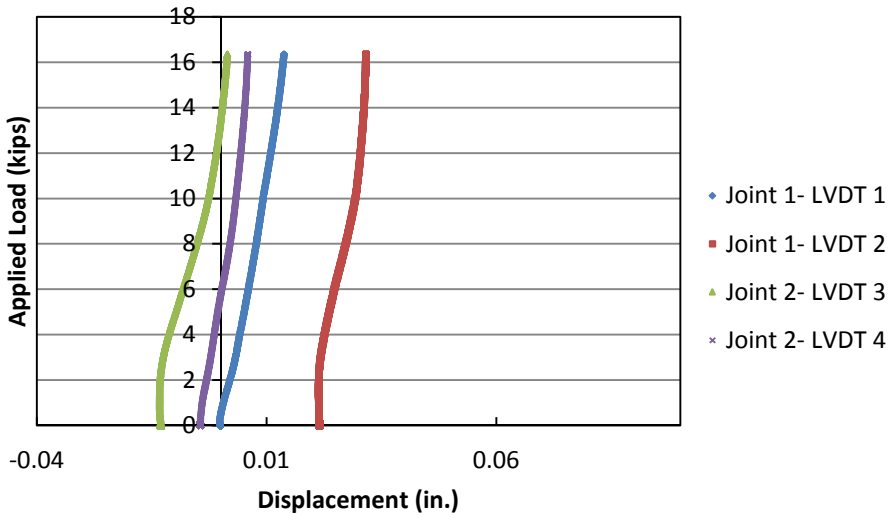

Figure A-90. Specimen A Vertical Joint Differential Deflection at 100,000 Cycles

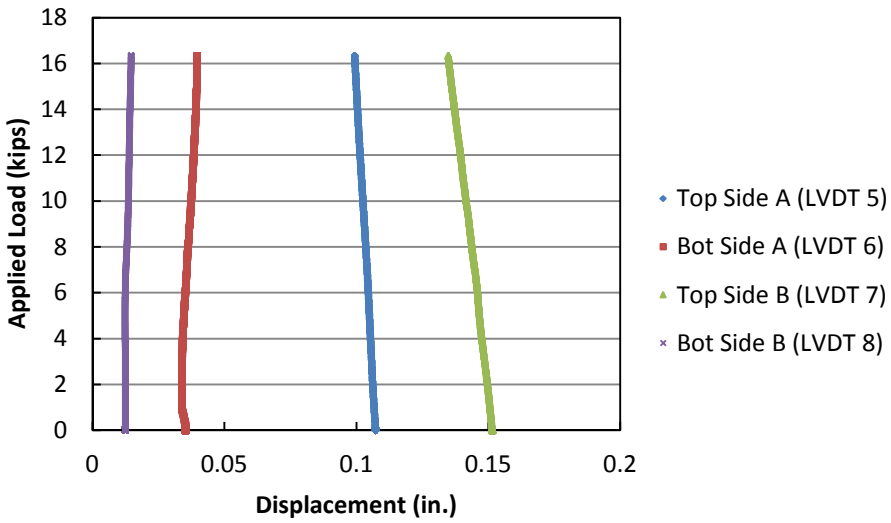

Figure A-91. Specimen A Horizontal Joint 1 Deflection at 100,000 Cycles

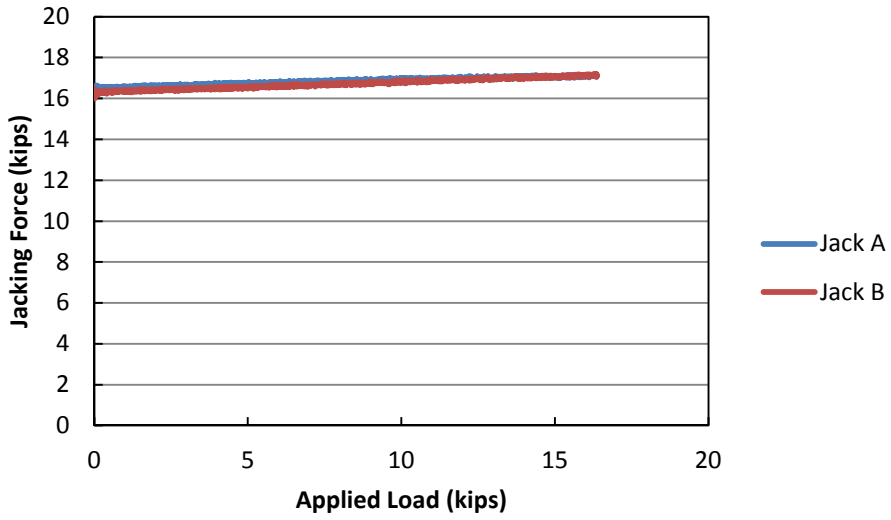

Figure A-92. Specimen A Jacking Forces During Static Test at 100,000 Cycles

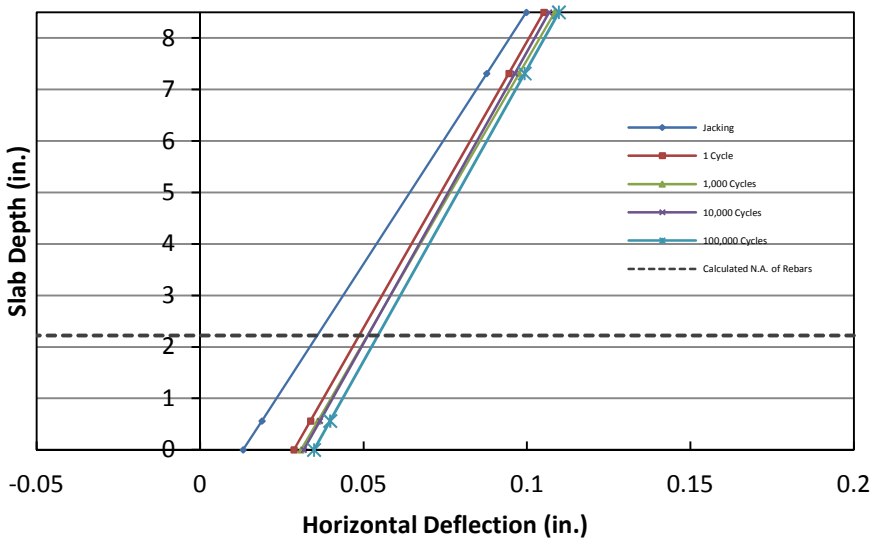

Figure A-93. Joint 1 Movement Throughout Cycling (Specimen A, Side A)

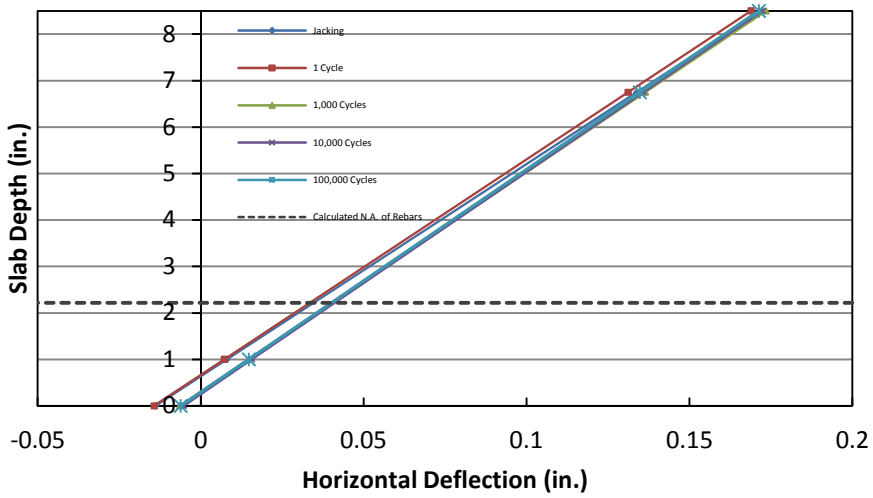

Figure A-94. Joint 1 Movement Throughout Cycling (Specimen A, Side B)

APPENDIX B- Bridge Cross-Section & Deck Slab Sketches with Test Specimens' Cut Location

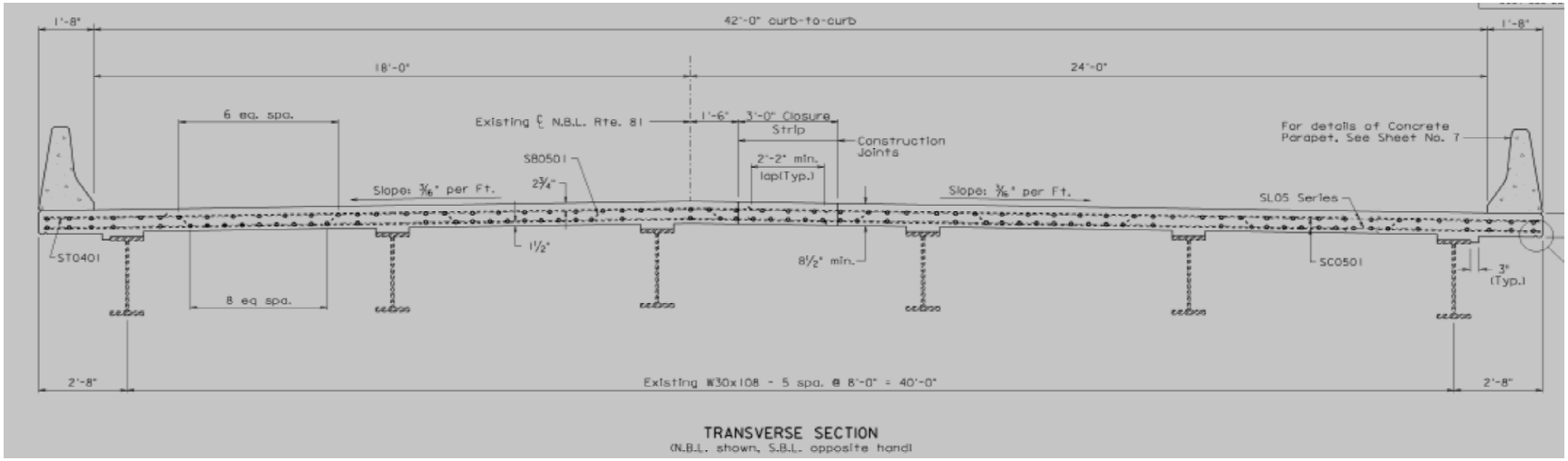

Figure B-1. Cross-Section of Interstate 81 Bridge with Closure Pour

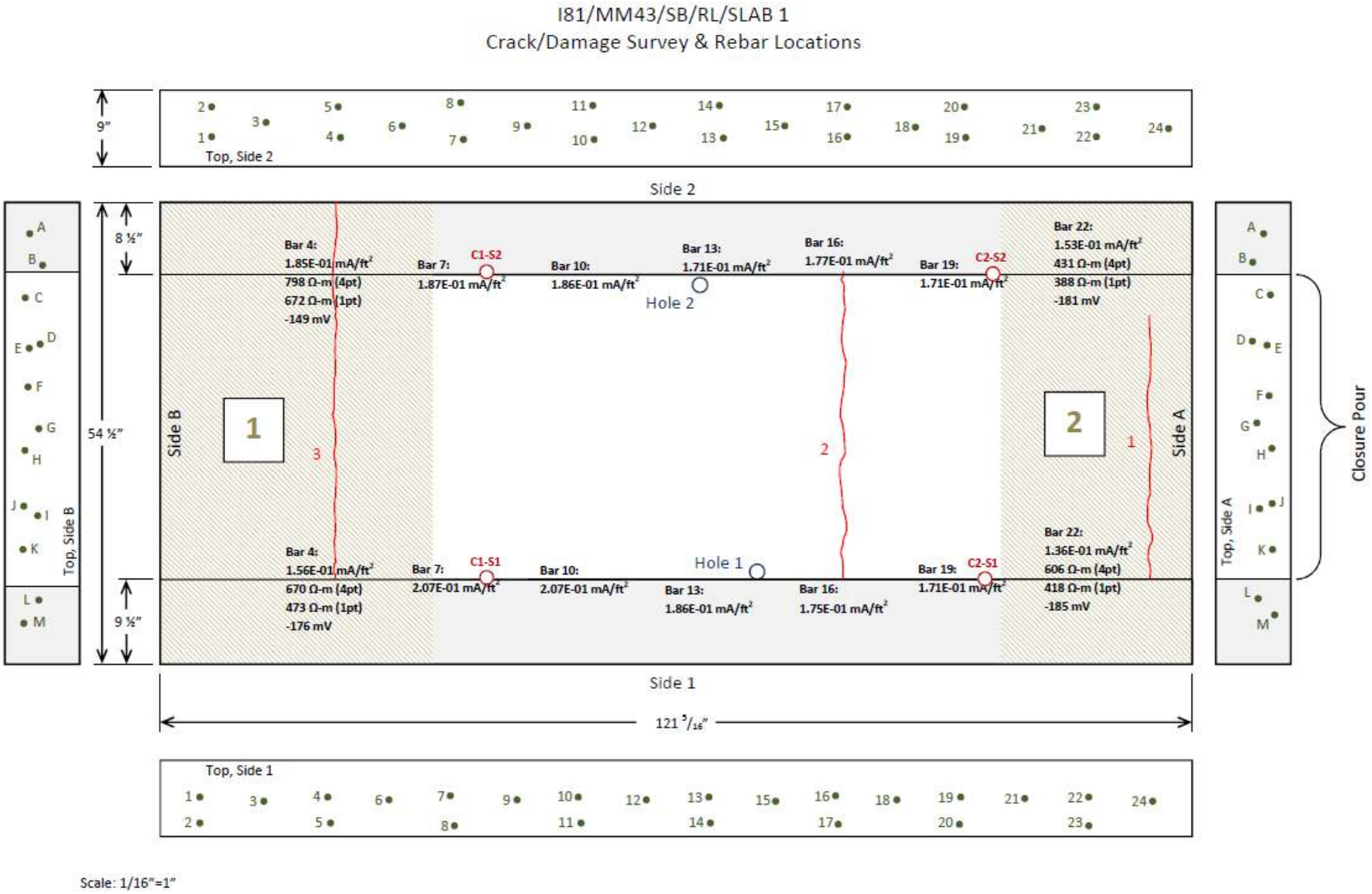

Figure B-2. Crack, Damage Survey and Rebar Locations for Slab 1

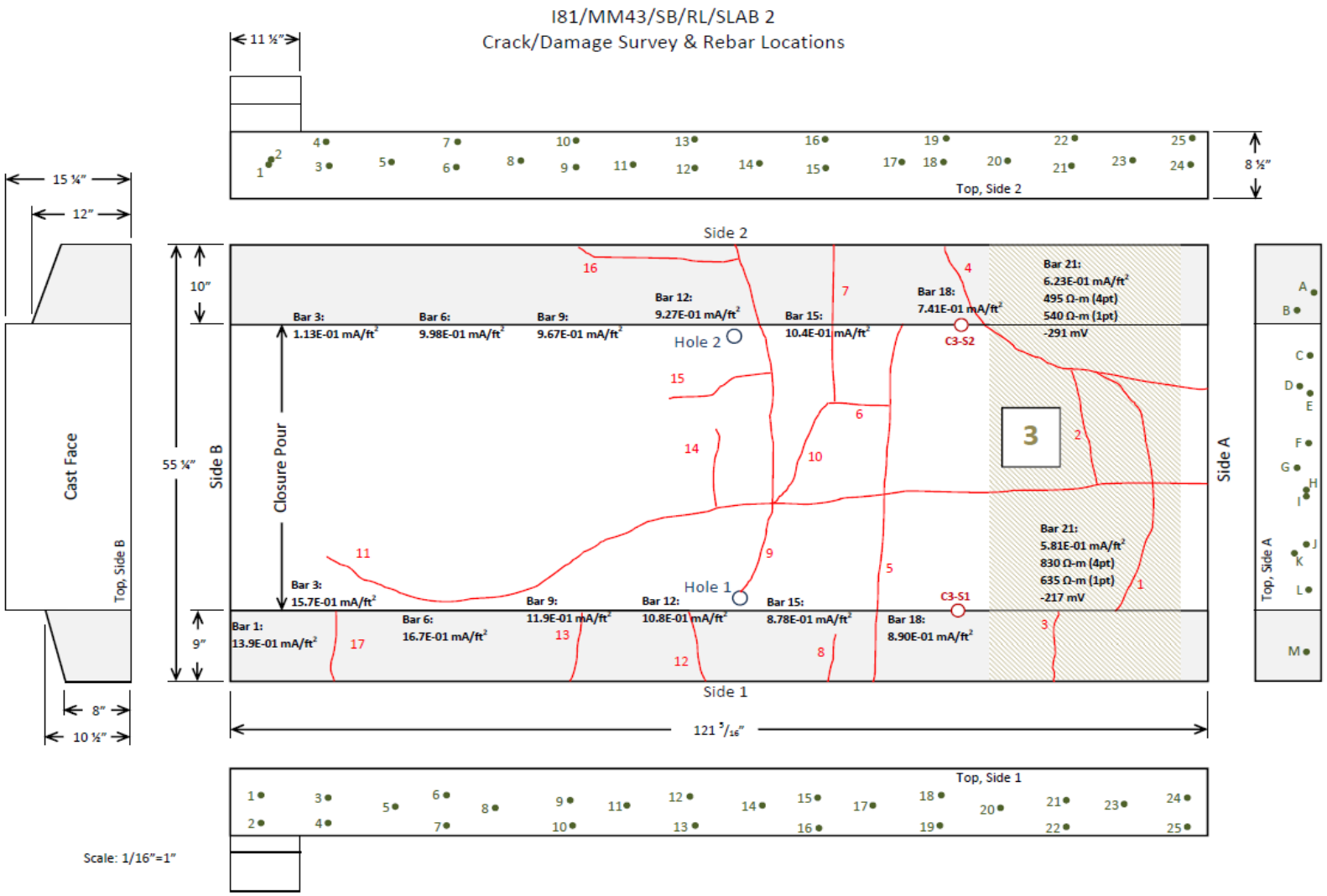

Figure B-3. Crack, Damage Survey and Rebar Locations for Slab 2

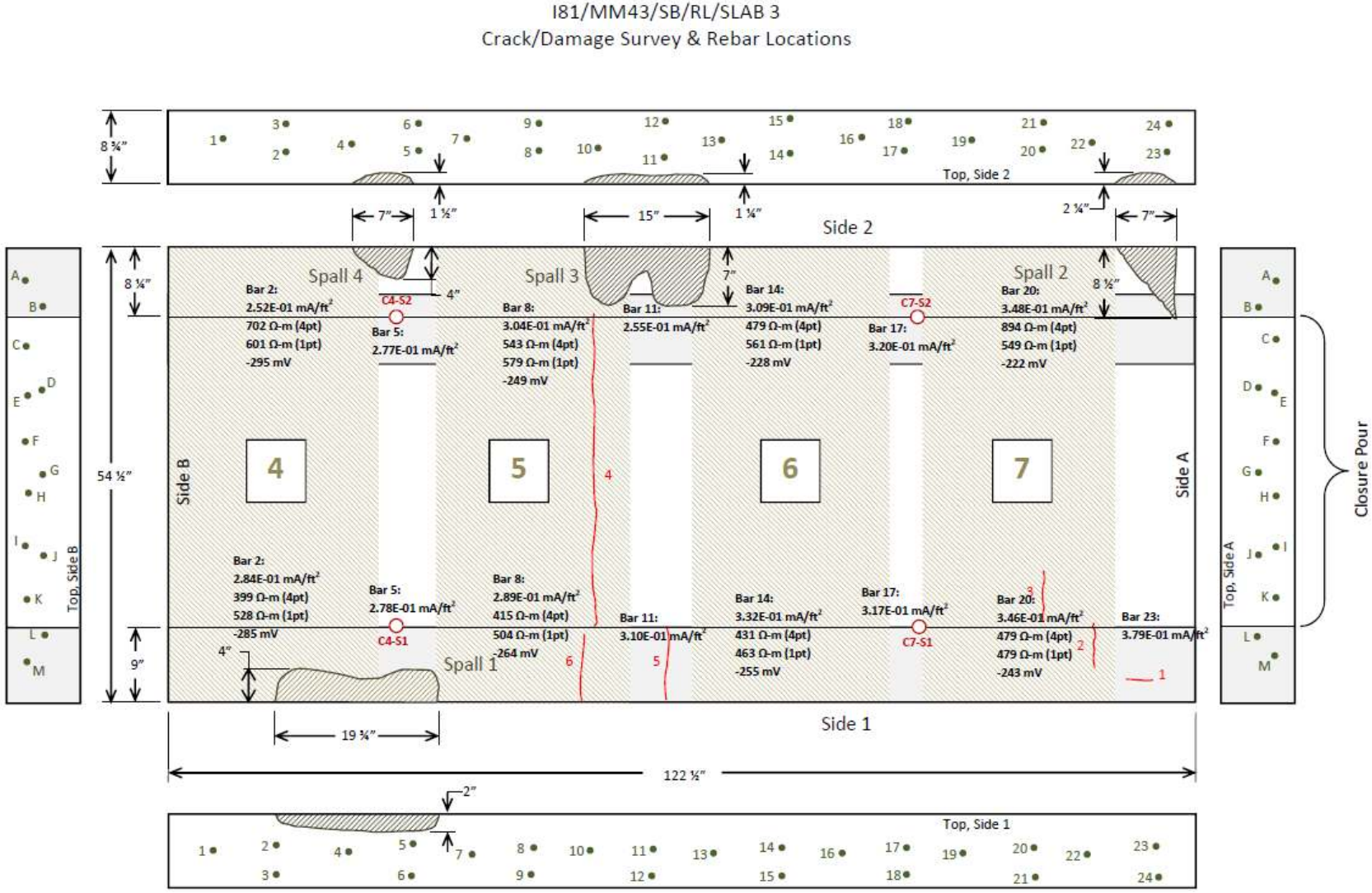

Figure B-4. Crack, Damage Survey and Rebar Locations for Slab 3

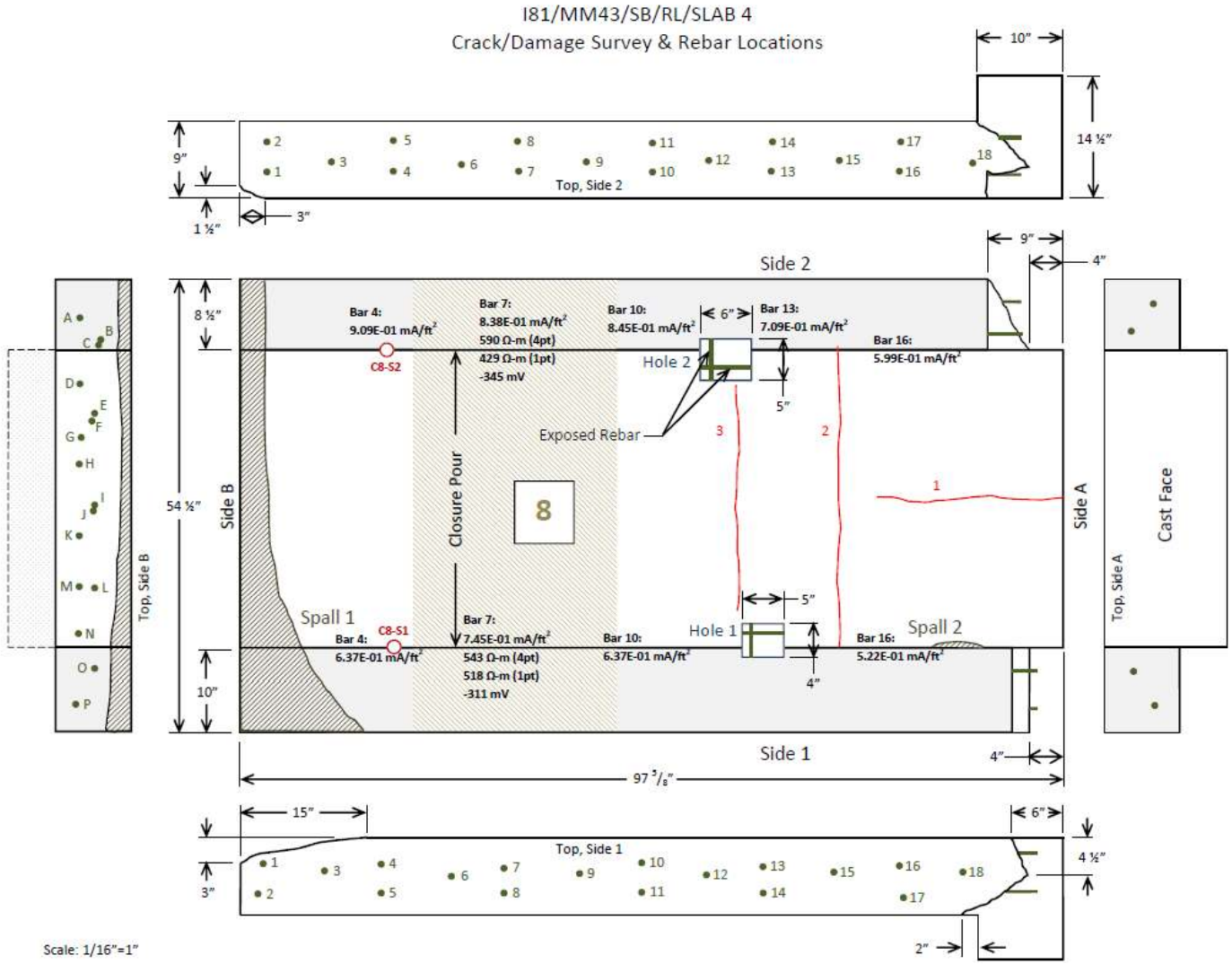

Figure B-5. Crack, Damage Survey and Rebar Locations for Slab 4

APPENDIX C- I-81 Test Specimen Dimensions and Bar Cover Depths

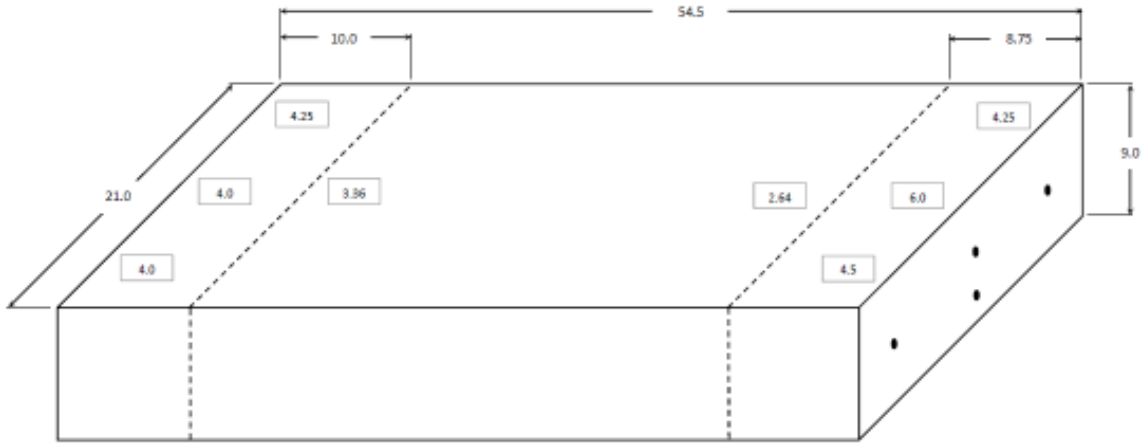

Figure C-1. Specimen 1 Dimensions and Bars Cover Depths

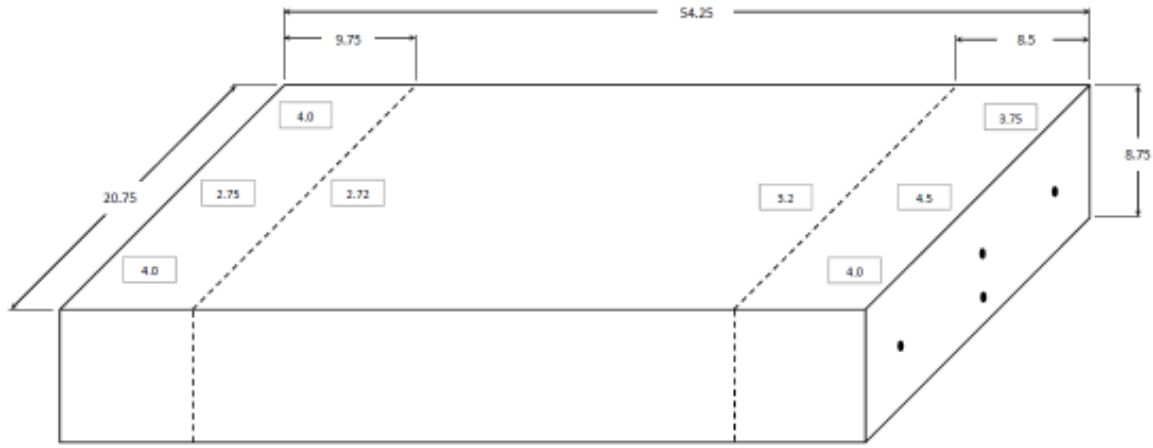

Figure C-2. Specimen 2 Dimensions and Bars Cover Depths

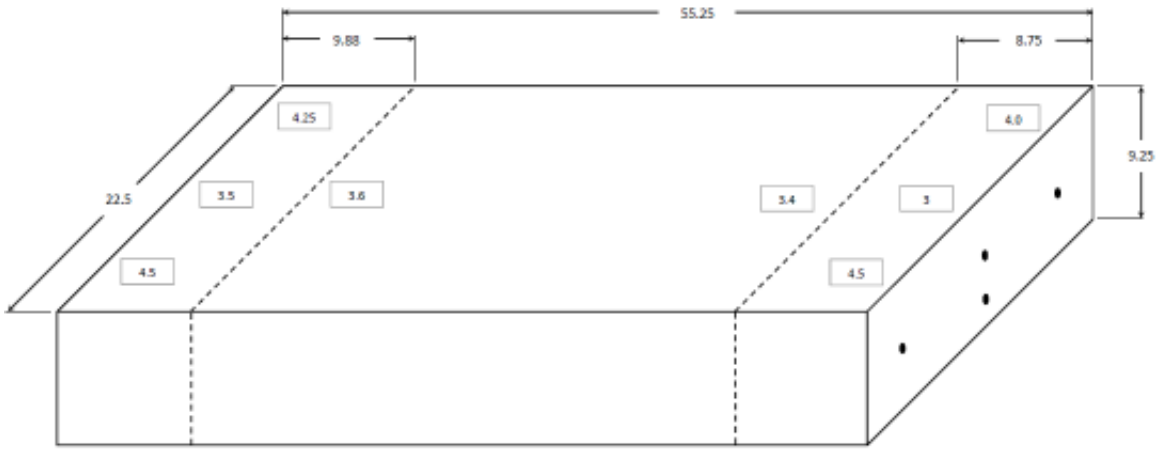

Figure C-3. Specimen 3 Dimensions and Bars Cover Depths

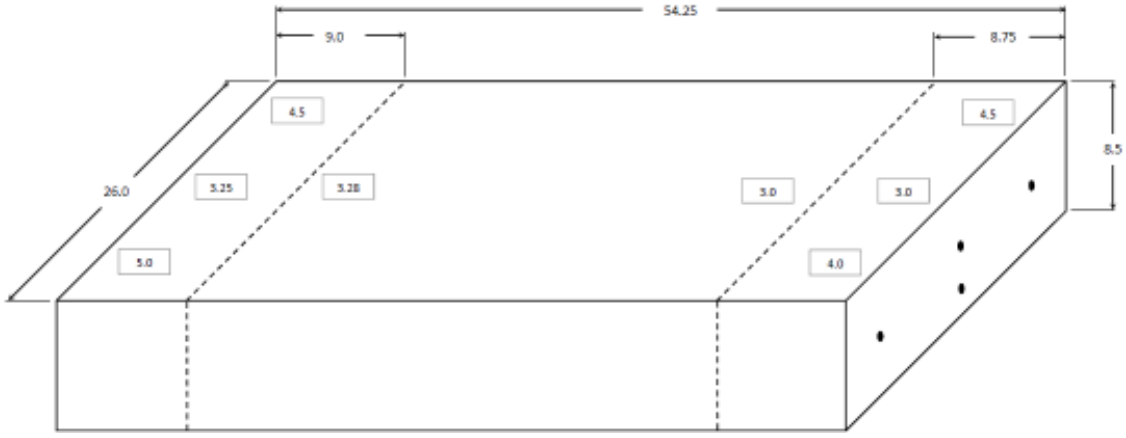

Figure C-4. Specimen 4 Dimensions and Bars Cover Depths

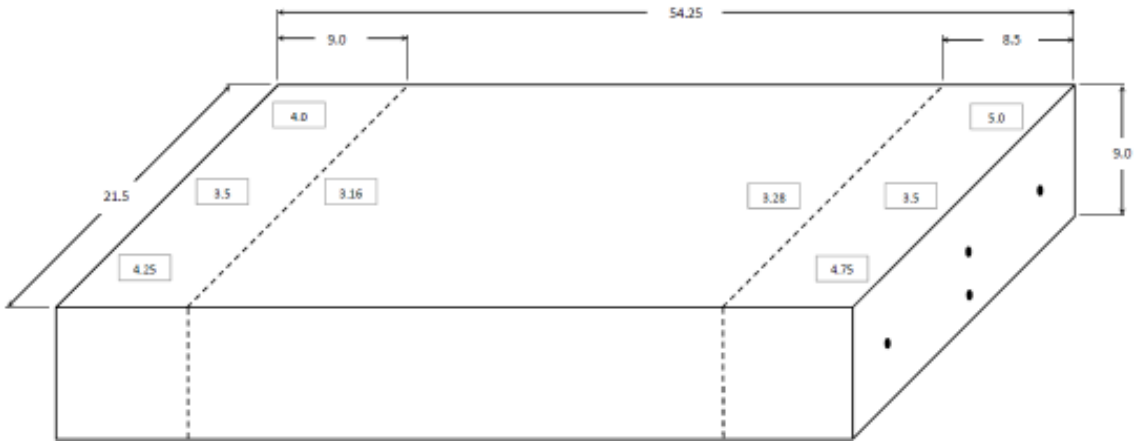

Figure C-5. Specimen 5 Dimensions and Bars Cover Depths

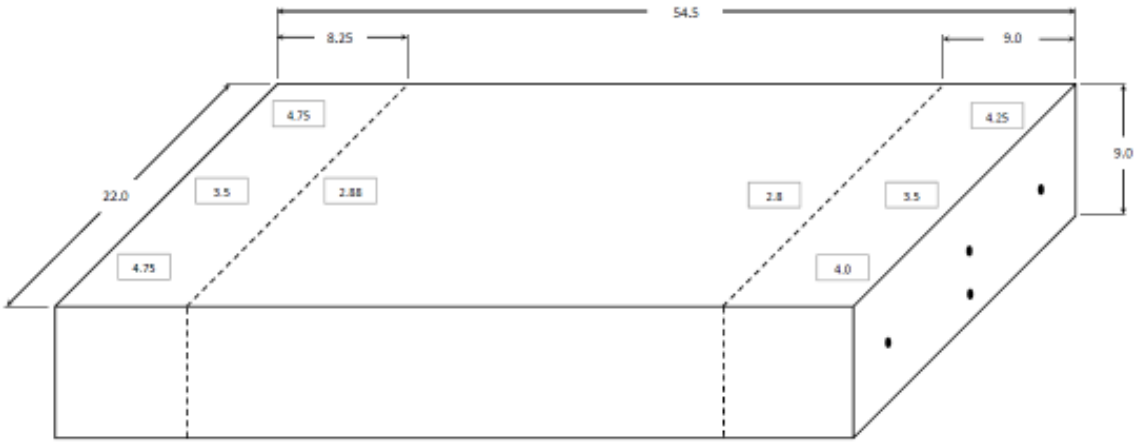

Figure C-6. Specimen 6 Dimensions and Bars Cover Depths

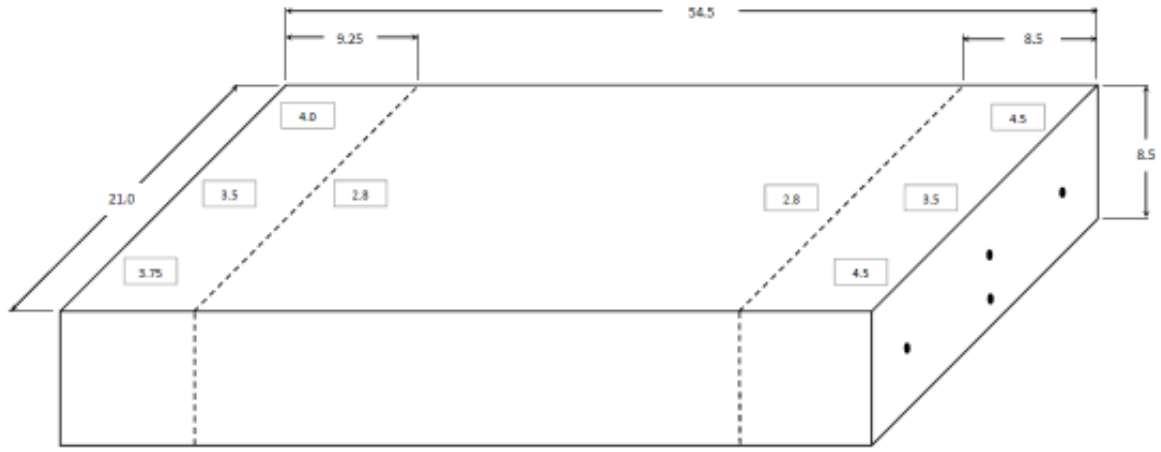

Figure C-7. Specimen 7 Dimensions and Bars Cover Depths

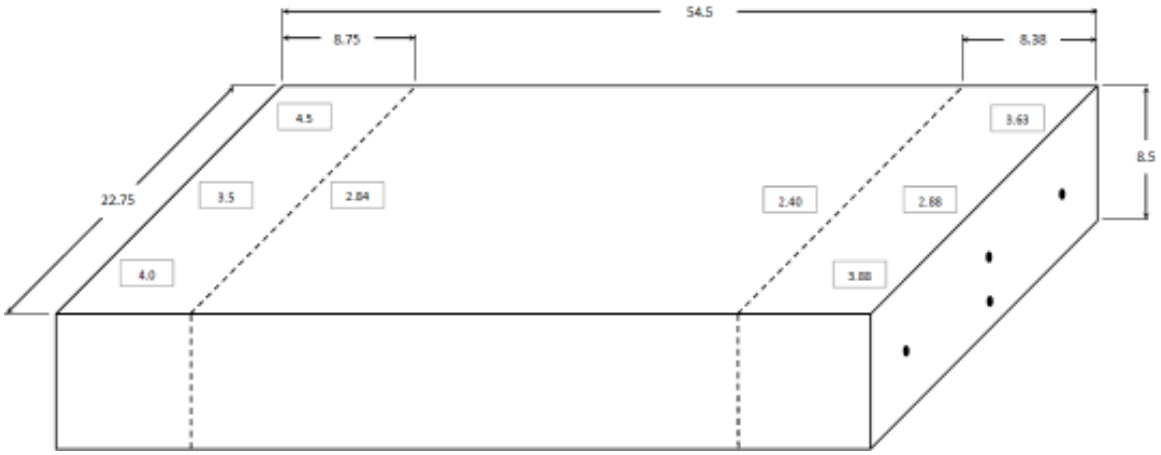

Figure C-8. Specimen 8 Dimensions and Bars Cover Depths

APPENDIX D- Failed Test Specimens

D.1 Strength Test Specimens

Figure D-1. Side A View of Failed Specimen 1

Figure D-2. Side B View of Failed Specimen 1

Figure D-3. Side A View of Failed Specimen 3

Figure D-4. Side B View of Failed Specimen 3

Figure D-5. Side A View of Failed Specimen 8

Figure D-6. Side B View of Failed Specimen 8

Figure D-7. Side A View of Failed Specimen C

Figure D-8. Side B View of Failed Specimen C

Figure D-9. Side A View of Failed Specimen B

Figure D-10. Side A View of Failed Specimen B with Focus on Joint 2 and Main Cracks

Figure D-11. Side B View of Failed Specimen B with Focus on Joint 2

Figure D-12. Side B View of Failed Specimen B with Focus on Joint 1

D.2 Fatigue Test Specimen- Specimen A

Figure D-13. Joint 2 after Top Rebar Failed in Fatigue (Jacking Setup in Place)

Figure D-14. Top View of Failed Rebar at Joint 2 (Spalled Concrete Removed)

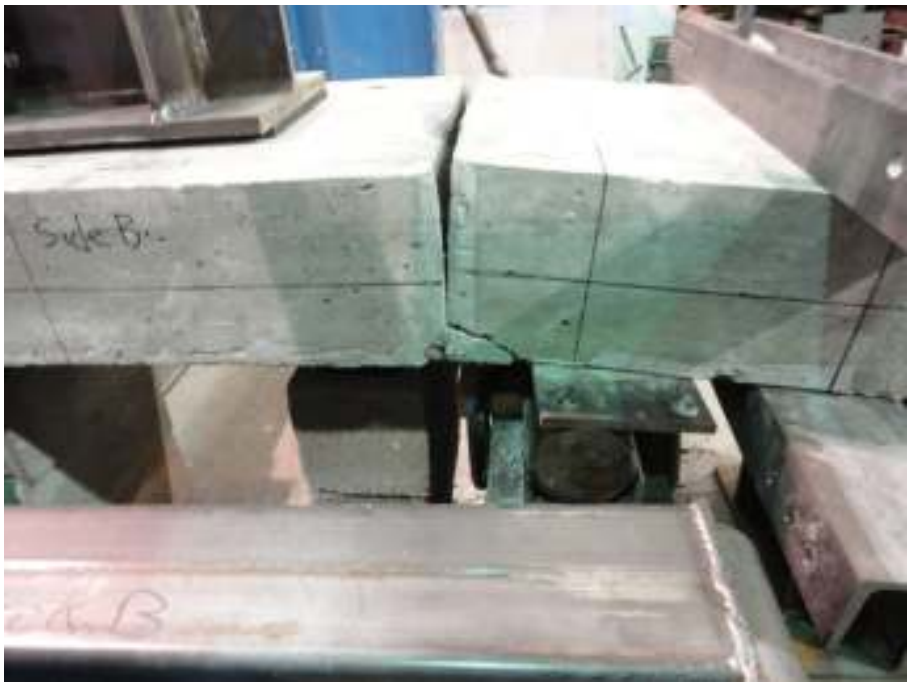

Figure D-15. Joint 2 with Jacking Struts and Connections Removed

Figure D-16. Joint 1 with Jacking Struts and Connections Removed (No Failed Fatigue Rebars)

Figure D-17. End Face of Joint 2 with Failed Top Rebar (Bottom Bars Were Cut)

Figure D-18. Closure Pour Face of Joint 2 with Failed Top Rebar

APPENDIX E- Calculations

E.1 I-81 Specimens Capacity and Load Limits

Section Data

Concrete:

$f_c := 7650$ psi (From core sample strength tests) $E_c := 57\cdot\sqrt{f_c} = 4985.464$ ksi

depth $:= 9$ in width $:= 22$ in $b :=$ width $A_c :=$ depth $\cdot$ width $= 198$ in^2

$d := 7.25$ in (distance from top surface to bottom three bars)

$d' := 3.75$ in (distance from top surface to top bar)

$$\beta_1 := 0.85 - \left(f_c - 4000\right)\cdot\frac{0.05}{1000} = 0.667$$ [ACI R10.2.7]

Steel:

#5 bars: $A_{s1} := 3\cdot 0.31 = 0.93$ in^2 $A_{s2} := 0.31$ in^2 $d_b := \frac{5}{8}$ in

$f_y := 67.5$ ksi $E_s := 25141$ ksi (from rebar tests) $\varepsilon_y := \frac{f_y}{E_s} = 0.00268$ $n := \frac{E_s}{E_c}$

Capacity of Section

Flexure:

Check if top steel in tension or compression:

Assume $c := d' = 3.75$ in $a := \beta_1\cdot c = 2.503$ in

$$C := 0.85\cdot\frac{f_c}{1000}\cdot a\cdot b = 358.085$$ kips

$T := A_{s1}\cdot f_y = 62.775$ kips (Top steel is in tension since C > T)

Assume top and bottom steel yield:

$$\Sigma F_H = 0 \qquad 0.85\cdot f_c\cdot\left(\beta_1\cdot c\right)\cdot b = f_y\cdot\left(A_{s1} + A_{s2}\right)$$

$$c := \frac{f_y\cdot\left(A_{s1} + A_{s2}\right)}{0.85\cdot\frac{f_c}{1000}\cdot\beta_1\cdot b} = 0.877$$ in $a := c\cdot\beta_1 = 0.585$ in

Check steel:

$$\varepsilon_{s1} := 0.003 \cdot \frac{d - c}{c} = 0.02181 \quad > \quad \varepsilon_y = 0.003$$ (bottom steel yields, strain hardening)

$$\varepsilon_{s2} := 0.003 \cdot \frac{d' - c}{c} = 0.00983 \quad > \quad \varepsilon_y = 0.003$$ (top steel yields)

$$M_n := f_y \cdot A_{s1} \cdot d + f_y \cdot A_{s2} \cdot d' - 0.85 \cdot \frac{f_c}{1000} \cdot a \cdot b \cdot \left(\frac{a}{2} \right) = 509.101 \quad \text{in·kips}$$

Shear:

Shear capacity due to concrete (no shear reinforcment):

Use lower layer of bars for d: $d = 7.25$ in

$$V_c := \frac{2 \cdot \sqrt{f_c} b \cdot d}{1000} = 27.901 \quad \text{kips}$$ (controls) [ACI Eq. 11-3]

At joints (assuming no concrete contact):

$$V_n := 0.6 \cdot f_y \cdot \left(A_{s1} + A_{s2} \right) = 50.22 \quad \text{kips}$$ [based on AISC Eq. G2-1]

Determination of Load Limits

Distributed Load Case:

Wheel Pressure = P/(20*10)

$$w_p = \frac{P}{20} \quad \frac{\text{kips}}{\text{in}}$$

Where P is the applied wheel load in kips over the 20x10" elastomeric pad

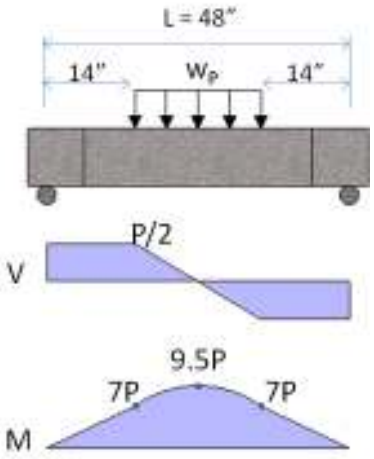

Shear and moment values in the figure to the right where determined by simple statics. Shear diagram, V, is in "kips". Moment diagram, M, is in "in-kips".

Flexure: $9.5 \cdot P = M_n \text{ solve}, P \rightarrow 53.59$ $P_{flex} = 53.6$ kips

Shear: $0.5 \cdot P = V_c \text{ solve}, P \rightarrow 55.802$ $P_{shear} = 55.8$ kips

Two Point-Loads Case:

Wheel Load = **P**

It was assumped that when the slabs deflected during loading, the top surface curvature would cause the load to be applied at two locations 8" from the slab's center.

Shear and moment values in the figure to the right where determined by simple statics. Shear diagram, V, is in "kips". Moment diagram, M, is in "in-kips".

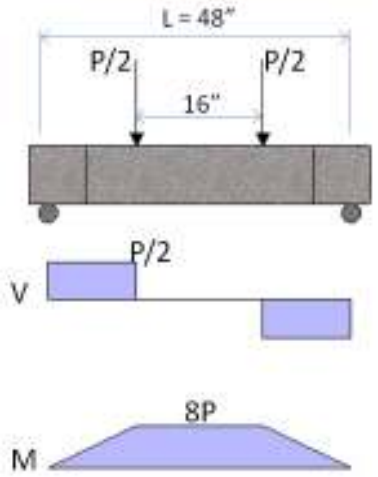

Flexure: $8 \cdot P = M_n \text{ solve}, P \rightarrow 63.64$ $P_{flex} = 63.6$ kips

Shear: $0.5 \cdot P = V_c \text{ solve}, P \rightarrow 55.802$ $P_{shear} = 55.8$ kips

E.2 Cast Specimens Capacity and Load Limits

Section Data

Concrete:

$f_c := 6325$ psi (From concrete mixture cylinder tests) $E_c := 57\cdot\sqrt{f_c} = 4533.203$ ksi

depth $:= 8.75$ in width $:= 22$ in $b := width$ $A_c := depth \cdot width = 192.5$ in^2

$d := 7.25$ in (distance from top surface to bottom three bars)

$d' := 3.375$ in (distance from top surface to top bar)

$$\beta_1 := 0.85 - \left(f_c - 4000\right)\cdot\frac{0.05}{1000} = 0.734$$ [ACI R10.2.7]

Steel:

#5 bars: $A_{s1} := 3\cdot 0.31 = 0.93$ in^2 $A_{s2} := 0.31$ in^2 $d_b := \frac{5}{8}$ in

$f_y := 67.5$ ksi $E_s := 25141$ ksi (from rebar tests) $\varepsilon_y := \frac{f_y}{E_s} = 0.003$ $n := \frac{E_s}{E_c}$

Capacity of Section

Flexure:

Check if top steel in tension or compression:

Assume $c := d' = 3.375$ in $a := \beta_1\cdot c = 2.476$ in

$$C := 0.85\cdot\frac{f_c}{1000}\cdot a\cdot b = 292.903 \text{ kips}$$

$T := A_{s1}\cdot f_y = 62.775$ kips (Top steel is in tension since C > T)

Assume top and bottom steel yield:

$$\Sigma F_H = 0 \qquad 0.85\cdot f_c\cdot\left(\beta_1\cdot c\right)\cdot b = f_y\cdot\left(A_{s1} + A_{s2}\right)$$

$$c := \frac{f_y\cdot\left(A_{s1} + A_{s2}\right)}{0.85\cdot\frac{f_c}{1000}\cdot\beta_1\cdot b} = 0.964 \text{ in} \qquad a := c\cdot\beta_1 = 0.708 \text{ in}$$

Check steel:

$$\varepsilon_{s1} := 0.003 \cdot \frac{d - c}{c} = 0.01955 \quad > \quad \varepsilon_y = 0.003$$ (bottom steel yields, strain hardening)

$$\varepsilon_{s2} := 0.003 \cdot \frac{d' - c}{c} = 0.0075 \quad > \quad \varepsilon_y = 0.003$$ (top steel yields)

$$M_n := f_y \cdot A_{s1} \cdot d + f_y \cdot A_{s2} \cdot d' - 0.85 \cdot \frac{f_c}{1000} \cdot a \cdot b \cdot \left(\frac{a}{2}\right) = 496.125 \quad \text{in·kips}$$

Shear:

Shear capacity due to concrete (no shear reinforcment):

Use lower layer of bars for d: $d = 7.25$ in

$$V_c := \frac{2 \cdot \sqrt{f_c} b \cdot d}{1000} = 25.37 \quad \text{kips}$$ (controls) [ACI Eq. 11-3]

At joints (assuming no concrete contact):

$$V_n := 0.6 \cdot f_y \cdot \left(A_{s1} + A_{s2}\right) = 50.22 \quad \text{kips}$$ [based on AISC Eq. G2-1]

Determination of Load Limits

Distributed Load Case:

Wheel Pressure = P/(20*10)

$$w_p = \frac{P}{20} \quad \frac{\text{kips}}{\text{in}}$$

Where P is the applied wheel load in kips over the 20x10" elastomeric pad

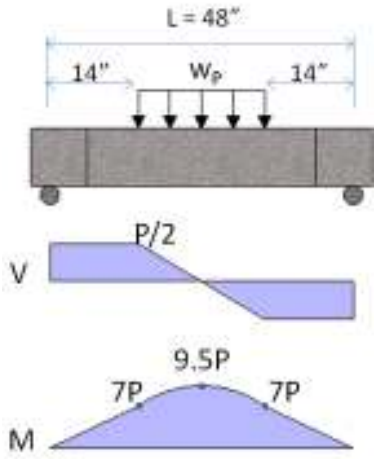

Shear and moment values in the figure to the right where determined by simple statics. Shear diagram, V, is in "kips". Moment diagram, M, is in "in-kips".

Flexure: $9.5 \cdot P = M_n \text{ solve}, P \rightarrow 52.22$ $P_{flex} = 52.2$ kips

Shear: $0.5 \cdot P = V_c \text{ solve}, P \rightarrow 50.74$ $P_{shear} = 50.74$ kips

Two Point-Loads Case:

Wheel Load = **P**

It was assumped that when the slabs deflected during loading, the top surface curvature would cause the load to be applied at two locations 8" from the slab's center.

Shear and moment values in the figure to the right where determined by simple statics. Shear diagram, V, is in "kips". Moment diagram, M, is in "in-kips".

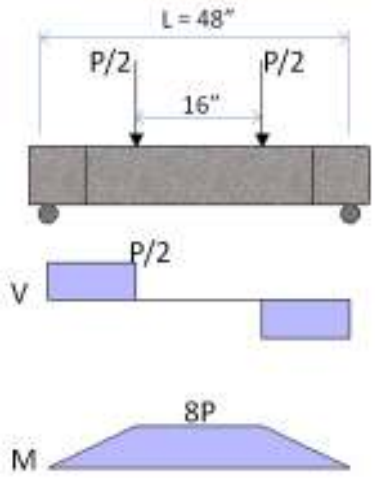

Flexure: $8 \cdot P = M_n \text{ solve}, P \rightarrow 62.02$ $P_{flex} = 62.0$ kips

Shear: $0.5 \cdot P = V_c \text{ solve}, P \rightarrow 50.74$ $P_{shear} = 50.7$ kips

E.3 I-81 Bridge Closure Pour Stresses and Deflections due to Shrinkage

Known Data

Concrete:

$f'_c := 6500$ psi $\qquad E_c := 57\cdot\sqrt{f'_c} = 4595$ ksi

$depth := 9$ in $\qquad width := 22$ in $\qquad A_c := depth \cdot width = 198$ in^2

Steel:

Four #5 bars: $A := 0.31$ in^2 $\qquad A_s := 4\cdot A = 1.24$ in^2 $\qquad d_b := \frac{5}{8}$ in

$E_s := 25141$ ksi (from tensile tests) $\qquad n := \frac{E_s}{E_c} = 5.471$

Creep and Shrinkage

Shrinkage: Using the ACI 290R-92 Model

$\varepsilon_{sh} := 700\cdot 10^{-6}$ (Taken Abbas (2011) report, plots for unrestrained prisms after 180 days)

Apply correction factor for volume and surface area of prisms and closure pour section

Prism dimensions: 3x3x11" Closure pour dimension: 9x22x36"

$V_{pr} := 3\cdot 3\cdot 11 = 99$ $\qquad V_{cp} := 9\cdot 22\cdot 36 = 7128$

$S_{pr} := 2\cdot(3\cdot 3) + 4\cdot(3\cdot 11) = 150$ $\qquad S_{cp} := 2\cdot(36\cdot 22 + 36\cdot 9) = 2232$

$\gamma_{sh.pr} := 1.2\cdot e^{\left(-0.12\cdot\frac{V_{pr}}{S_{pr}}\right)}$ $\qquad \gamma_{sh.cp} := 1.2\cdot e^{\left(-0.12\cdot\frac{V_{cp}}{S_{cp}}\right)}$ [ACI 290R-92]

$\gamma_{sh.pr} = 1.109$ $\qquad \gamma_{sh.cp} = 0.818$

$\varepsilon_{shu} := \varepsilon_{sh}\cdot\frac{\gamma_{sh.cp}}{\gamma_{sh.pr}} = 0.00052$ $\qquad \frac{\varepsilon_{shu}}{10^{-6}} = 516$ $\mu\varepsilon$

Shrinkage Function Over Time:

Take: $\alpha := 1$ $\qquad f := 35$ (Assuming 7 day moist curing)

$$\varepsilon_{sh}(t) := \frac{t^{\alpha}}{f + t^{\alpha}} \cdot \varepsilon_{shu}$$ (Where t is the age since curing)

For I-81 closure pour, assume first and second adjacent slabs had an age of 30 and 100 days, respectively, when the closure pour was cast.

$\varepsilon_{sh.30} := \varepsilon_{sh}(30 - 7) = 0.0002$ $\varepsilon_{sh.100} := \varepsilon_{sh}(100 - 7) = 0.00038$

Aging Coefficient:

$$\mu(t_o) := \frac{t_o^{0.5}}{1 + t_o^{0.5}}$$ [MacGregor & Wight Eq. 3-41]

Loading at 7 days: $\mu(7) = 0.726$

Loading at 14 days: $\mu(14) = 0.789$ Take aging coefficient as: $\mu := 0.75$

Creep Coefficient:

Use ACI 209R-92 Model:

$\phi_u = 2.35 \cdot \gamma_c$

Assume loading at 10.5 days (in between 7 and 14 days) $t_o := 10.5 \quad \text{days}$

$\gamma_{c.to} := 1.25 \cdot (t_o)^{-0.118} = 0.947$

From relative humidity map, average RH in VA: $RH := 0.70$

$\gamma_{c.RH} := 1.27 - 0.67 \cdot RH = 0.801$ For RH > 40%

$V := 9 \cdot 22 = 198$ $S := 2 \cdot (9 + 22) = 62$

$$\gamma_{c.vs} := \frac{2}{3} \cdot \left[1 + 1.13 \cdot e^{\left(-0.54 \cdot \frac{V}{S}\right)}\right] = 0.801$$

$\gamma_c := \gamma_{c.to} \cdot \gamma_{c.RH} \cdot \gamma_{c.vs} = 0.608$

$\phi_u := 2.35 \cdot \gamma_c = 1.428$

Creep Function Over Time:

Take: $d := 10$ $\psi := 0.6$

$$\phi_c(t) := \frac{t^{\psi}}{d + t^{\psi}} \cdot \phi_u$$ (Where t is the number of days since loading)

For I-81 closure pour, assume first and second adjacent slabs had an age of 30 and 100 days, respectively, when the closure pour was cast.

$\phi_{c.30} := \phi_c(30 - t_o) = 0.532$ $\phi_{c.100} := \phi_c(100 - t_o) = 0.853$

Internal Stresses of Adjacent Slabs (prior to closure pour)

Older Slab (100 days):

$\Delta\varepsilon_s = \Delta\varepsilon_c$

$$\frac{\Delta P_s}{A_s \cdot E_s} = \frac{\Delta P_c}{A_c \cdot E_c}\left(1 + \mu \cdot \phi_{c.100}\right) - \varepsilon_{sh.100}$$

Since $\Delta P_s = -\Delta P_c$

$$\frac{-\Delta P_c}{A_s \cdot E_s} = \frac{\Delta P_c}{A_c \cdot E_c}\left(1 + \mu \cdot \phi_{c.100}\right) - \varepsilon_{sh.100} \text{ solve}, \Delta P_c \rightarrow 11.076$$

$\Delta P_{c.old} := 12.673$ kips (T)

$\Delta f_c := \frac{\Delta P_{c.old}}{A_c} = 0.064$ ksi (T) $\Delta f_s := \frac{-\Delta P_{c.old}}{A_s} = -10.22$ ksi (C)

Newer Slab (30 days):

$\Delta\varepsilon_s = \Delta\varepsilon_c$

$$\frac{\Delta P_s}{A_s \cdot E_s} = \frac{\Delta P_c}{A_c \cdot E_c}\left(1 + \mu \cdot \phi_{c.30}\right) - \varepsilon_{sh.30}$$

Since $\Delta P_s = -\Delta P_c$

$$\frac{-\Delta P_{c.new}}{A_s \cdot E_s} = \frac{\Delta P_{c.new}}{A_c \cdot E_c}\left(1 + \mu \cdot \phi_{c.30}\right) - \varepsilon_{sh.30} \text{ solve}, \Delta P_{c.new} \rightarrow 6.093$$

$\Delta P_{c.new} := 6.979$ kips (T)

$$\Delta f_c := \frac{\Delta P_{c.new}}{A_c} = 0.035 \text{ ksi (T)} \qquad \Delta f_s := \frac{-\Delta P_{c.new}}{A_s} = -5.628 \text{ ksi (C)}$$

Long Time After Closure Pour was Set

The following approach to estimate stresses and crack opening is based on Gilbert (1992)

Assume $L := 8 \cdot 12 = 96$ in (Take L as 8-ft beam spacing)

$$\rho := \frac{A_s}{A_c} = 0.006 \qquad s_o := \frac{d_b}{10 \cdot \rho} = 9.98 \qquad \text{use} \quad s_o := 10 \text{ in}$$

System divided into three regions of uniform internal steel and concrete stresses and four transition regions, each with a length of s_o.

Number of unknowns:

Forces: ΔP_{s1} ΔP_{c1} ΔP_{s2} ΔP_{c2} ΔP_{s3} ΔP_{c3} P (7 unknown forces)

Strains: $\Delta \varepsilon_{s1}$ $\Delta \varepsilon_{c1}$ $\Delta \varepsilon_{s2}$ $\Delta \varepsilon_{c2}$ $\Delta \varepsilon_{s3}$ $\Delta \varepsilon_{c3}$ (6 unknown strains)

Steel def. in transition region: Δl_{so1} Δl_{so2} Δl_{so3} Δl_{so4} (4 unknown deformations)

17 Total Unknown Values

Equations of Equilibrium:

1) $\Delta P_{s1} + \Delta P_{c1} = P$ 2) $\Delta P_{s2} + \Delta P_{c2} = P$ 3) $\Delta P_{s3} + \Delta P_{c3} = P$

Constitutive Equations:

4) $$\Delta \varepsilon_{s1} = \frac{\Delta P_{s1}}{A_s \cdot E_s} \rightarrow \Delta \varepsilon_{s1} = 3.20771 \times 10^{-5} \cdot \Delta P_{s1}$$

5) $$\Delta \varepsilon_{s2} = \frac{\Delta P_{s2}}{A_s \cdot E_s} \rightarrow \Delta \varepsilon_{s2} = 3.20771 \times 10^{-5} \cdot \Delta P_{s2}$$

6) $\Delta\varepsilon_{s3} = \frac{\Delta P_{s3}}{A_s \cdot E_s} \rightarrow \Delta\varepsilon_{s3} = 3.20771 \times 10^{-5} \cdot \Delta P_{s3}$

From earlier :

$\varepsilon_{shu} = 0.001 \qquad \mu = 0.75 \qquad \phi_u = 1.428$

$P_{o.100} := \Delta P_{c.old} = 12.673 \text{ kips} \qquad P_{o.30} := \Delta P_{c.new} = 6.979 \text{ kips}$

Simplify:

$$E_{c.eff} := \frac{E_c}{1 + \mu \cdot \phi_u} = 2218.996 \text{ ksi}$$

7)

$$\Delta\varepsilon_{c1} = \frac{P_{o.30}}{A_c \cdot E_c} \cdot \phi_u + \frac{\Delta P_{c1}}{A_c \cdot E_{c.eff}} - \varepsilon_{shu} \rightarrow \Delta\varepsilon_{c1} = 2.276 \times 10^{-6} \cdot \Delta P_{c1} - 5.0554 \times 10^{-4}$$

8) No initial axial load for closure pour

$$\Delta\varepsilon_{c2} = \frac{\Delta P_{c2}}{A_c \cdot E_{c.eff}} - \varepsilon_{shu} \rightarrow \Delta\varepsilon_{c2} = 2.276 \times 10^{-6} \cdot \Delta P_{c2} - 5.1649 \times 10^{-4}$$

9)

$$\Delta\varepsilon_{c3} = \frac{P_{o.100}}{A_c \cdot E_c} \cdot \phi_u + \frac{\Delta P_{c3}}{A_c \cdot E_{c.eff}} - \varepsilon_{shu} \rightarrow \Delta\varepsilon_{c3} = 2.276 \times 10^{-6} \cdot \Delta P_{c3} - 4.966 \times 10^{-4}$$

10)

$$\Delta l_{so1} := \frac{s_o}{A_s \cdot E_s} \cdot \left(\frac{P}{3} - \frac{2}{3} \cdot \Delta P_{s1} \right) \rightarrow 1.0692 \times 10^{-4} \cdot P + -2.1385 \times 10^{-4} \cdot \Delta P_{s1}$$

11)

$$\Delta l_{so2} := \frac{s_o}{A_s \cdot E_s} \cdot \left(\frac{P}{3} - \frac{2}{3} \cdot \Delta P_{s2} \right) \rightarrow 1.0692 \times 10^{-4} \cdot P + -2.1385 \times 10^{-4} \cdot \Delta P_{s2}$$

12)

$$\Delta l_{so3} := \frac{s_o}{A_s \cdot E_s} \cdot \left(\frac{P}{3} - \frac{2}{3} \cdot \Delta P_{s2} \right) \rightarrow 1.0692 \times 10^{-4} \cdot P + -2.1385 \times 10^{-4} \cdot \Delta P_{s2}$$

13)

$$\Delta l_{so4} := \frac{s_o}{A_s \cdot E_s} \cdot \left(\frac{P}{3} - \frac{2}{3} \cdot \Delta P_{s3} \right) \rightarrow 1.0692 \times 10^{-4} \cdot P + -2.1385 \times 10^{-4} \cdot \Delta P_{s3}$$

Equations of Compatability:

14) $\Delta\varepsilon_{c1} = \Delta\varepsilon_{s1}$

15) $\Delta\varepsilon_{c2} = \Delta\varepsilon_{s2}$

16) $\Delta\varepsilon_{c3} = \Delta\varepsilon_{s3}$

Define section lengths:

$L_1 := 0.5L - 0.5 \cdot 36 = 30$ in $\quad L_2 := 36$ in $\quad L_3 := L_1 = 30$ in

$l_1 := L_1 - s_o = 20$ in $\quad l_2 := L_2 - 2 \cdot s_o = 16$ in $\quad l_3 := L_3 - s_o = 20$ in

17)

$$\Delta\varepsilon_{s1} \cdot l_1 + \Delta\varepsilon_{s2} \cdot l_2 + \Delta\varepsilon_{s3} \cdot l_3 + \Delta l_{so1} + \Delta l_{so2} + \Delta l_{so3} + \Delta l_{so4} = 0$$

$$20\Delta\varepsilon_{s1} + 16\Delta\varepsilon_{s2} + 20\Delta\varepsilon_{s3} + \Delta l_{so1} + \Delta l_{so2} + \Delta l_{so3} + \Delta l_{so4} = 0$$

Solve System of Equations:

$$\text{Coef} := \begin{pmatrix}
1 & 1 & 0 & 0 & 0 & 0 & -1 & 0 & 0 & 0 & 0 & 0 & 0 & 0 & 0 & 0 \\
0 & 0 & 1 & 1 & 0 & 0 & -1 & 0 & 0 & 0 & 0 & 0 & 0 & 0 & 0 & 0 \\
0 & 0 & 0 & 0 & 1 & 1 & -1 & 0 & 0 & 0 & 0 & 0 & 0 & 0 & 0 & 0 \\
.00002781 & 0 & 0 & 0 & 0 & 0 & 0 & -1 & 0 & 0 & 0 & 0 & 0 & 0 & 0 & 0 \\
0 & 0 & .00002781 & 0 & 0 & 0 & 0 & 0 & 0 & -1 & 0 & 0 & 0 & 0 & 0 & 0 \\
0 & 0 & 0 & 0 & .00002781 & 0 & 0 & 0 & 0 & 0 & 0 & -1 & 0 & 0 & 0 & 0 \\
0 & 2.276\cdot10^{-6} & 0 & 0 & 0 & 0 & 0 & 0 & -1 & 0 & 0 & 0 & 0 & 0 & 0 & 0 \\
0 & 0 & 0 & 2.276\cdot10^{-6} & 0 & 0 & 0 & 0 & 0 & 0 & -1 & 0 & 0 & 0 & 0 & 0 \\
0 & 0 & 0 & 0 & 0 & 2.276\cdot10^{-6} & 0 & 0 & 0 & 0 & 0 & -1 & 0 & 0 & 0 & 0 \\
-.0001854 & 0 & 0 & 0 & 0 & 0 & .00009270 & 0 & 0 & 0 & 0 & 0 & -1 & 0 & 0 & 0 \\
0 & 0 & -.0001854 & 0 & 0 & 0 & .00009270 & 0 & 0 & 0 & 0 & 0 & 0 & -1 & 0 & 0 \\
0 & 0 & -.0001854 & 0 & 0 & 0 & .00009270 & 0 & 0 & 0 & 0 & 0 & 0 & 0 & -1 & 0 \\
0 & 0 & 0 & 0 & -.0001854 & 0 & .00009270 & 0 & 0 & 0 & 0 & 0 & 0 & 0 & 0 & -1 \\
0 & 0 & 0 & 0 & 0 & 0 & 0 & -1 & 1 & 0 & 0 & 0 & 0 & 0 & 0 & 0 \\
0 & 0 & 0 & 0 & 0 & 0 & 0 & 0 & 0 & -1 & 1 & 0 & 0 & 0 & 0 & 0 \\
0 & 0 & 0 & 0 & 0 & 0 & 0 & 0 & 0 & 0 & 0 & -1 & 1 & 0 & 0 & 0 \\
0 & 0 & 0 & 0 & 0 & 0 & 0 & 20 & 0 & 16 & 0 & 20 & 0 & 1 & 1 & 1 & 1
\end{pmatrix} \quad E := \begin{pmatrix}
0 \\ 0 \\ 0 \\ 0 \\ 0 \\ 0 \\ 0.0005055 \\ 0.0005165 \\ 0.0004966 \\ 0 \\ 0 \\ 0 \\ 0 \\ 0 \\ 0 \\ 0 \\ 0
\end{pmatrix}$$

Note: The rows of matrix Coef and vector E correspond the equation numbers from the calculations. Also, the columns of matrix Coef correspond to the following variables in the order presented:

$$\Delta P_{s1} \quad \Delta P_{c1} \quad \Delta P_{s2} \quad \Delta P_{c2} \quad \Delta P_{s3} \quad \Delta P_{c3} \quad P \quad \Delta\varepsilon_{s1} \quad \Delta\varepsilon_{c1} \quad \Delta\varepsilon_{s2} \quad \Delta\varepsilon_{c2} \quad \cdots$$

$$\cdots \quad \Delta\varepsilon_{s3} \quad \Delta\varepsilon_{c3} \quad \Delta l_{so1} \quad \Delta l_{so2} \quad \Delta l_{so3} \quad \Delta l_{so4}$$

$$\text{Ans} := \text{Coef}^{-1} \cdot E = \begin{pmatrix}
-14.41894 \\ 45.91792 \\ -14.78456 \\ 46.28354 \\ -14.12312 \\ 45.6221 \\ 31.49898 \\ -0.0004 \\ -0.0004 \\ -0.00041 \\ -0.00041 \\ -0.00039 \\ -0.00039 \\ 0.00559 \\ 0.00566 \\ 0.00566 \\ 0.00554
\end{pmatrix}$$

Results:

Forces:

$\Delta P_{s1} := Ans_1 = -14.419$ kips $\quad \Delta P_{c1} := Ans_2 = 45.918$ kips

$\Delta P_{s2} := Ans_3 = -14.785$ kips $\quad \Delta P_{c2} := Ans_4 = 46.284$ kips

$\Delta P_{s3} := Ans_5 = -14.123$ kips $\quad \Delta P_{c3} := Ans_6 = 45.622$ kips

$P := Ans_7 = 31.499$ kips

Stress on Rebars: $f_s := \frac{P}{A_s} = 25.402$ ksi

Strains:

$\Delta\varepsilon_{s1} := \frac{Ans_8}{10^{-6}} = -401$ με $\quad \Delta\varepsilon_{c1} := \frac{Ans_9}{10^{-6}} = -401$ με

$\Delta\varepsilon_{s2} := \frac{Ans_{10}}{10^{-6}} = -411$ με $\quad \Delta\varepsilon_{c2} := \frac{Ans_{11}}{10^{-6}} = -411$ με

$\Delta\varepsilon_{s3} := \frac{Ans_{12}}{10^{-6}} = -393$ με $\quad \Delta\varepsilon_{c3} := \frac{Ans_{13}}{10^{-6}} = -393$ με

Steel Def. in Transition Zones:

$\Delta l_{so1} := Ans_{14} = 0.00559$ in $\quad \Delta l_{so3} := Ans_{16} = 0.00566$ in

$\Delta l_{so2} := Ans_{15} = 0.00566$ in $\quad \Delta l_{so4} := Ans_{17} = 0.00554$ in

Construction Joint Widths:

$$w_1 := \Delta l_{so1} + \Delta l_{so2} - \left(\frac{2}{3}\cdot\Delta\varepsilon_{c1}\cdot s_o + \frac{2}{3}\cdot\Delta\varepsilon_{c2}\cdot s_o\right)\cdot 10^{-6} = 0.017 \text{ in}$$

$$w_2 := \Delta l_{so3} + \Delta l_{so4} - \left(\frac{2}{3}\cdot\Delta\varepsilon_{c2}\cdot s_o + \frac{2}{3}\cdot\Delta\varepsilon_{c3}\cdot s_o\right)\cdot 10^{-6} = 0.017 \text{ in}$$

E.4 Reinforcing Bar Stresses and Strains due to Jacking

Section Data

Concrete:

Slab dimensions:

$h := 8.75 \ \text{in}$ (slab depth) $b := 22 \ \text{in}$ (width)

$l_{closurepour} := 36 \ \text{in}$ $l_{ends} := 34 \ \text{in}$ $L := l_{closurepour} + 2 \cdot l_{ends} = 104 \ \text{in}$

$A_c := h \cdot b = 192.5 \ \text{in}^2$

Steel:

No. 5 Bars:

$A_{s.top} := 0.31 \ \text{in}^2$ $A_{s.bot} := 0.31 \cdot 3 = 0.93 \ \text{in}^2$

From tensile tests of No. 5 bars:

$f_y := 67.5 \ \text{ksi}$ $E_s := 25140 \ \text{ksi}$ $\varepsilon_y := 0.002677$ $\varepsilon_{sh} := 0.01196$

Location of steel bars at joint cross-section:

$d := 7.25 \ \text{in}$ (distance from top surface to bottom three bars)

$d' := 3.375 \ \text{in}$ (distance from top surface to top bar)

Other Dimensions:

Distance from support to joint: $d_{sj} := 6 \ \text{in}$

Distance from joint to jacking strut pivot point: $d_{jp} := 12.5 \ \text{in}$

Find Bar Stresses and Strains

Dead Load:

Total slab weight:

$$W := \frac{h \cdot b \cdot L}{12^3} \cdot \left(\frac{150}{1000} \right) = 1.738 \ \text{kips}$$

Reaction at supports:

$$R_{DL} := \frac{W}{2} = 0.869 \quad \text{kips}$$

Sum moments about bottom bars of the end section cut at the joint:

$$\Sigma M_{bot} = 0 \qquad (d - d') \cdot P_{DL.top} - d_{sj} \cdot R_{DL} = 0 \text{ solve}, P_{DL.top} \rightarrow 1.345 \quad \text{kips}$$

(compression)

$$P_{DL.top} := -1.345 \text{ kips} \qquad P_{DL.bot} := 1.345 \text{ kips}$$

Jack Load:

Sum moments about bottom bars of a cut section at the joints:

$$\Sigma M_{bot} = 0$$

$$(d - d') \cdot P_{jack.top} - (d - 0.5 \cdot h) \cdot P_{jack} = 0 \text{ solve}, P_{jack.top} \rightarrow 0.74194 P_{jack}$$

$$P_{jack.top} = 0.74194 P_{jack}$$

Sum horizontal forces:

$$\Sigma F_{hor} = 0 \qquad P_{jack.top} + P_{jack.bot} = P_{jack}$$

$$0.74194 P_{jack} + P_{jack.bot} = P_{jack} \text{ solve}, P_{jack.bot} \rightarrow 0.25806 P_{jack}$$

$$P_{jack.bot} = 0.25806 P_{jack}$$

First Yield:

Top bar force at yield: $P_{y.top} := f_y \cdot A_{s.top} = 20.925 \quad \text{kips}$

Corresponding jack force:

$$0.74194 P_{jack} + P_{DL.top} = P_{y.top} \text{ solve}, P_{jack} \rightarrow 30.016 \quad \text{kips}$$

$$P_{y.jack} := 30.016 \quad \text{kips} \qquad (15.01 \text{ kips per jack})$$

Bottom bars force at yield:

$$P_{y.bot} := 0.25806 P_{y.jack} + P_{DL.bot} = 9.091 \quad \text{kips}$$

Bar Stress and Strain at Yield:

Stress:

$$f_{top} := \frac{P_{y.top}}{A_{s.top}} = 67.5 \quad ksi \qquad f_{bot} := \frac{P_{y.bot}}{A_{s.bot}} = 9.775 \quad ksi$$

Strain:

$$\varepsilon_{top} := \frac{f_{top}}{E_s} = 0.00268 \qquad \varepsilon_{bot} := \frac{f_{bot}}{E_s} = 0.000389$$

Joint Curvature:

$$\rho_y := \frac{\varepsilon_{top} - \varepsilon_{bot}}{d - d'} = 0.000593 \quad in^{-1}$$

$$\theta_y := \operatorname{asin}\left(\frac{\rho_y}{\sqrt{1^2 + \rho_y{}^2}}\right) = 0.000593 \quad rad$$

Vertical displacement of jack load due to joint curvature:

$$\Delta_{jack} := d_{jp} \cdot \sin(\theta_y) = 0.00741 \quad in$$

An Excel spreadsheet was made to calculate the stress and strains when jacked to 36 kips and the follow formulas were used.

Converge to Jacking Force Accounting for P-? Effects:

$$\Sigma M_{bot} = 0$$

$$P_{jack} \cdot \left[\cos(\theta_y) \cdot (d - 0.5 \cdot h) - \sin(\theta_y) \cdot d_{jp}\right] + R_{DL}\left[\sin(\theta_y) \cdot (h - d) - \cos(\theta_y) \cdot d_{sj}\right] = P_{y.top} \cdot (d - d')$$

$$P_{jack} := \frac{P_{y.top} \cdot (d - d') - R_{DL} \cdot \left[\sin(\theta_y) \cdot (h - d) - \cos(\theta_y) \cdot d_{sj}\right]}{\cos(\theta_y) \cdot (d - 0.5 \cdot h) - \sin(\theta_y) \cdot d_{jp}} = 30.094 \quad kips$$

$$P_{bot} := P_{jack} \cdot \cos(\theta_y) - P_{y.top} - R_{DL} \cdot \sin(\theta_y) = 9.168 \quad kips$$

Converges after 2 cycles

Add Increments of Strain to Bars:

Determine increment:

$$\varepsilon_{inc} := \frac{\varepsilon_{sh} - \varepsilon_y}{100} = 9.283 \times 10^{-5}$$ 1% increment of (e_{sh} - e_y)

Add increment to top and bottom steel (keeps curvature constant):

$$\varepsilon_{top} := \varepsilon_y + \varepsilon_{inc} = 0.00277$$

$$\varepsilon_{bot} := 0.000392 + \varepsilon_{inc} = 0.000485$$ (The 0.000392 value was taken from spreadsheet)

$$f_{bot} = \varepsilon_{bot} \cdot E_s$$

$$P_{bot} = f_{bot} \cdot A_{s.bot}$$

$$\Sigma F = 0$$

$$P_{jack} = \frac{1}{\cos(\theta)} \cdot \left(P_{y.top} + P_{bot} + R_{DL} \cdot \sin(\theta)\right)$$

Stop Incrementing Strain When Jack Reaches 36 kips:

Specimen A was jacked up to 18 kips per jack (36 kips total)

$$P_{jack} := 36 \quad \text{kips}$$

$$P_{bot} := P_{jack} \cdot \cos\left(\theta_y\right) - P_{y.top} - R_{DL} \cdot \sin\left(\theta_y\right) = 15.074 \quad \text{kips}$$

$$f_{bot} := \frac{P_{bot}}{A_{s.bot}} = 16.209 \quad \text{ksi}$$

$$\varepsilon_{bot} := \frac{f_{bot}}{E_s} = 0.000645 < \varepsilon_y = 0.00268$$ (Has not yielded)

$$\varepsilon_{top} := \rho_y \cdot (d - d') + \varepsilon_{bot} = 0.00294 < \varepsilon_{sh} = 0.01196$$ (Has not gone into strain hardening)

Excel Spreadsheet Used:

Input Values		
h	8.75	*in*
b	22	*in*
L	104	*in*
A_s.top	0.31	*in^2*
A_s.bot	0.93	*in^2*
f_y	67.5	*ksi*
E_s	25140	*ksi*
e_y	0.002677	*in/in*
e_sh	0.01196	*in/in*
d	7.25	*in*
d`	3.375	*in*
d_sj	6	*in*
d_jp	12.5	*in*
R_DL	0.869	*kips*
P_DL.top	-1.345	*kips*
P_DL.bot	1.345	*kips*
e_inc	9.28E-05	*1%*

	P_top/P_jack	P_bot/P_jack	P_top	P_bot	P_jack	f_bot	e_bot	f_top	e_top	rho	delta_v
	-	-	*kip*	*kips*	*kips*	*ksi*	*in/in*	*ksi*	*in/in*	*rad/in*	*in*
No jacking	0	0	0	0	0	0	0	0	0	0	0
First Yield	0.74194	0.25806	20.925	9.090904	30.0159	9.775166	0.000389	67.5	0.002677	0.00059	0.007381
Converge to jacking force accounting for P-delta effects			20.925	9.168307	30.09383	9.858395	0.000392	67.5	0.002677	0.00059	0.007371
			20.925	9.168196	30.09371	9.858275	0.000392	67.5	0.002677	0.00059	0.007371
Add 1% increments to e_top & e_bot of (e_sh - e_y)			20.925	11.33858	32.2641	12.19202	0.000485	67.5	0.00277	0.00059	0.007371
			20.925	13.50896	34.43448	14.52577	0.000578	67.5	0.002863	0.00059	0.007371
Final state when jacked to 36 kips			20.925	15.07448	36	16.20912	0.000645	67.5	0.00293	0.00059	0.007371
							In Elastic Range		**No Strain Harding**		

Conclusion:

Although the top steel was yielded during the jacking process, it did not go into strain hardening. When the wheel load (16.5 kips) was applied to Specimen A, the bending caused the top steel to tend to go into compression. Therefore, any compressive stress component due to slab bending caused the stress and strain to be reduced along a line parallel to the elastic portion of the bar stress-strain curve. As the the specimen was cycled the stress and strain cyled elastically along the this parallel line.

E.5 Reduced Wheel Load using Equivalent Slab Width

Equivalent Strip

Truck wheel load:

$P_{wheel} := 16 \quad kips$

Spacing of supporting components:

$S := 8 \quad ft$

Type of deck: Cast-in-place

$M_{positive} := 26 + 6.6 \cdot S = 78.8 \quad in$ [AASHTO Table 4.6.2.1.3-1]

$M_{negative} := 48 + 3.0 \cdot S = 72 \quad in$

Equivalent width:

$w_{eq} := \min\left(M_{positive}, M_{negative}\right) = 72 \quad in$

Slab specimen width:

$w_{specimen} := 22 \quad in$

Reduced Load

Equivalent reduced wheel load for test specimens:

$$P_{reduced} := \frac{w_{specimen}}{w_{eq}} \cdot P_{wheel} = 4.9 \quad kips$$

E.6 Stress Range Components for Failed Fatigue Reinforcing Bar

Stress Range Components of Fatigue Fracture Face

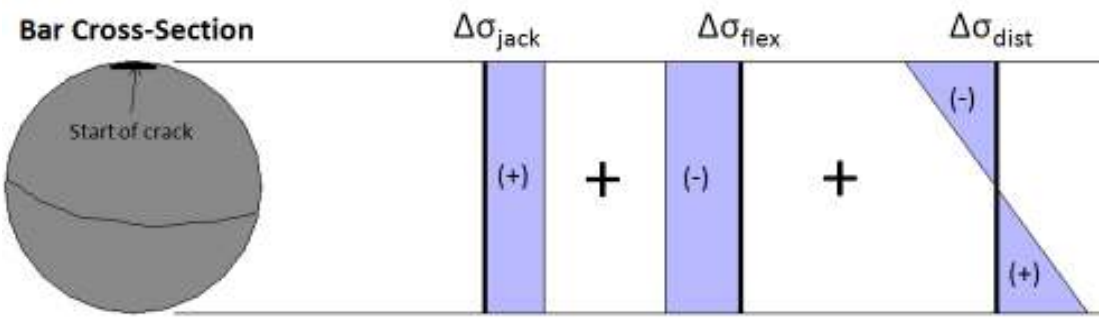

$f_r = \Delta\sigma_{bend} + \Delta\sigma_{dist} - \Delta\sigma_{jack}$

f_r = Total stress range corresponding to fatigue failure at N cycles in S-N plot

$\Delta\sigma_{bend}$ = Stress change from one-way bending of slab specimen due to applied wheel load

$\Delta\sigma_{dist}$ = Stress change from distorsional local bending of top bar due to applied wheel load (related to shear deformation)

$\Delta\sigma_{jack}$ = Stress change from axial jacking load due to wheel load

Determination of Stress Change due to Local Distorsional Bending

Stress Range from S-N Plot:

Failure at: $N := 282000$ cycles

Mean stress range:

$\log(N) = 6.9690 - 0.0383 f_r \text{ solve}, f_r \rightarrow 39.654$ ksi [Equation 5-1]

$f_{r.mean} := 39.654$ ksi

Stress range tolerance limits:

$\log(N) = 6.9690 + 0.3586 - 0.0383 f_r \text{ solve}, f_r \rightarrow 49.017$ ksi [Equation 5-2]

$\log(N) = 6.9690 - 0.3586 - 0.0383 f_r \text{ solve}, f_r \rightarrow 30.291$ ksi [Equation 5-2]

$f_{r.high} := 49.017$ ksi $f_{r.low} := 30.291$ ksi

Change in Stress from Slab One-Way Bending:

Moment at joint due to wheel load:

$P_{wheel} := 16 \quad kips \qquad \Delta P := P_{wheel}$

$\Delta M_{joint} := 3 \cdot \Delta P = 48 \quad in \cdot kip$ (From moment diagram)

$h := 8.75 \quad in$ (slab depth) $\qquad b := 22 \quad in$ (slab width) $\qquad L := 104 \quad in$ (slab length)

$d := 7.25 \quad in$ (distance from top surface to bottom three bars)

$d' := 3.375 \quad in$ (distance from top surface to top bar)

$A_{s.top} := 0.31 \quad in^2 \qquad A_{s.bot} := 0.31 \cdot 3 = 0.93 \quad in^2$

Reaction due to applied load: $R := \frac{\Delta P}{2} + \frac{b \cdot h \cdot L}{12^3} \cdot (0.150) = 9.738 \quad kips$

Sum moments about bottom bars of a cut section at the joints:

$\Sigma M_{bot} = 0$

$(d - d') \cdot \Delta P_{bend.top} + \Delta M_{joint} - 6 \cdot R = 0 \text{ solve}, \Delta P_{bend.top} \rightarrow 2.691 \quad kips$

$\Delta P_{bend.top} := 2.691 \quad kips$

Change in stress:

$\Delta \sigma_{bend} := \frac{\Delta P_{bend.top}}{A_{s.top}} = 8.681 \quad ksi$

Change in Stress from Axial Jacking Load:

Change in jacking force during 0.5 to 16.5 kip applied loading:

$\Delta P_{jack} := \frac{1}{3} \cdot (0.958 + 0.940 + 0.977) = 0.958 \quad kips$ (values averaged from static tests at 10^3, 10^4, and 10^5 cycles)

Sum moments about bottom bars of a cut section at the joints:

$$\Sigma M_{bot} = 0 \quad (d - d') \cdot \Delta P_{j.top} - \left(d - \frac{h}{2}\right) \cdot \Delta P_{jack} = 0 \text{ solve}, \Delta P_{j.top} \rightarrow 0.711 \quad \text{kips}$$

$$\Delta P_{j.top} := 0.711 \quad \text{kips}$$

Change in stress:

$$\Delta\sigma_{jack} := \frac{\Delta P_{j.top}}{A_{s.top}} = 2.294 \quad \text{ksi}$$

Change in Stress from Distorsional Local Bending:

Using Equations 5-1 (mean stress range):

$$f_{r.mean} = \Delta\sigma_{bend} + \Delta\sigma_{dist} - \Delta\sigma_{jack} \text{ solve}, \Delta\sigma_{dist} \rightarrow 33.267 \quad \text{ksi}$$

Using Equations 5-2 (mean stress range):

$$f_{r.high} = \Delta\sigma_{bend} + \Delta\sigma_{dist} - \Delta\sigma_{jack} \text{ solve}, \Delta\sigma_{dist} \rightarrow 42.63 \quad \text{ksi}$$

$$f_{r.low} = \Delta\sigma_{bend} + \Delta\sigma_{dist} - \Delta\sigma_{jack} \text{ solve}, \Delta\sigma_{dist} \rightarrow 23.904$$

$$\frac{33.267}{f_{r.mean}} \cdot 100 = 83.893 \quad \%$$

By using the mean stress range corresponding to failure at 282,000 cycles, the change in stress from distorsional local top bar bending due to applied wheel load appears to be the primary stress component since it takes up 83.9% of the mean stress range.